UNIVERSITY OF ALBERTA

Lightning strikes in Alberta thunderstorms: climatology and case studies

by

Steven Alexander Kozak

©

A thesis submitted to the Faculty of Graduate Studies and Research in partial fulfillment of the requirements for the degree of Master of Science

Department of Earth and Atmospheric Sciences

Edmonton, Alberta

Fall 1998

National Library of Canada
Acquisitions and Bibliographic Services
395 Wellington Street
Ottawa ON K1A 0N4
Canada

Bibliothèque nationale du Canada
Acquisitions et services bibliographiques
395, rue Wellington
Ottawa ON K1A 0N4
Canada

Your file Votre référence

Our file Notre référence

The author has granted a non-exclusive licence allowing the National Library of Canada to reproduce, loan, distribute or sell copies of this thesis in microform, paper or electronic formats.

L'auteur a accordé une licence non exclusive permettant à la Bibliothèque nationale du Canada de reproduire, prêter, distribuer ou vendre des copies de cette thèse sous la forme de microfiche/film, de reproduction sur papier ou sur format électronique.

The author retains ownership of the copyright in this thesis. Neither the thesis nor substantial extracts from it may be printed or otherwise reproduced without the author's permission.

L'auteur conserve la propriété du droit d'auteur qui protège cette thèse. Ni la thèse ni des extraits substantiels de celle-ci ne doivent être imprimés ou autrement reproduits sans son autorisation.

0-612-34385-5

Canada

UNIVERSITY OF ALBERTA

LIBRARY RELEASE FORM

Name of Author: Steven Alexander Kozak

Title of Thesis: Lightning strikes in Alberta thunderstorms: climatology and case studies

Degree: Master of Science

Year this Degree Granted: 1998

Permission is hereby granted to the University of Alberta Library to reproduce single copies of this thesis and to lend or sell such copies for private, scholarly, or scientific research purposes only.

The author reserves all other publication and other rights in association with the copyright in the thesis, and except as hereinbefore provided, neither the thesis nor any substantial portion thereof may be printed or otherwise reproduced in any material form whatever without the author's prior written permission.

Steven Kozak

21 Sept 1998

5420-110 St.
Edmonton, AB T6H 3E1

UNIVERSITY OF ALBERTA

FACULTY OF GRADUATE STUDIES AND RESEARCH

The undersigned certify that they have read, and recommend to the Faculty of Graduate Studies and Research for acceptance, a thesis entitled *Lightning strikes in Alberta thunderstorms: climatology and case studies* submitted by Steven Alexander Kozak in partial fulfillment of the requirements for the degree of Master of Science.

G.W. Reuter

D.P. Hube

E.P. Lozowski

J.D. Wilson

approved 17 September 1998

ABSTRACT

The spatial and temporal distributions of cloud-to-ground (CG) lightning strikes are investigated for Alberta. The first part of the thesis documents the summertime CG lightning climatology, using 12 years of data from 1984 to 1995. The second part analyzes four severe thunderstorms to relate the location and timing of lightning strikes to the intensity and depth of the precipitation pattern as observed by radar.

On average, July has the highest CG lightning strike frequency for Alberta, the average July total being 122 000. The diurnal cycle shows a peak of lightning frequency at 1900 MDT. Maps of average CG lightning strike density, high lightning strike positions, and average lightning day counts are shown for the entire summer, and every two weeks from 1 June to 31 August. Most lightning occurs in western Alberta, typically in the Edson-Rocky Mountain House corridor. The combined effects of topography, vegetation, elevation, and latitude impact the average spatial distribution of lightning. CG lightning activity intensifies during June and July, accompanied with a northward shift of the main lightning area. During August, the lightning frequency decreases and the main lightning area shifts (back) south.

The case studies show that the spatial distribution of CG lightning strikes in supercell thunderstorms is not uniform. About 60-85% of lightning strikes occur on the upshear side. The left side of the moving storm tends to have more lightning strikes compared to the right side. Most CG lightning strikes occur just outside the precipitation core, within 30 km from its center. The CG lightning frequency tends to lag peaks in the precipitation intensity by about 90 minutes for 19 August 1992, and by 10-30 minutes for 30 July 1993.

ACKNOWLEDGEMENTS

I would like to thank Dr. Reuter, my supervisor, for his guidance and advice throughout the project. Thanks are also due to Bruno Larochelle of Environment Canada and the Alberta Forest Service for collecting and providing the lightning data. Financial support for this research was provided by NSERC and the Atmospheric Environment Service.

TABLE OF CONTENTS

		Page
1.	INTRODUCTION	
	1.1 Overview	1
	1.2 Theory of lightning formation	2
	1.3 Review of lightning climatology studies	4
	1.4 Review of case studies focusing on lightning in thunderstorms	7
	1.5 Alberta thunderstorms	8
	1.6 Statement of research problems	11
2.	DATA SETS AND METHOD OF ANALYSIS	
	2.1 Lightning detection network for Alberta	14
	2.2 Methods of analyzing lightning climatology	15
	2.3 Radar data	16
	2.4 Methods used for analyzing case study storms	17
3.	SUMMER LIGHTNING CLIMATOLOGY	
	3.1 Introduction	19
	3.2 Temporal distribution of CG lightning strikes	19
	3.3 Spatial distribution of CG lightning strikes	21
	3.4 Effects of mountains on CG lightning strikes	25
	3.5 Intraseasonal variations in lightning strike distribution	27
	3.6 Discussion and conclusions	30
4.	LIGHTNING STRIKES AND PRECIPITATION IN ALBERTA THUNDERSTORMS	
	4.1 Introduction	35
	4.2 Significant weather and synoptic conditions	36
	4.3 Spatial organization of lightning strikes relative to the geometric storm center	38
	4.4 Spatial organization of lightning strikes relative to the center of the precipitation core	40
	4.5 Number of lightning strikes as a function of rainfall rate	42
	4.6 Temporal correlation of rainfall and lightning	44
	4.7 Displacement of lightning strikes from precipitation core center	45
	4.8 Conclusions	46

5. SUMMARY AND CONCLUSIONS 48

APPENDIX A 51

APPENDIX B 52

REFERENCES 53

FIGURES 57

TABLES 111

LIST OF TABLES

Table		Page
3.1	1984-95 average strike count over Alberta. Data are in units of thousands of strikes.	111
3.2	Two regions used to analyze the impact of vegetation coverage on CG lightning strike density [strikes $(10\ km)^{-2}$].	111
3.3	Average June, July, and August temperatures in °C and precipitation in mm, for Lethbridge, Edmonton Municipal Airport, and Fort Vermillion. The periods of observations are shown in brackets.	112
3.4	Average percentage of CG lightning strikes that occur in June, July, and August, with respect to the summer total, for Alberta, Manitoba, and southern Ontario. Percentage of strikes that occur in the morning (0-12 Local Time), and afternoon and evening (12-24), with respect to the daily total, are also shown.	112
4.1	Number of lightning strikes #STR within storm quadrants and number of lightning strikes #STR within storm as a function of time, for storm 1. Averages and totals are also included. Numbers in bold indicate the location of the precipitation core center.	113
4.2	Same as in Table 4.1 except for storm 2.	114
4.3	Same as in Table 4.1 except for storm 3.	115
4.4	Same as in Table 4.1 except for storm 4.	116
4.5	Percentages of CG lightning strikes that accumulate throughout the observing period of the four storms.	117
4.6	Number of lightning strikes #STR within core quadrants and number of lightning strikes #STR within storm as a function of time, for storm 1. Averages and totals are also included.	118
4.7	Same as in Table 4.6 except for storm 2.	119
4.8	Same as in Table 4.6 except for storm 3.	120
4.9	Same as in Table 4.6 except for storm 4.	121

4.10 Number of lightning strikes #STR within maximum rain rate intervals and number of lightning strikes #STR within storm as a function of time, for storm 1. Rain rate interval and storm areas (number of pixels) and lightning strike averages, totals, and weighted totals are also included. 122

4.11 Same as in Table 4.10 except for storm 2. 123

4.12 Same as in Table 4.10 except for storm 3. 124

4.13 Same as in Table 4.10 except for storm 4. 125

4.14 Evolution of Storm 1. STSIZE is the storm size [km^2], H is the maximum 40 dBz height [km], R is the rainfall rate maximum above 2 km [mm h^{-1}], #STR is the number of strikes in the previous 10 minutes, and DR is the average distance of lightning strikes [km] from the center of the rainfall rate maximum. 126

4.15 Same as in Table 4.14 except for storm 2. 127

4.16 Same as in Table 4.14 except for storm 3. 128

4.17 Same as in Table 4.14 except for storm 4. 129

LIST OF FIGURES

Figure		Page
1.1.	The top of the storm is positively charged with the exception of a thin layer of negative charge right at the cloud top. Centered near –15°C is a layer of negative charge. Positive charge is frequently found near cloud base in rain shafts (after Cotton, 1990).	57
1.2	Illustration of the convective charging theory. Positive ions are swept aloft, where they attract negative ions at the cloud boundaries. Downdrafts at the cloud edges sweep the negative ions downward where they induce point discharges at the Earth's surface supplying more positive ions (after Cotton, 1990).	57
1.3	Topographical map for Alberta contoured every 1000 feet (300 m) up to 4000 feet. Lakes and rivers are also indicated.	58
1.4	Map of vegetation types for Alberta.	59
2.1	The Alberta Forest Service's LLP lightning detection network consists of 16 direction finders.	60
2.2	Transforming x-y coordinate system to an x′ -y′ coordinate system by rotating around the z-axis (0,0) with an angle θ.	60
2.3	The supercell storm of elliptical form is divided into quadrants relative to the storm center (left) and relative to the precipitation core center (right). The storm motion is in the direction of the major axis of the ellipse. LB(C) is left back, LF(C) is left front, RB(C) is right back, and RF(C) is right front.	61
3.1	Summertime CG lightning strike totals over Alberta from 1984-95.	62
3.2	Average percentages of CG lightning strikes that occur in June, July, and August, with respect to the summer total.	62
3.3	Average CG lightning strikes per day.	63
3.4	Average diurnal cycle of CG lightning strikes.	63
3.5	Average summer CG lightning strike density [strikes per 10 km squared].	64
3.6	Average annual hours (× 100) of sunshine, from 1931-60..	65
3.7	Total 1984-95 summer high CG lightning strike positions [strikes per km squared].	66

3.8 Average summer lightning day count [lightning days per km squared]. 67

3.9 CG lightning strikes from 12-24 MDT, in three hour intervals, as a function of the distance from the Continental Divide in km. 68

3.10 Contour plot of CG lightning strikes as a function of time of day [MDT] and distance from the Continental Divide [km]. 69

3.11 Average June 1-15 lightning strike density. 70

3.12 Average June 16-30 lightning strike density. 71

3.13 Average July 1-15 lightning strike density. 72

3.14 Average July 16-31 lightning strike density. 73

3.15 Average August 1-15 lightning strike density. 74

3.16 Average August 16-31 lightning strike density. 75

3.17 June 1-15 high lightning strike positions. 76

3.18 June 16-30 high lightning strike positions. 77

3.19 July 1-15 high lightning strike positions. 78

3.20 July 16-31 high lightning strike positions. 79

3.21 August 1-15 high lightning strike positions. 80

3.22 August 16-31 high lightning strike positions. 81

3.23 Average June 1-15 lightning day count. 82

3.24 Average June 16-30 lightning day count. 83

3.25 Average July 1-15 lightning day count. 84

3.26 Average July 16-31 lightning day count. 85

3.27 Average August 1-15 lightning day count. 86

3.28 Average August 16-31 lightning day count. 87

3.29 Average annual hailstorm frequency, from 1943-57, shown with a grey-scale. Average annual thunderstorm hours depicted with labeled contours. 88

4.1 The 850 mb analysis at 0000 UTC on August 1992. Solid lines are geopotential height contours in decameters while dashed lines are isotherms in °C. Wind barbs are in knots. A short windbarb is 5 knots, and a long wind barb is 10 knots (analysis by Environment Canada). 89

4.2 Sounding recorded at Stony Plain at 0000 UTC on 19 August 1992. The solid line depicts temperature and the dashed line depicts the dewpoint. 90

4.3 Same as in Fig. 4.2 except for 30 July 1993. 90

4.4 Radar observations sampled by Carvel radar at 0350 UTC on 19 Aug 1992. The top map shows the maximum rainfall rate [mm h^{-1}] above 2 km. The Severe Storm Map (bottom) displays the maximum height [km] of the 40 dBz radar reflectivity factor. The location of CG lightning strikes are also shown. 91

4.5 Time history of number of lightning strikes per minute within each of the four quadrants (Right Front, Left Front, Right Back, and Left Back) for (a) storm 1 and (b) storm 2 on 19 August 1992. 92

4.6 Radar observations sampled by Carvel radar at 0120 UTC on 30 July 1993. The top map shows the maximum rainfall rate [mm h^{-1}] above 2 km. The Severe Storm Map (bottom) displays the maximum height [km] of the 40 dBz radar reflectivity factor. The location of the CG lightning strikes are also shown. 93

4.7 Time history of number of lightning strikes #STR per minute within each of the four quadrants (Right Front, Left Front, Right Back, and Left Back) for (a) storm 3 and (b) storm 4 on 30 July 1993. 94

4.8 Accumulated number of lightning strikes #STR in each quadrant for (a) storm 1 and (b) storm 2. 95

4.9 Accumulated number of lightning strikes #STR in each quadrant for (a) storm 3 and (b) storm 4. 96

4.10 Time history of number of lightning strikes #STR per minute within each of the four quadrants (Right Front Core, Left Front Core, Right Back Core, and Left Back Core) for (a) storm 1 and (b) storm 2 on 19 August 1992. 97

4.11 Accumulated number of lightning strikes #STR in each core quadrant for (a) storm 1 and (a) storm 2. 98

4.12 Time history of number of lightning strikes #STR per minute within each of the four quadrants (Right Front Core, Left Front Core, Right Back Core, and Left Back Core) for (a) storm 3 and (b) storm 4 on 30 July 1993. 99

4.13 Accumulated number of lightning strikes #STR in each core quadrant for (a) storm 3 and (b) storm 4. 100

4.14 Percentage values of CG lightning strikes for different rainfall rate intervals in mm h^{-1} for (a) storm 1 and (b) storm 2, and adjusted for area for (c) storm 1 and (d) storm 2. 101

4.15 Percentage values of CG lightning strikes for different rainfall rate intervals in mm h^{-1} for (a) storm 3 and (b) storm 4, and adjusted for area for (c) storm 3 and (d) storm 4. 102

4.16 Number of lightning strikes #STR (circles) compared with (a) maximum 40 dBz height H in km (crosses), and (b) maximum rainfall rate R in mm h^{-1} (squares) for storm 1. 103

4.17 Same as in Fig. 4.16 except for storm 2. 104

4.18 Correlation coefficient (CC) plotted versus time delay of lightning strikes with maximum 40 dBz height H in km (crosses) and maximum rainfall rate R in mm h^{-1} (squares) for (a) storm 1, and (b) storm 2 of 19 August 1992. 105

4.19 Number of lightning strikes #STR (circles) compared with (a) maximum 40 dBz height H km (crosses), and (b) maximum rainfall rate R in mm h^{-1} (squares) for storm 3. 106

4.20 Same as in Fig. 4.19 except for storm 4. 107

4.21 Correlation coefficient (CC) plotted versus time delay of lightning strikes with maximum 40 dBz height H in km (crosses) and maximum rainfall rate R in mm h^{-1} (squares) for (a) storm 3, and (b) storm 4 of 30 July 1993. 108

4.22 Time histories of distance of lightning from rainfall maximum in km (DR in circles) and rainfall rate in mm h^{-1} (R in crosses) for (a) storm 1 and (b) storm 2. 109

4.23 Time histories of distance of lightning from rainfall maximum in km (DR in circles) and rainfall rate in mm h^{-1} (R in crosses) for (a) storm 3 and (b) storm 4. 110

1. INTRODUCTION

1.1 Overview

When a significant amount of latent energy stored in the unstable stratification of moist air is released, cumulonimbus clouds develop. They are often accompanied by lightning strikes and thunder. Strikes of lightning travel from cloud to ground or within clouds. Lightning heats the air along its path to about 50 000 K, causing the air to expand explosively to produce thunder. Up to four million joules of energy are delivered to the ground by a single lightning strike (Uman, 1971). Lightning kills about 60 people annually in Canada on average. The annual expense of property damage due to lightning is in the billions of dollars for Canada. These losses include damage to structures, damage to aircraft, disruption of power lines, livestock deaths and injuries, and building fires. Lightning is also a direct cause of forest fires when dry conditions are present. While lightning annually starts one-third of all forest fires in Canada, it is responsible for about 90% of the total forested area burned because it is difficult for fire-fighting crews to reach many of the remote fires (Anderson, 1991).

How are lightning strikes in thunderstorms related to geographical properties of the surface and meteorological conditions? Specifically, how are the locations of cloud-to-ground lightning strikes related to the surface topography, vegetation coverage, and distance from the mountains? How are lightning strikes distributed within individual storms? How is the timing of the lightning related to the evolution of storm dynamics? These questions are investigated in this thesis for the province of Alberta. The analysis is based on twelve years (1984-95) of lightning data from the lightning detection network operated by the Alberta Forest Service (AFS). The radar reflectivity data measured by the Carvel radar are also used in the cases studies.

The focus of this thesis is on documenting the spatial and temporal distributions of lightning strikes in Alberta. How the spatial and temporal distributions of lightning strikes are affected by geographical features and meteorological conditions is also

studied. Before the specific objectives of this thesis are given, it is necessary to provide sufficient background by reviewing the major theories of charge separation and lightning formation. The major findings from lightning research conducted over the last century also need reviewing. And finally, the essential background on Alberta thunderstorm research is presented.

1.2. Theory of lightning formation

In effect, prior to discharge by lightning, the storm system could be considered as an enormous capacitor, or battery. Many theories have been suggested in an attempt to explain how this separation of electrical charge occurs. Yet, despite the many attempts, there is still no consensus on the mechanisms that produce lightning in thunderclouds.

Any good theory for lightning formation must be consistent with typical thunderstorm conditions, summarized as follows (Cotton and Anthes, 1989):

a. average duration of precipitation and electrical activity from a single thunderstorm cell is about 30 minutes,
b. regions of separated charge are bounded by the –5°C and –40°C levels and have a typical radius of 2km,
c. charge structure in mature cumulonimbus clouds as shown in Fig. 1.1,
d. charge generation and separation processes are closely associated with the development of precipitation,
e. the charge center appears to be displaced both vertically and horizontally from the main precipitation core,
f. sufficient charge must be separated to supply the first lightning flash within about 20 minutes of the appearance of precipitation particles of radar-detectable size.

There are two major theories for lightning formation that satisfy the above thunderstorm conditions: the so-called "convection theory" and the so-called "precipitation-related theory". The relative merits and shortcomings of the two were

debated by Mason (1976) and Moore (1976). Other scientists (e.g. Schonland, 1953) suggested that no single explanation can satisfy all the thunderstorm characteristics and thus a combination of convection and precipitation-related theories would best explain charge generation and separation in clouds.

The convection theory postulates that differential convective motions of cloudy air transport and accumulate externally derived charges in opposition to forces imposed by the electric field (Moore and Vonnegut, 1977). To begin the process, the existence of a electric field or space charge beneath the cloud layer is required during the initial phase of the cloud's development. The electric field is available from several combinations of sources: point discharges from a net positively charged earth under fair-weather conditions, electrified ocean spray, blowing dust, charged precipitation, and nearby clouds that have already become electrified (Vonnegut, 1963). Convective updrafts raise the positive ions into a newly formed cumulus cloud. The rising positively charged cumulus cloud preferentially attracts negative ions produced in the ionosphere, or produced above 6 km by cosmic radiation, resulting in a negatively charged cloud top. Instead of neutralizing the positive charges in the cloud, the negative charges are transported to the lower part of the cloud by convective downdrafts at the cloud edges (Fig. 1.2). The downward-transported, negative charges induce further point discharges at the Earth's surface, which supply more positive ions to the lower troposphere. The process begins all over again, leading to an exponentially increasing cloud polarity (Cotton and Anthes, 1989).

Precipitation-charging theories do not depend solely on convective motions of clouds for charge separation. According to Mason (1976), the principal mechanism for the separation of electric charge is the vertical separation of larger hydrometers from smaller ones, as a result of their differing terminal velocities. Precipitation charging by induction is the most popular theory. The basic concept is that in the presence of a fair-weather field, cloud and precipitation particles become polarized, as shown in Fig. 3.23 of Cotton (1990). The lower parts of the particles become positively charged and the upper parts become negatively charged. The large falling particles collide with the slower-moving small particles. After colliding, the smaller particles become positively charged, and are swept into the upper portions

of the cloud, while the larger particles become negatively charged, and settle in the lower portions. This results in a polarized cloud with positive space charge in the upper part of the cloud, and negative space charge in the lower part of the cloud.

Once the charge separation is sufficiently large, a lightning flash is initiated (Cotton, 1990). Lightning discharges can be initiated between the ground and a cloud (cloud-to-ground or CG lightning), or confined to the cloud itself (intra-cloud lightning). This thesis focuses on CG lightning strikes. For intra-cloud lightning the reader is referred to Brook and Ogawa (1977).

The middle-to-lower part of a thundercloud is usually negatively charged, while its upper part has a positive charge. The polarity of the prevailing cloud charge defines the polarity of the lightning current (Berger, 1977). The discharge of positive cloud charge to ground is called a positive CG strike, while the discharge of negative cloud charge to ground is called a negative CG strike. Approximately one in ten lightning strikes are positive. No distinction is made between positive and negative CG lightning in this thesis.

Thunder arises from the expansion of air in a lightning channel caused by intense localized heating (Uman, 1971). The heated air in a lightning channel, usually only a few centimetres in diameter, can reach temperatures of 50 000 K before it has time to expand. After each lightning strike, the high-pressure channel expands explosively into the surrounding air and compresses it, creating shock waves that are later heard as thunder by an observer.

1.3 Review of lightning climatology studies

This section is organized by starting off with lightning climatologies on the global scale. Thereafter the focus shifts to regional lightning climatologies. In the first global study of thunderstorms, Brooks estimated that 100 lightning flashes occur on the Earth every second (Orville and Spencer, 1979). This 1925 estimate was based on the results of Brooks' climatological survey of thunderstorm frequencies from meteorological station records and ocean ship logs. Brooks' data coverage was

heavily weighted to central Europe and eastern North America with sparse coverage elsewhere.

The advent of satellites improved estimations of spatial and temporal lightning distributions on a global scale. In particular, the satellites from the Defense Meteorological Satellite Program (DMSP) improved the recording of lightning data. Using DMSP satellite data, Orville and Spencer (1979) found that the annual average global (between 60°S and 60°N) intra-cloud and CG lightning flash frequency was 123 s^{-1}. Lightning frequency was found to be 25% greater in summer over the northern hemisphere than during summer in the southern hemisphere. In localized regions, the frequency of lightning that occurred within a few minutes of local midnight was found to be up to 20 times greater over land than over water. The locations of 32 000 lightning strikes, recorded from September 1977 to August 1978, were found to be in good agreement with general global circulation patterns (Orville and Henderson, 1986). For example, more lightning flashes occur over the Southern Hemisphere compared with the Northern Hemisphere in January, over the Northern Hemisphere compared with the Southern Hemisphere in July, and over moist compared with arid regions throughout the year. This indicates that the distribution of lightning is not only strongly influenced by the presence of land, but also by seasonal and regional variations in climate.

Satellite data have limitations for global lightning studies. Most importantly, DMSP satellites cannot detect lightning strikes during the day. In addition, DMSP satellites cannot differentiate between positive and negative lightning polarity, nor between intra-cloud and CG lightning strikes.

Regional networks of magnetic direction finders (DFs) can sample lightning data with a better spatial resolution of a few km and they are operational 24 hours a day. These regional networks differentiate between positive and negative CG lightning strikes, and can determine the number of return strokes. However, it is difficult for the networks to record intra-cloud lightning.

The first regional networks to measure the CG lightning strike locations began in the United States in 1976 (Krider et al., 1980), with the establishment of the western

lightning detection network. This was followed by research networks in Oklahoma and New York (Orville, 1990). All three regional networks grew until complete coverage of the contiguous United States was obtained in 1989.

Regional lightning climatologies have been compiled from these regional detection networks. The results indicate that the spatial distribution of CG lightning is affected by geographical properties such as topography, vegetation cover, and water cover. From January to March 1986, CG lightning frequency over the warm Gulf Stream was up to 4 times greater than that over the adjacent land (Biswas and Hobbs, 1990). Orville (1990) found that most of the lightning along the East Coast of the United States occurred over the Atlantic Ocean in the vicinity of the Gulf Stream. In both cases maximum lightning strike density was closely correlated with the maximum sea surface temperature. Orville (1991) summarized annual CG lightning strike densities [km^{-2}] in the contiguous United States for 1989. A peak in lightning strike density (per 10 km^2 per year) was found in central Florida. Local strike maxima were observed in eastern Texas, Kansas, on the Illinois-Indiana border, and along the Carolina Coast. Orville (1994) published CG lightning strike density charts for the three years 1989-91 for almost the entire mainland United States. Lightning strike density was found to increase from north to south in North America. Mackerras and Darveniza (1994) found there is more convection and more lightning at lower latitudes, coinciding with more heat and moisture. The lightning strike rate increased by about 7% every 100 km displacement toward the equator.

An extensive regional CG lightning climatology was compiled for the southern Great Lakes region of Ontario (Clodman and Chisholm, 1996). For the period of 2 May to 7 September 1989, 23 April to 26 September 1990, and 25 April to 23 October 1991, the major findings are summarized as follows:

- high surface temperature and moisture lead to an increase in lightning generation, thus, lake areas usually had fewer lightning strikes than nearby land areas, and warm water usually had more lightning strikes than cold water,
- convergence lines of lake breezes and other mesoscale lake circulations were possible sites for storms with intense lightning,

- upslope flow increased the frequency of lightning-producing storms.

Regional lightning studies have focused on the impact of geography and atmospheric circulation patterns on the diurnal variations of CG lightning strike frequency. Maier et al. (1984) showed that the average diurnal patterns of CG lightning in southern Florida, during the summers of 1976-78, were consistent with previous determinations of the times of maximum rainfall and maximum rainfall rate. They also determined that South Florida lightning data showed substantially less diurnal variation over the Atlantic Ocean and Gulf of Mexico than over land. Lopez and Holle (1986) confirmed these findings using summertime CG lightning data in Colorado and Florida for the summer months of 1983. They also found that lightning centers in Florida were found to be the most intense in the mid-afternoon along the coastline, due to ocean breezes, and did not move in any particular direction. In Colorado, lightning strikes were concentrated just east of the Continental Divide in the morning due to low-level upslope flow caused by heating of the foothills; the lightning centers moved eastward later in the day. The progression of thunderstorm activity eastward from the late afternoon to the early part of the morning was also seen east of the Rockies in Alberta (Summers and Paul, 1970). Hanuta and LaDochy (1989) documented eastward movements of lightning strike frequency peaks in Manitoba. Near midnight, the western sector decreased, but the central plains region continued to have relatively high activity, which shifted farther east by mid-morning.

1.4 Review of case studies focusing on lightning in thunderstorms

Research has been conducted to investigate the occurrence of lightning within a particular convective storm. Rust et al. (1981) found that source-locations for CG lightning strikes occurred in regions of weaker updrafts (<10 ms^{-1}) adjacent to downdrafts. Few lightning strikes occurred in the major precipitation shaft as indicated by a high radar reflectivity core. Contrary to that, Krehbiel et al. (1983) observed that CG lightning discharges formed throughout the precipitating region of New Mexico storms, and appeared to be bounded by the precipitation region. Williams (1985) determined that, in many cases, the regions of intense precipitation

are not regions of maximum space charge density. Ray et al. (1987) found that CG lightning tended to be located downshear (in front) of the main storm updraft and radar reflectivity core in supercell storms, and concentrated in the updraft and core of multicell storms. Keighton et al. (1991) studied the evolution of a severe Mesoscale Convective System (MCS) in Oklahoma on 23 May 1981 (see Hane (1986) for description of MCSs). They found that before the storm became a supercell, the majority of CG lightning strikes emanated from the anvil to the left of the precipitation core, with respect to storm motion. After the storm became a supercell, CG lightning strikes clustered closer to, but still to the left of, the core. For two MCSs studied in Oklahoma (MacGorman and Nielsen, 1991), most CG lightning strikes were found to occur near (~10 km from center) or in radar reflectivity cores. Holle et al. (1994) found that lightning strike density in the precipitation core of a MCS exceeded the lightning strike density in the remainder of the storm. The precipitation core was the region of the storm with the greatest reflectivity, and had the strongest reflectivity gradients.

Case studies of thunderstorms have also dealt with the temporal patterns of CG lightning strikes with respect to the precipitation field. Rust et al. (1981) found that increases in radar reflectivity magnitudes were correlated with increases in CG lightning strikes. Goodman and MacGorman (1986) support these findings for Mesoscale Convective Systems: lightning discharge rates were positively correlated with the intensification and decay of MCSs. Their study also suggested that storm organization has an important control on the rate of thunderstorm discharge; the frequency of CG lightning discharges is primarily a function of precipitation core depth, and the number of multicellular convective elements in MCSs. In a study of a MCS, Rutledge and MacGorman (1988) observed that maximum CG activity is approximately coincident with the period of most intense rainfall, on the time scale of hours.

1.5 Alberta thunderstorms

In mid-latitudes, the prevailing upper level wind is westerly. Thus Alberta is located on the lee side of the Continental Divide. Fig. 1.3 shows the topography of

Alberta. The airmass subsides when passing over the Rocky Mountains, and produces a stable inversion layer often referred to as the capping lid. The capping lid allows for the build-up of latent energy during summer days. Warm moist boundary-layer air is trapped by the capping lid. Above the cap, the environmental temperature lapse rate can become very steep. Under these conditions, parcels of air lifted from the surface become highly buoyant with respect to the environmental air, setting the stage for strong convective overturning and severe storm formation. Storms occur almost every day during the three summer months in Alberta (Reuter and Aktary, 1995).

Convective overturning in Alberta can be weak or strong, depending on the temperature stratification and moisture contents. Strong convection requires a large amount of Convective Available Potential Energy (CAPE), wind shear and mechanisms capable of releasing the latent energy (Smith and Yau 1993). Severe convection tends to begin in the foothills where convergence zones are formed with upslope flow (Wojtiw, 1977). Severe convective storms frequently drop hail and almost always have lightning activity. Severe hailstorms can maintain their structure for several hours as they develop and move over the plains of Alberta. Hail swaths are often up to 100 km long, and occasionally contain golfball-sized hail (Deibert, 1977). Severe convective hail storms have been investigated extensively in the Alberta Hail Project. Wojtiw (1986) lists hundreds of conference papers and journal articles, dealing with various aspects of Alberta hailstorms.

Smith and Yau (1993) found that a favorable phasing of mesoscale and synoptical scale circulations is required to obtain sufficient lifting of the surface air to break through the capping lid and trigger the release of the vast amount of latent energy stored in the atmosphere. At dawn, the foothills facing directly into the rays of the sun are warmed before the eastern plains. The warm air rises, and an upslope surface flow develops as air from the plains rushes in. This is called a mountain-plain mesoscale circulation. A morning surface inversion layer prevents significant turbulent mixing, therefore surface heat and moisture slowly accumulate in the lower 1 to 2 km of the atmosphere. In the afternoon, a coinciding surface synoptic pressure gradient produces a northeasterly wind that advects a tongue of warm moist air into the lower branch of the mountain-plain circulation. At the same

time, there is increased convective instability as cold air at the upper levels enters Alberta, associated with a synoptic-scale short-wave trough. By this time, the inversion layer has eroded, particularly over the foothills, and explosive development of deep convective clouds ensues.

The mesoscale mountain-plain circulation depends largely on properties of the surface. Specifically, surface fluxes of sensible and latent heat depend on latitude, local cloud cover, surface albedo, surface moisture content, and heat capacity of the surface. Dark surfaces with a low albedo absorb more shortwave radiation than light surfaces with a high albedo. Therefore, the surface energy balance is affected by the type of vegetation. Transpiration from plants, and evaporation of water surfaces tend to decrease the surface sensible heat flux, but increase the surface moisture flux. Fig. 1.4 shows the vegetation cover for Alberta. Significant spatial variations occur in the type of vegetation. The northern region is mostly covered by coniferous and deciduous forests. It also contains many lakes and swaths of muskeg. There is a stretch of farmland southwest of the town of Peace River towards the foothills. In the south, Alberta contains mostly farming regions, irrigated cropland (near Lethbridge), and dry rangeland (from Medicine Hat toward the Neutral Hills). The Rocky Mountains and Foothills are covered by thick groves of coniferous and deciduous trees.

Despite the many studies of Alberta summer hailstorms, little research has been conducted on lightning strikes. Pakiam and Maybank (1975) estimated the number of lightning strikes from satellite imagery and motion picture cameras in multicell and supercell hailstorms. The frequency of lightning discharges tended to depend on the depth and size of the storms. In 1984, the Alberta Forest Service (AFS) started to operate a network of lightning detectors to record the locations of cloud to ground lightning strikes. Anderson (1991) used these lightning data to find statistical relationships between lightning occurrence and meteorological variables. The frequency of lightning was mostly affected by the amount of the CAPE as sampled with the Stony Plain sounding. Higher CAPE values were correlated with more lightning strikes.

With the exception of Anderson's (1991) thesis research, no other research has made use of the lightning data collected. This is found to be surprising because of the major damage by forest fires started by lightning. This thesis is the first to compile and analyze summertime lightning climatology and case studies in Alberta.

1.6 Statement of the research problems

This thesis consists of two major parts. The first will document the summertime lightning climatology for Alberta and analyze the geographical and meteorological properties that determine spatial and temporal distributions of summer CG lightning strikes. The second part contains detailed case studies of four severe thunderstorms. Here the focus will be on relating the location and timing of lightning strikes relative to the precipitation structure. For the first part (containing the lightning climatology) this thesis will focus mainly on the following issues:

- Is there significant variation of summer CG lightning strike frequency on a yearly, monthly, and daily basis? How does summer CG lightning strike frequency vary diurnally?
- Is the spatial distribution of summer CG lightning strikes influenced by topography and surface properties such as vegetation cover, water cover, and urban areas? Does the frequency of CG lightning strikes vary with distance from the mountains?
- How does the spatial distribution of summer CG lightning strikes vary on an intra-seasonal basis? Is there spatial movement of CG lightning strikes?

To determine if there are significant yearly and monthly variations of summer CG lightning strikes over Alberta, CG lightning strike frequency will be calculated for each year between 1984-95. An average strike frequency will be calculated for the summer season and each day within it. An investigation of the diurnal variation of summer CG lightning strikes, will be achieved by calculating the frequency for each hour of the day, averaged over 12 years.

To determine how CG lightning strikes are related to the geographical features, there will be a comparison of maps of CG lightning strike density, high strike density positions, and lightning-day count, against elevation and vegetation cover maps. The lightning data will be averaged over 12 years from 1984-95 to "filter" out individual storm events. Also, the frequency of CG lightning strikes will be calculated as a function of the distance from the mountains for each hour of the day. For the intra-seasonal analysis, the three month summer time period will be divided into six half-month periods. Maps of CG lightning strike density, high strike density positions, and lightning-day count will be obtained for each of the half-month periods (averaged over 12 years).

The second component of this thesis deals with four individual thunderstorms. Here the focus will be on the relationship between CG lightning and precipitation (as observed by weather radar). Two days, 18 August 1992 and 29 July 1993, will be analyzed in detail. For both of these days, the focus will be on two long-lived supercell storms. The following issues will be investigated:

- Where are the majority of CG lightning strikes located relative to the geometric center of the storm?
- Where are the majority of CG lightning strikes located relative to the center of the precipitation core?
- Does the frequency of CG lightning strikes depend on precipitation intensity?
- Deep and intense radar echoes are followed by a large number, and high spatial density, of lightning strikes (e.g. Rutledge and MacGorman, 1988). What is the time lag that maximizes the positive correlation of echo height and intensity with CG lightning occurrence?

- Does the displacement of CG lightning strikes from the center of the precipitation core temporally depend on the core's intensity?

This thesis consists of 5 chapters. After introducing the problem in Chapter 1, a detailed description of the lightning detection network and the Carvel radar will be given in Chapter 2. The methodology used for the lightning climatology will also be described. Chapter 3 contains the lightning climatology for Alberta. The temporal

climatology of CG lightning strikes on an interannual, intraseasonal, and daily basis will first be discussed. This will be followed by a presentation of the spatial climatology of summertime CG lightning strikes. The intraseasonal variability of CG lightning strike distributions will finally be analyzed in a combined temporal and spatial approach. The four case studies will be described in Chapter 4. The spatial organizations of CG lightning strikes will be determined relative to the storm center, relative to the center of the precipitation core, and as a function of precipitation intensity. The temporal correlation between precipitation core height and intensity and lightning strike occurrence will also be determined. The last chapter (Chapter 5) will summarize the major results.

2. DATA SETS AND METHOD OF ANALYSIS

2.1 Lightning detection network for Alberta

In 1984, the Alberta Forest Service (AFS) started to operate a dense network of lightning detection sensors. The detectors use a wide-band, magnetic gate design, and are manufactured by Lightning Location and Protection Inc. of Tucson, Arizona. Hermann et al. (1976) and Krider et al. (1980) give detailed descriptions of these detectors. A network consists of roughly equally spaced sensors that can be combined to estimate the time and location of CG lightning strikes.

The lightning detection network consists of three components: the direction finder, the position analyzer, and the remote display processor. The direction finder (DF) senses the electromagnetic field radiated by a CG lightning strike using two erect, orthogonal wire loop antennas and a horizontal flat plate antenna. The antenna's bandwidth is 1 kHz to 1 MHz. The radiated field of a lightning flash induces a current in the loops. The voltage signal measured in the loops is related to the strike's generated magnetic field strength by the cosine of the angle between the loop antenna and the direction to the strike. By comparing the voltage signals from the two loops, a direction to the strike can be determined.

The direction finder can discriminate a CG strike from other forms of lightning by its characteristic electromagnetic "signature". When the leader reaches the ground, the return stroke is triggered producing a sharp voltage rise. This rise is used to distinguish a CG strike from other electromagnetic noise.

The direction finder sends the data of each registered CG lightning strike to a centralized position analyzer (PA). The PA triangulates data from direction finders to locate the position of a CG lightning strike. If the strike is in line with, or directly between, two direction finders (called the baseline), the PA considers the ratio of the signal strengths as well. From the PA, users can view a map of the lightning data on a remote display processor (RDP). The RDP can focus on desired time and location

windows covered by the detection network and can show up to 30 000 strikes at a time.

When using remotely sensed data, the quality of the measurements is an important issue. The manufacturers of the lightning detectors claim a detection rate of 80% within a 400 km radius of the detector. They also claim that the direction of a strike is recorded accurately within 2°.

Fig. 2.1 shows the location of the detectors in the Alberta network; it consists of 16 direction finders. The coverage over the forested areas in the west is better than over the farming areas in the east. The AFS lightning detection network position analyzer is located at the AFS headquarters in Edmonton. The lightning database consists of information collected year-round, from 1984 to the present.

2.2 Methods for analyzing lightning climatology

The lightning observations are analyzed by using a "book keeping" method in which the numbers of CG lightning strikes are added for different windows in time and space. For analyzing the diurnal cycle of lightning frequency, a time step of one hour is chosen; i.e. the number of lightning strikes is counted for each hourly interval starting at 0000 MDT (Mountain Daylight Time). The average hourly number of lighting strikes is computed by averaging 3 months of summer data for the 12 years (1984-1995). Similarly, daily lightning frequency values are found by counting CG lightning strikes for each of the 91 days of the 12 year period and then averaging.

For analyzing the spatial variability of lightning activity, the following procedures are used. Average CG lightning strike densities are determined by using grid elements with spatial dimensions of 1/3° latitude by 2/3° longitude. Lightning strikes are added up in each grid element, over the time period of interest. Areas are calculated as a function of latitude, and are used to determine average CG lightning strike densities. The densities are computed by dividing the number of strikes by surface area. The high CG lightning strike positions are determined by using Clodman and Chisholm's (1996) method. Here the grid elements are chosen to be

1/10° latitude by 1/6° longitude. A grid element is marked if it's lightning strike density exceeds 0.5 strikes km^{-2} for at least one day.

Lightning day counts are calculated by a method that is used by Clodman and Chisholm (1996). A day is counted as a lightning day if multiple CG lightning strikes are recorded in a given grid element of size 1/3° latitude by 2/3° longitude. The size of the grid element is chosen such that a human observer located at the center of a grid element would see all the CG lightning strikes.

One section of our analysis requires the distance of CG lightning strikes from the Continental Divide. Fig. 2.2 shows the transformation of coordinates used. First, the latitude-longitude grid is transformed into a Cartesian x-y coordinate system with its origin located at 49°N and 120°W. The y-axis points north. The x-y system is then transformed to an x′-y′ coordinate system, by rotating by an angle θ, such that the x′-axis is perpendicular to the Continental Divide.

2.3 Radar Data

In Chapter 4, two case days (18 August 1992 and 29 July 1993) are analyzed to determine the spatial and temporal distribution of CG lightning strikes relative to the precipitation field. The precipitation fields within these storms were monitored by weather radar; the C-band radar, located at Carvel (53.34°N, 114.09°W) recorded the radar reflectivity factor and Doppler estimates of the radial wind components. Since the analysis focuses on reflectivity data, Doppler measurements are not dealt with.

The Carvel radar operates at a wavelength of 5.34 cm. The transmitted pulses have a peak power of 260 kW, a repetition frequency of 250 Hz, and a duration of 2 μs. The antenna diameter is 3 m and rotates at a rate of 6 rpm. The beamwidth of the emitted power cone is 1.1°. The range resolution is 300 m with a bin length of 1000 m. The radar scans at 24 different elevation angles ranging from 0.4° to 24.6°, every 10 minutes (Reuter and Beaubien, 1996).

The radar reflectivity Z is converted to rain rate R using the Marshall-Palmer Z-R relationship $Z=200R^{1.6}$. Here Z is in mm^6m^{-3} and R is in mm h^{-1}. In the presence of hail, the rainfall tends to be less than the value obtained from the Z-R relationship. Also for heavy convective rainfall the Marshall-Palmer estimate tends to overestimate the rainfall (Xin and Larochelle, 1997).

2.4 Methods used for analyzing case study storms

The synoptic analyses of the two case study days use standard data. The synoptic maps at standard pressure levels are examined for the synoptic flow pattern. The upper air sounding data sampled at Stony Plain at 1200 UTC is used for the sounding analysis of convective instability.

Lightning observations from the AFS network are examined in conjunction with the 2 km Constant Altitude Planar Position Indicator (CAPPI) depicting rainfall rate obtained from the Carvel radar. The Severe Storm map that shows the maximum height of the 40 dBz radar reflectivity is also analyzed.

The storm precipitation areas are determined on the CAPPI maps (obtained at time steps of 10 minutes), and approximated by ellipses. The major axes of the ellipses usually point in the direction of storm motion (approximately the wind direction at 500 mb). The storm ellipse is divided into four equally sized quadrants, as shown on the left side of Fig. 2.3. The four quadrants are labeled as Left Front (LF), Right Front (RF), Left Back (LB) and Right Back (RB), respectively. "Left" means left of the major axis, and back means behind the minor axis.

On the CAPPI maps, identification of the location of the precipitation core, as defined by the largest rainfall rate, is done. The storm ellipse area is also divided into four core quadrants, which are labeled Left Front Core (LFC), Right Front Core (RFC), Left Back Core (LBC) and Right Back Core (RBC), respectively; the right side of Fig. 2.3 shows the geometry. "Left" means left of the line passing through the precipitation core, in the direction of storm motion. "Back" means behind the precipitation core.

The time evolution of the lightning data and the radar-derived rainfall parameters is analyzed by computing correlation coefficients. The method used pairs present values of lightning data with past values of rainfall. A complete description of regression and correlation is given in Devore and Peck (1990).

3. SUMMERTIME LIGHTNING CLIMATOLOGY

3.1 Introduction

This chapter presents the climatology of cloud-to-ground (CG) lightning strikes for Alberta. The analysis is based on 12 years of observations from 1984 to 1995. As discussed in Chapter 1, CG lightning occurs only in deep cumulonimbus clouds developing in convectively unstable conditions. Reuter and Aktary (1995) found that convective instability in Alberta is frequent for the three summer months, yet rare for the period 1 September to 30 May. Analysis of Alberta lightning has thus been confined to the period from 1 June to 31 August.

The organization of this chapter is as follows: first the temporal variation of CG lightning strikes is presented. The inter-annual variability, the month-to-month variability, and the diurnal cycle is investigated in turn. Next, an analysis of the spatial variability of CG lightning strikes, and the relationship of CG lightning with topographic features, distance from the Rocky Mountains, and surface coverage is done. Thereafter, an examination of the combined effect of spatial and temporal variability is done to investigate systematic intraseasonal effects for different locations.

3.2 Temporal distribution of CG lightning strikes

The CG lightning strikes for the entire province of Alberta are counted for each of the 92 summer days (1 June-31 August) for each of 12 years (1984-1995). By adding the number of recorded lightning strikes for the 92 summer days, the total annual number of lightning strikes is estimated. These annual values are listed in Table 3.1 and plotted in Fig 3.1. By averaging over the 12 years of data, the mean value of CG lightning strikes recorded for Alberta was 268 800 CG lightning strikes per summer (1 June to 31 August). However, the variability from year to year is significant: the 12-year low of 102 700 strikes occurred in 1984, while the 12-year high of 561 300 strikes was recorded in 1994. There seems to have been a

systematic increase of about 30 000 CG lightning strikes per summer from the mid-1980's to mid-1990's. However, 1995 was an exception in having less than average lightning activity.

Fig. 3.2 shows the monthly variation of CG lightning strikes for the 12 year period. Of the 268 800 CG lightning strikes that occur on average every summer, 61 700 strikes occur in June (23% of the total), 122 000 occur in July (45%), and 85 100 occur in August (32%). July, the warmest month for Alberta, has almost twice as many lightning strikes as June.

Fig. 3.3 shows the average number of CG lightning strikes that occur on each day during the period from 1 June to 31 August. 12 years of data are insufficient to mask the significant variability in the day-to-day CG lightning strike frequency. Still, a systematic increase is apparent from the beginning of June towards a peak near the end of July, followed by a gradual decline towards the end of the summer. CG lightning strike frequencies of less than 1 000 are common during the first half of June and the second half of August. CG lightning strike frequencies larger than >5 000 occur mostly during the latter half of July and the beginning of August. Overall, CG lightning strike frequency gradually increases during June and most of July (peaking in the last week of July), and decreases during August.

The focus of this chapter now turns to the diurnal cycle in observed lightning frequency for Alberta. Fig. 3.4 displays the number of CG lightning strikes, as a function of MDT time, averaged over all the summer days of the 12-year analysis period. From 5-12 MDT, few CG lightning strikes per hour are recorded. The first significant CG lightning strike frequencies begin at about 12 MDT, which is consistent with a strengthening mountain-plain mesoscale circulation (Smith and Yau, 1993). During the period 13-18 MDT, there is an increase in the lightning strike frequency. About 20% of CG lightning strikes are recorded in the night and morning, while about 80% of CG lightning strikes occur in the afternoon and evening; the number of CG lightning strikes peak at 19 MDT at approximately 286. In later sections the diurnal cycle in lightning activity will be further interpreted in terms of the triggering, development, and movement of typical summertime convection over central Alberta.

3.3 Spatial distribution of CG lightning strikes

Fig. 3.5 displays the CG lightning strike density for Alberta when averaging the observations for 12 years of summer days. The data are plotted in units of number of strikes per summer per surface area of 10 km x 10 km. As the lightning strike density spans a wide range of values, the data are displayed with non-uniform contour intervals. Consecutive contour threshold values are doubled: 1, 2, 4, 8, 16, 32, 64, and 128. The contour plot reveals that the lightning strike density is not uniform throughout Alberta. Instead there are regions with pronounced lightning activity. The greatest CG lightning strike densities occur in two areas: one approximately 20 km north of Edson, and the other 50 km southeast of Edson. These two regions are only on the order of 10-15 km wide, but represent CG lightning strike densities greater than 128 strikes $(10\ km)^{-2}$. The region with between 64-128 strikes $(10\ km)^{-2}$ covers a significantly large area of Alberta; it stretches from the Edmonton region to the east, the Hinton region to the west, the Slave Lake region to the north, and the northwestern Calgary region to the south. The alignment of the 64 strikes $(10\ km)^{-2}$ contour resembles the 1 km (3 kft) contour elevation shown in Fig. 1.3.

Smith and Yau (1993) identified the frequent occurrence of convergence zones in western Alberta formed by upslope flow. Usually the upslope flow arises from mountain plain circulation due to differential heating. The two areas of maximum lightning strike densities correspond well with the most prevalent convergence localities.

The northeastern corner of the province, north of Lake Athabasca, has the lowest lightning strike density at 4-8 strikes $(10\ km^{-2})$ per summer. This region is flat, and furthest from the Rocky Mountain range. Other regions with low CG lightning densities are found in the northwestern part of Alberta, over the mountains near the continental divide southeast of Jasper town site, and in the southern part of Alberta; these regions have generally between 8-32 strikes $(10\ km)^{-2}$ per summer and are characterized by elevations significantly higher and not as flat as the northeastern corner of Alberta. The mountains, northwest, and south, would have higher CG lightning strike densities if topography were the only factor.

As the surface radiation budget depends on surface albedo, heat capacity and smoothness properties, the lightning strike density should be related to surface vegetation coverage. Fig. 1.4 displays vegetation types in Alberta. To determine the possible impact of the vegetation coverage on CG lightning strike density, we compare the two regions in Table 3.2. The comparison suggests that a forested surface yields a higher lightning strike density than a surface covered by grassland or cultivated cropland. It is speculated that forests can increase the atmospheric moisture by evapotranspiration. This increase in vapor would likely stimulate cumulus convection and thus enhance lightning activity.

Northern Alberta contains many muskeg areas, rivers, and lakes (see Fig. 1.4) which provide ample moisture to the boundary layer air. Nevertheless, northern Alberta has relatively low CG lightning strike densities. The observations in Fig. 3.5 do not support the notion of a lake breeze-induced enhancement of CG lightning strike densities over land adjacent to the lakes. For example, the regions surrounding Lake Athabasca and Lake Claire do not have any enhancement of lightning strike density. CG lightning strike densities increase slowly towards the south; a possible explanation for this is that hours of sunshine increase with decreasing latitude (see Fig. 3.6). The lack of atmospheric moisture, however, can diminish the frequency of convection and lightning strike density. For example, the Medicine Hat to Lethbridge corridor receives the greatest amount of sunlight in a year, but is the driest region of Alberta. The lightning strike density is relatively small in this particular region. The southern half of the province contains several small lakes (Gull Lake for example). The lightning strike density observations suggest that the these lakes are too small to affect the overall CG lightning density pattern.

The data shown in Fig. 3.5 do not reveal significant effects of the major urban areas of Calgary and Edmonton. The region surrounding Calgary has 32-64 strikes $(10\ km)^{-2}$ with no indication of a change in lightning strike density at Calgary. The Edmonton region also has 32-64 strikes $(10\ km)^{-2}$ region. A narrow band of 30 km width just south of the city has a higher lightning strike density of 64-128 strikes $(10\ km)^{-2}$. It is not clear that this higher lightning frequency south of Edmonton is related to the surface cover or local heat source of the city.

So far we have examined CG lightning strike density (i.e. the number of strikes per 10 km by 10 km area) as a measure of lightning activity. Clodman and Chisholm (1996) suggested to also use high CG lightning strike positions for analyzing the spatial variation of lightning. The grid elements used to define high lightning strike positions are 1/10° latitude by 1/6° longitude (see section 2.3). Fig. 3.7 shows the high CG lightning strike positions averaged for the 12 years of summer data. The symbolism is as follows: a plus sign represents 0.5-1.0 CG lightning strikes km^{-2}, a triangle represents 1.0-1.5 km^{-2}, a square represents 1.5-2.0 km^{-2}, and a circle represents 2.0-4.0 km^{-2}. Most of Alberta falls within the 0.5-1.0 km^{-2} zone. High lightning strike positions greater than 1.0 km^{-2} tend to occur in clusters. The squares and circles, for instance, concentrate themselves strictly within small clusters northwest of Rocky Mountain House, extending into the Grande Prairie region. There are a few other small clusters of squares and circles: two in the Fort McMurray area, and two northeast of Calgary. Most of the high CG lightning strike positions are within 200 km of the mountains in elevated regions with northeast-facing slopes (see Fig. 1.4). The only exception is a pair of clusters near Fort McMurray, in an area with an elevation of about 1000 feet. The triangles, squares, and circles appear to be favored by highly elevated land, with east-facing slopes. Therefore, in general, there is a tendency for high CG lightning strike positions to be in the west-central region of the province, particularly over the foothills. These conditions apply to the region west of Lethbridge as well, but very few high strike density positions are found there. Therefore, as for CG lightning strike densities, high CG lightning strike positions seem to be affected by surface properties such as vegetation cover and water cover.

To identify the possible effects of vegetation cover on lightning strike frequency, two regions are chosen with similar elevations and northeast-facing slopes, similar distances from the Continental Divide, and similar coverage of the lightning detection network. The first region is southwest of Grande Prairie, and is mostly covered by uncultivated deciduous and coniferous forests, and characterized by numerous high CG lightning strike positions. The second region is west of Lethbridge, and is covered by partly-cultivated grasslands with a very small band of mixed deciduous and coniferous forests near the foothills, and is characterized by a few high CG

lightning strike positions between 0.5-1.0. It appears as though high CG lightning strike positions occur in regions with, and upwind of, mostly heavily treed forests compared with grassy and cultivated regions.

The far northern part of the province is significantly covered with bodies of water such as muskeg, rivers, and lakes. Despite the moisture, there are few high CG lightning strike positions north of High Level and Lake Athabasca. Further towards the south and west (approaching the northern Slave Lake region), the number of high CG lightning strike position clusters increases five-fold.

The lack of high CG lightning strike positions near Edmonton and Calgary, confirm that urban areas in Alberta have little or no effects on lightning activity.

In addition to CG lightning strike density and high CG lightning strike positions, the CG lightning day counts can also be used to quantify the lightning activity. If there were 2 or more lightning strikes within visible range from an observer, a day was counted as a lightning day. As described in Section 2.3, the grid elements were 1/3° latitude by 2/3° longitude to accommodate the visible range criterion. Fig. 3.8 displays the CG lightning day count based on the entire 12 years of lightning observations. A region with more than 30 lightning days per summer extends from the foothills to the west of Calgary and into the Swan Hills region south of Lesser Slave Lake; it is roughly parallel to the Rocky Mountain range in the Hinton region. The position of this region is similar to that for large CG lightning strike densities (shown in Fig. 3.5). As discussed before, elevation and slope are important for convergence zones to form. For example, lower elevations from Hinton to the Swan Hills produce approximately the same number of lightning days as higher elevations to the west of Calgary, but the slope of the land is much the same. There are several pockets of lightning day minima. There are fewer than 18 lightning days in the northeastern and southeastern corners of Alberta. Also, Jasper National Park along the continental divide has only about 14 lightning days. This finding is consistent with that found for CG lightning strike density (Fig. 3.5) and high lightning strike positions (Fig. 3.6).

Comparing Alberta's vegetation cover (Fig. 1.5) with Fig. 3.7 shows that nearly two-thirds of the center of large lightning day count (>30), from west of Calgary to the Swan Hills and Hinton region, is covered by uncultivated coniferous and deciduous forests. The greatest lightning day count (>38) is situated in a band of forest, approximately 50 km north of Rocky Mountain House, just east of a region of mostly coniferous trees covering the foothills. The remainder of the >30 lightning day count on the east side of the lightning day center is composed of small lakes and rivers and partly cultivated forests further east toward Edmonton and Red Deer. Lightning day gradients are greatest between the continental divide and the foothills; a distance of approximately 50-100 km. The gradients are much smaller over the plains. Low lightning days (potentially <14) in Jasper National Park are almost exclusively associated with rock barrens. There appears to be a decrease in the number of lightning days away from the continental divide in the central part of the province, and as one approaches the northern and eastern borders of Alberta. Regions with lightning day counts less than 18 in the southeast corner of the province consist of partly cultivated grasslands, and a very small uncultivated area of forest on the Cypress Hills. Low lightning day counts in the northeastern corner of the province are accompanied by significantly different vegetation cover. This region contains the greatest concentration of large open (cool) bodies of water, including Lake Athabasca and Lake Claire. Further towards the south and west (approaching the northern Slave Lake region), lightning day counts increase slowly. Muskeg is commonly found in these regions and the elevation is not much higher than near Lake Athabasca. Urban area effects are not obvious in the lightning day count data. Calgary does not show any significant effect, while Edmonton may have contributed towards the bulge in the 26-30 lightning day count south of the city.

3.4 Effects of Mountains on CG Lightning Strikes

The spatial analysis of lightning strikes has indicated the importance of topography, and the Rocky Mountains in particular. The proximity of the Rocky Mountain range was found to be important in determining the lightning strike density. This section analyzes the proximity of the mountains in greater detail. Fig. 3.9 plots the number of lightning strikes as a function of the distance from the Continental

Divide. The five curves correspond to three-hourly time intervals starting at 12, 15, 18, 21 and 24 MDT, respectively. At 12 MDT, the number of lightning strikes is very low and is independent of the distance from the Continental Divide. At 15 MDT, the number of lightning strikes increases markedly to peak at 1700 strikes, at 100 km from the Continental Divide. At 18 MDT, the number of CG lightning strikes increases further; the main peak in CG lightning strikes is still at 100 km, but a secondary peak develops at about 450 km.

At 21 MDT, the number of lightning strikes begins to decrease. There is a shift of the curve away from the Continental Divide by approximately 50 km relative to the 18 MDT observations. At 24 MDT, the number of lightning strikes is reduced even more. There is also a continued shift of the maximum away from the Continental Divide; the peak is now located at about 200 km. We roughly estimate that from 18-24 MDT the primary peak in CG lightning strikes shifts eastward from the mountains at a speed of about 15 km h^{-1} by determining the distance covered by the 1000-1250 contour interval from 14 to 16 MDT.

Fig. 3.10 contours the CG lightning strikes in a distance-time diagram. The horizontal axis is local time, while the vertical axis is distance from the Continental Divide. The movement of the lightning away from the mountains is apparent. After 13 MDT, the contour of 250 CG lightning strikes begins to occur up to 650 km away from the Continental Divide. Over the foothills, approximately 100 km away from the Continental Divide, the number of lightning strikes ranges from fewer than 500 to more than 2000 within the time interval of 14 to 17 MDT. The variability in the number lightning strikes diminishes further away from the Continental Divide. The peak in the number of lightning strikes is tilted towards the right, indicating the eastward movement of lightning with time. The most dramatic shift of peak lightning activity away from the Continental Divide occurs from 14 to 24 MDT for CG lightning strike counts greater than 1000.

3.5 Intraseasonal variations in lightning strike distribution

The intra-seasonal variability of CG lightning strikes is now examined by analyzing the lightning density, high CG lightning strike positions, and lightning day counts. The 91 summer days are divided into 6 intervals; 1-15 June, 16-30 June, 1-15 July, 16-31 July, 1-15 August, and 16-31 August. The emphasis is on identifying the seasonal pattern (see Table 3.3): during June, southern Alberta (south of Red Deer) is the warmest and wettest part of the province. In July, the storm track migrates northward. The south still remains warm but, in July, storm systems pass more towards central and northern Alberta. August tends to be the driest month of the three. How does the spatial distribution of summer CG lightning strikes vary on an intra-seasonal basis? Do CG lightning strikes follow the movement of the storm track?

In the first 15 days of June (Fig. 3.11), the largest CG lightning strike density (from 8-16 strikes $(10\ km)^{-2}$) occurs around the Edson region. Other maxima of similar intensity are found near Grand Prairie, 30 km west of Cold Lake, near the Lesser Slave Lake, and 50 km east of Red Deer. A broader area of 4-8 strikes $(10\ km)^{-2}$ covers much of the foothills west of Lethbridge to west of Grande Prairie and northeastward to approximately 150-200 km from the Continental Divide. The lightning strike density in the northeastern corner of Alberta (0-0.5 strikes $(10\ km)^{-2}$) is the provincial minimum for the period from June 1-15. The rest of the northern one-third of the province contains low CG lightning strike densities as well (mostly from 1-4 strikes $(10\ km)^{-2}$). There are other CG lightning strike minima of considerable size: one located in Jasper National Park southeast of the town of Jasper (0-0.5 strikes $(10\ km)^{-2}$), and the other in the southeastern corner of Alberta (1-2 strikes $(10\ km)^{-2}$), south of Medicine Hat.

In general, CG lightning strike densities rise by up to 50% in Alberta from the first to the last half of the month of June (Fig. 3.12). This is consistent with the warming trend in the province as the summer solstice approaches. The maximum near Edson has grown from 8-16 to 16-32 strikes $(10\ km)^{-2}$, and has approximately doubled in area. The regions with minimum lightning strike densities remain virtually unchanged during June.

The first half of July shows an increase in the size of the west-central maximum of lightning activity (Fig. 3.13). It now extends from south of Rocky Mountain House to Lesser Slave Lake. However, the intensity remains about the same. With the significant northern expansion of CG lightning strike densities between 4-16 strikes $(10\ km)^{-2}$, comes a retreat of the minimum over the northeast, indicating a northward shift of the prevailing storm tracks during late summer. The southeastern part of Alberta continues to have a low lightning strike density as most of the convective storms pass further north over the prairies. The second half of July continues with the northward shift of the lightning activity (Fig. 3.14). The northward and eastward expansion of the 16-32 strikes $(10\ km)^{-2}$ center of lightning days has reached its peak. All minima have increased to their highest levels of the summer so far.

In August (Fig. 3.15) the CG lightning strike densities weaken away from the north, east, and southeast. There is also a shift towards higher strike densities along the southern foothills west of Lethbridge and Calgary. The center of maximum CG lightning strike density in the western part of the province has shrunk. However, its magnitude has increased to 32-64 strikes $(10\ km)^{-2}$. The southward shift of the storm track during early August is associated with the southern shift in higher CG lightning strike densities. During the last half of August (see Fig. 3.16), the widespread cooling and drying of Alberta, as the sunshine decreases, is evident. The center of maximum CG lightning strike density is less than half what it was during the first half of August. All CG lightning strike density minima have nearly doubled in size and intensity.

The intraseasonal shift is also apparent in the maps displaying the high lightning strike positions (Fig. 3.17-3.22). Many high CG lightning strike positions appear during the first half of July (Fig. 3.19), most of which are within 200 km of the Continental Divide. Towards the second half of July, the number of high lightning strike positions increases. There is a marked northeastward expansion of high lightning strike positions, particularly north of Red Deer. A fairly large number of high lightning strike positions are in the Grande Prairie and Peace River areas during the second half of July. During August (Fig. 3.21) the major storm tracks shift southward causing a southwestward retreat of high lightning strike positions toward the

mountains. Fig. 3.22 shows the continuation of the gradual decline in the number of high lightning strike positions during the second half of August.

The intraseasonal maps for lightning day count (Fig. 3.23 to Fig. 3.28) show the summertime variation of lightning day count in half-month increments. The number of lightning days from June 1-15 (Fig. 3.23) shows 5-6 lightning days near Edson and Drayton Valley. A larger region of between 4-5 lightning days extends from 50 km north-northwest of Edson to Rocky Mountain House. Between 3-4 lightning days are found along the foothills from Milk River northeastward to Grande Cache. The northern quarter of Alberta and the mountainous regions have generally <2 lightning days; a 50 km by 50 km region of from 0-1 lightning days is situated north and northwest of Lake Athabasca, and southeast of Jasper. The number of lightning days increases from early June to late June (Fig. 3.24). The largest lightning day count (7-8 lightning days), stretches from Edson southeastward to Rocky Mountain House. A smaller area of 7-8 lightning days is situated on the southwestern corner of the Swan Hills. Overall, the center of greatest lightning days increases by 2 or 3, and now covers a third more area; the center expands in all directions. The lightning day count data for the first half of July indicate a northward expansion (Fig. 3.25). This is consistent with the storm tracks moving northward during July. The region with the highest lightning day counts, shifts northward by about 50 km towards the Swan Hills area. Lightning day counts decrease by about 1 lightning day in southeastern Alberta from the second half of June to the first half of July even with the warming trend, due to the northern movement of the storm track. The second half of July shows the largest lightning days (Fig.3.26). The overall pattern of lightning days shifts towards the east-northeast. Lightning day contour lines of 5 or more move from the Edmonton and Slave Lake regions during the first half of July, to the Lloydminster and Fort McMurray regions during the second half of July. The center of greatest lightning day counts (7-8) grows considerably when compared with the first half of July; it covers approximately 4 times as much area stretching from Rocky Mountain House to Slave Lake.

In the first half of August, the region with lightning day counts of 7-8 become smaller and move southwestward towards the mountains (Fig.3.27). Also the regions with >4 lightning days shift towards the mountains. North of Lake Athabasca

there is a patch with 0-1 lightning days, which is the minimum for August 1-15. During the second half of August, there is a further reduction of lightning day activity as the solar radiation weakens. The greatest number of lightning days (5-6) occur near Rocky Mountain House. The smallest number of lightning days now encompasses the Lake Athabasca regions and northward to the NWT border.

3.6 Discussion and Conclusions

CG lightning strike frequency in Alberta varies significantly on an interannual, intraseasonal and daily basis. In 1984, there was a 12-year low of approximately 100 000 CG lightning strikes, and in 1994 there was a 12-year high of approximately 560 000 CG lightning strikes. On average there are 270 000 CG lightning strikes per year. The monthly distribution of lightning strikes are on average: June 23%, July - 45%, and August 32%. Table 3.4 compares Alberta average lightning with those reported for Manitoba (by Hanuta and LaDochy, 1989) and southern Ontario (Clodman and Chisholm, 1996). All three locations had the most lightning strikes during the month of July.

The lightning data for Alberta has a large day-to-day variability of CG lightning strikes. This suggests that a few storms with many CG lightning strikes can significantly affect the overall pattern. Small lightning frequencies (<1000) are common during the first half of June and the second half of August. Large frequencies (>5000) are common during the second half of July and the first half of August. Overall, CG lightning strike frequency gradually increases during June and most of July, peaks in the last week of July, and then decreases during August. We should point out that these findings for Alberta are very similar to those found in northeastern Colorado by Lopez and Holle (1986).

In Alberta, hourly CG lightning strike frequency increases during the afternoon, peaks at about 1900 MDT, and decreases during the rest of the evening and into the early morning hours. This diurnal pattern is similar to that recorded for Manitoba (Hanuta and LaDochy, 1989), southern Ontario (Clodman and Chisholm, 1996) and northeastern Colorado (Lopez and Holle, 1986). In Alberta, 80% of CG lightning

strikes occur during the afternoon and evening, and 20% occur during the morning. These numbers are similar to those for Manitoba and southern Ontario (see Table 3.4).

Average summertime CG lightning strikes are not uniformly distributed throughout Alberta. Major features include two 10-15 km wide maxima near Edson with >128 lightning strikes $(10\ km)^{-2}$, a large region of 64-128 strikes $(10\ km)^{-2}$ over western Alberta, a minimum with 4-8 strikes $(10\ km)^{-2}$ in the northeastern corner of the province near Lake Athabasca, and minima with between 8-16 strikes $(10\ km)^{-2}$ over the mountains and in the southeastern corner of the province. High lightning strike positions tend to occur in clusters, within about 200 km of the Continental Divide. The lightning day count distribution has its maximum stretched along the foothills bordered by Swan hills, Hinton, and Calgary.

It should be pointed out that lightning detectors are not evenly distributed in Alberta (see Section 2.1). Coverage is very good in the northern and western parts of the province, but there are few sensors covering the eastern plains (particularly in a line from Lloydminster to Medicine Hat). The non-uniform distribution of the network could give rise to a negative bias for the lightning counts in the southeastern part of Alberta.

The average spatial distribution of summer CG lightning strikes, high CG lightning strike positions, and lightning days are all influenced by topography. For example, the region with in excess of 64 strikes $(10\ km)^{-2}$ in west-central Alberta coincides with sloped land surfaces, generally facing northeast, with elevations generally >3000 feet. CG lightning strike densities are up to 90% smaller in flat and low areas of far northeastern Alberta, when compared with regions near Edson. The frequency of high CG lightning strike positions and lightning day counts also increase in sloped and elevated areas near the foothills in west-central Alberta and decrease in relatively flat and low areas to the north and east. Orographic lift caused by upslope wind produces storms over higher terrain. This condition is predominant near the foothills, partly because of the mountain-plain circulation (Smith and Yau, 1993). In Alberta, hailstorms occur frequently near the foothills of central and south-central Alberta (see Fig. 3.29); the largest frequency of hail (>9 strikes per sector) is

concentrated from Rocky Mountain House to Calgary. Severe hailstorms tend to begin in the foothills where convergence zones are formed with upslope flow (Wojtiw, 1977).

A similar topographic effect was evident in lightning observations for northeastern Colorado (Lopez and Holle, 1986). Court and Griffiths (1986) suggested that even the gentle slope of the Florida peninsula enhances lightning at the higher elevations. Clodman and Chisholm (1996) reported that lightning strike densities in upslope regions were about 30% higher than that for downslope areas of southern Ontario.

There are, however, exceptions to the correlation between sloped and elevated land surfaces and greater lightning activity in Alberta. For example, the foothills west of Lethbridge in southern Alberta yield generally <32 strikes $(10\ km)^{-2}$, approximately 5 high CG lightning strike positions between 0.5-1.0 km^{-2}, and 18-26 lightning days. In contrast the region west of Rocky Mountain House (with similar elevation, slope, and distance from the Continental Divide) has >64 strikes $(10\ km)^{-2}$ and >38 lightning days. Different vegetation can largely account for this. Different types of vegetation have different surface albedos, heat capacities, and moisture storage properties. These factors affect the surface energy balance and thereby the near surface temperature and humidity (Changnon and Semonin, 1979; Clodman and Chisholm, 1996; Rabin et al., 1990). Convective storms with CG lightning strikes seem to develop preferentially over.

Average spatial CG lightning strike density, high CG lightning strike position, and lightning day count patterns are also affected by water cover. Near and northeast of Rocky Mountain House, moisture from lakes tends to enhance lightning activity. Northern Alberta has sufficient moisture (from muskeg, rivers, and lakes), but often lacks sufficient sensible heat to spawn major convective storms. In addition, the region is flat and therefore has no prevalent convergence zones.

Clodman and Chisholm (1996) noted a lake-breeze effect on lightning strike distribution for southern Ontario. Alberta data do not indicate strong lake-breeze effects. Large lakes are found in northern Alberta but the daily heating of the

surrounding forested area is probably insufficient for the development of a lake breeze that impacts lightning activity.

Average spatial CG lightning strike density, high CG lightning strike position, and lightning day count patterns are influenced by latitude, vegetation cover, water cover, and topography. There is an increase in CG lightning strikes densities from north to south in the Lake Athabasca – Slave Lake corridor. This southward increase is likely due to the increase in sunshine hours. Higher elevations and sloping land surfaces also create a southward increase of CG lightning strike densities, the number of high CG lightning strike positions, and lightning day counts, particularly in central Alberta. Orville (1994) compiled CG lightning flash density charts for the three years 1989-91 for almost the entire mainland United States. Lightning strike density was found to increase from north to south in North America. Mackerra and Darveniza (1994) found there is more convection and more lightning at lower latitudes, coinciding with more heat and moisture. The lightning strike rate increased by about 7% every 100 km. Clodman and Chisholm (1996) determined that there is a 50% increase per 100 km of lightning densities and lightning day counts in southern Ontario. They found that the north-south surface temperature and moisture gradients caused by differences in solar radiation, vegetation cover, water cover, and topography were contributing factors.

There is movement in the average peak of CG lightning strike frequency, as a function of distance from the Continental Divide in Alberta. From hour 15-24 MDT the primary peak in CG lightning strikes moves away from the Continental Divide with a speed of about 15 km/h. Hanuta and LaDochy (1989) also documented similar eastward movements of lightning strike frequency peaks in Manitoba. Near midnight, the western sector decreased, but the central plains region continued to have relatively high activity, which shifted farther east by mid-morning. The progression of thunderstorm activity eastward from the late afternoon to the early part of the morning was also seen east of the Rockies in Colorado (Lopez and Holle, 1986).

The average spatial distribution of CG lightning strike densities, high CG lightning strike positions, and lightning day counts vary intraseasonally. Lightning strikes

occur primarily in the Edson and Rocky Mountain House regions in June. CG lightning strike densities and lightning day counts approximately double in intensity from early to late June. This is consistent with the warming trend experienced, on average, during this period. High CG lightning strike positions spread north and eastward during the first half of July. CG lightning densities and lightning day counts increase by as much as 50% from the second half of June to the first half of July over the High Level-Grande Prairie corridor, indicative of a northward movement of the prevailing convective storm track. The second half of July shows a continuation of the warming. This period is the most active part in terms of thunderstorms. CG lightning strike densities (and lightning day counts) have reached their peak values. Interestingly, the number of high CG lightning strike positions peaks during the first half of August, indicating that the greatest number of high intensity thunderstorms occur in the first half of August. The first half of August indicates a retreat of CG lightning strike densities, high CG lightning strike positions, and lightning day counts away from the north, east, and southeast; for example, there is a 25% decrease in strike density and lightning day count in the Lloydminster area. While at the same time CG lightning strike density, high CG lightning strike positions, and lightning day counts over the southern foothills west of Lethbridge and Calgary are up by 50%. The southern movement of the storm track during the early part of August, and the slow cooling trend over the north, would explain the southern shift of lightning activity. The gradual drying trend over the plains also contributes to a suppression in lightning activity. The widespread cooling and drying of Alberta is evident during the last half of August. The center of maximum CG lightning strike density, for example, is less than half of what it was during the first half of August, and all CG lightning strike density minima have nearly doubled in size and intensity.

4. LIGHTNING STRIKES AND PRECIPITATION IN ALBERTA THUNDERSTORMS

4.1 Introduction

This chapter looks at the relationship between lightning strikes and the precipitation structure for four case study storms. A common feature of the four storms is that they were large severe hailstorms that lasted for several hours. They developed in an environment with strong moist convective instability and had large vertical shear of the horizontal wind. Both storm 1 and storm 2 occurred on 19 August 1992 [UTC, or 18 August MDT], while storm 3 and storm 4 developed on 29-30 July 1993 [UTC, or 29 July MDT]. Our analysis of these four storms is focused on the following issues:

- Where are the majority of CG lightning strikes located relative to the geometric center of the storm?
- Where are the majority of CG lightning strikes located relative to the center of the precipitation core?
- Does the frequency of CG lightning strikes correlate with the precipitation intensity?
- Deep and intense radar echoes are followed by a frequent and dense number of CG lightning strikes (e.g. Rutledge and MacGorman, 1988). What is the time lag that maximizes the positive correlation of echo height and intensity with CG lightning occurrence?
- Is the displacement of CG lightning strikes from the center of the precipitation core temporally dependent on the core's intensity?

The findings for each of the four storms are compared with each other to determine how the storm structure, and thus lightning distribution, is affected by meteorological conditions. Section 4.2 presents a discussion on the synoptic conditions and significant weather for the two days. Then follows an analysis of the spatial organization of the CG lightning strikes with respect to the geometric storm center (Section 4.3) and main precipitation core (Section 4.4), and an investigation of

how the CG lightning strike frequency is related to the rainfall rate (Section 4.5). The temporal correlation between the number of lightning strikes and rainfall parameters is presented in Section 4.6. Temporal variation in the distance of lightning strikes from the precipitation core is dealt with in Section 4.7. The last section summarizes the results and provides a possible explanation for the findings.

All these sections have a common structure. First, the results for storm 1 and storm 2 (of 19 August 1992) are presented. This is followed by a briefer discussion of the results for storm 3 and storm 4 (of 30 July 1993). Here the emphasis is on highlighting the major similarities and differences between the two case study days.

4.2 Significant weather and synoptic conditions

(a) 19 August 1992

The lightning detection network recorded about 15 000 CG lightning strikes on 19 August 1992 in a wide band from Grande Cache to Cold Lake. Hailstones as large as golfballs were recorded near Barrhead at 0130 UTC 19 August, and also at Morinville at 0525 UTC 19 August. Pea-sized hailstones were reported at Redwater, Fox Creek, Edmonton, Whitecourt, Grande Prairie, Edson and Slave Lake. At 0130 UTC a tornado damaged a mobile home near Fort Assiniboine. At 0315 UTC a second tornado (possibly from storm 1) was recorded near Morinville. More information about the storm observations can be found in Xin and Reuter (1996) and Xin and Reuter (1998).

Fig. 4.1 shows the 850 mb weather map valid at 0000 UTC on 19 August 1992. At that time deep convection had started in the Swan Hills region. The 850 mb geopotential height field shows a short-wave trough axis passing through central Alberta. The southerly airflow advected heat that tended to strengthen the convective instability and reduce the capping lid on the lee side of the mountains. There was significant baroclinicity over western Canada with isotherms ranging from 8-26°C.

The Stony Plain sounding for 0000 UTC on 19 August 1992 is plotted in Fig. 4.2. The ambient temperature profile was close to dry adiabatic from the surface to about 750 mb. For the observed surface conditions, the lifting condensation level was estimated at about 700 mb. The airmass was convectively unstable with a Convective Available Potential Energy (CAPE) of about 610 J kg^{-1}. The wind was generally unidirectional, except for some backing at the top of boundary layer.

(b) 30 July 1993

Several severe storms developed on 29-30 July 1993 [UTC] over central Alberta. All of them tracked from the southwest towards the northeast at a speed of about 50 km h^{-1}. Two of these storms are analyzed here in detail. At 0345 UTC 30 July (1945 MDT 29 July) a tornado, with a maximum intensity of F3 on the Fujita scale, touched down to the west of Holden, Alberta. The storm responsible for the tornado is identified as storm 4 in this thesis. Near 0356 UTC, the tornado flipped over a mobile home, resulting in injuries to its owner. The tornado continued north-northeastward and damaged or destroyed several other structures in the process. The tornado lasted a total of about 15 minutes, and the damage path was about 20 km long with a width of up to 200 m.

Fig. 4.3 shows the 0000 UTC 30 July 1993 sounding released from Stony Plain. The CAPE value was computed as 1768 J kg^{-1}, indicating the potential for very intense deep convection. The atmosphere was very moist (T_d approximately 16 C) in the lowest 100 mb providing ample "fuel" for the release of the latent instability. Vertical shear in the horizontal wind was generally moderate. According to the hodograph, the wind backed in the lowest 200 mb, then veered up to the 400 mb level; this indicates that there was a cooling trend at lower levels and a warming trend aloft (the atmosphere was becoming more stable during the evening).

4.3. Spatial organization of lightning strikes relative to the geometric storm center

(a) Storms 1 and 2 on 19 August 1992

At all times, both storms 1 and 2 remained well-defined entities that were easily tracked on the Constant Altitude Planar Position Image (CAPPI) maps that depict radar reflectivity at 2 km above ground (Fig. 4.4). The top panel shows the maximum rainfall rate above the 2 km level. This was derived from radar reflectivity measurements using the Marshall-Palmer Z-R relationship (see Section 2.4). The Severe Storm Map (bottom panel) shows the maximum height of the 40 dBZ radar reflectivity factor and the position of CG lightning strikes that occurred in the previous 10 minutes. The shape of the heavy rainfall area remained close to an ellipse with its major axis parallel to the downwind direction (i.e. northeast). On each CAPPI map (produced every 10 minutes), a geometric center is marked at the intersection of the major and minor axes of the ellipse, which closely approximated the storm area (see Fig. 2.3). The storm area is then divided into four equally-sized storm quadrants: Right Front (RF), Left Front (LF), Right Back (RB) and Left Back (LB). The number of CG lightning strikes occurring in the storm every 10 minutes is referred to as #STR.

Fig. 4.5a shows the time history of CG lightning strikes (#STR min^{-1}) for storm 1 (The numerical data are listed in Table 4.1). From 0040 to 0210 UTC the lightning frequency is relatively low, ranging from 0.5 to 2 min^{-1}. From 0210 to 0330 UTC, #STR increases to 5 min^{-1}. For the next 30 minutes, the lightning strike frequency subsides, before developing a new peak of 5.5 min^{-1} at 0430 UTC. The lightning diminishes rapidly, ceasing at 0520 UTC. A total of 574 CG lightning strikes accumulated during the 4½ hours. Fig. 4.5a also shows the contributions of the lightning strike frequency among the four quadrants. Most of the lightning strikes occur in the two back quadrants, with very few strikes in the front (i.e. downshear) side. From 0040 to 0210 UTC, the RB storm quadrant has slightly more lightning strikes than the LB quadrant. During this time, the maximum radar echo is located in the LB quadrant. After 0210 UTC, the maximum precipitation shifts into the LB

quadrant. This is accompanied by an increase of lightning in the RB quadrant. Throughout the remainder of the storm's lifetime, the largest relative contribution towards lightning comes from the RB quadrant.

Storm 2 (Fig. 4.5b) is similar to storm 1 in that it develops multiple peaks in CG lightning frequencies. In both storms, most of the lightning occurs in the two back quadrants (i.e. on the upshear side of the storms). The left quadrants of the storms (i.e. the northwest flank) have more lightning than the right quadrants (i.e. the southeast flank).

(b) Storms 3 and 4 on 30 July 1993

Storm 3 and storm 4 occurred over the radar area on 29-30 July 1993 [UTC]. Again, the storms could be tracked on the radar imagery (Fig. 4.6). The relative contributions of the four storm quadrants, toward CG lightning strike frequency, are plotted in Fig. 4.7 (and listed in Tables 4.3 and 4.4). In both storms, most of the lightning strikes occur in the two back quadrants (i.e. on the upshear side of the storms). In fact, very little lightning is found ahead of the geometric storm center. However, the relative importance of the LB and RB quadrants differs for the two cases. In storm 3, the two back quadrants contribute about equally. However, in storm 4 far more lightning strikes occur in the LB quadrant than in the RB quadrant.

Figures 4.8 and 4.9 compare the total number of CG lightning strikes that accumulated throughout the observing period for the four storms. Table 4.5 lists these data in percentage values. Storm 1 and storm 2, which occurred on 19 August 1992, had more lightning strikes than those associated with the storms forming on 30 July 1993. For storms 1, 2, and 3, about 85% of their total lightning strikes are in the back two quadrants (i.e. in the southwest or upshear side). In storm 4, the back half contributes 60%; still higher than the front side. Storms 1, 2, and 4 have more lightning on the left flank (i.e. northwest side), while storm 3 has more lightning on the right flank (i.e. southeast side).

4.4. Spatial organization of lightning strikes relative to the center of the precipitation core

(a) Storms 1 and 2 on 19 August 1992

The location of the precipitation core is identified on the CAPPI maps depicting maximum rainfall above 2 km (e.g. Fig. 4.4). By carefully tracking the rainfall data in time, we can follow the major precipitation core shaft. The storm area, divided into four unequally-sized "quadrants", is shown in Fig. 2.3. The two lines that define the quadrants are intersecting at the center of the precipitation core. One is parallel to the storm movement, while the other is perpendicular to it. The four areas are labeled as Right Front Core (RFC), Left Front Core (LFC), Right Back Core (RBC) and Left Back Core (LBC).

Fig. 4.10 shows the time history of CG lightning strikes (#STR min^{-1}) for storm 1 and storm 2 (The numerical data are listed in Tables 4.6 and 4.7, respectively). Overall, the largest #STR occurs in the left back core quadrant for both storms. For storm 1, the second largest #STR occurs in the right back core quadrant with the front core quadrants generally following closely behind, except after 0400 UTC, when the #STR in the front core quadrants increases significantly. For storm 2, the second largest #STR occurs in the left front quadrant throughout the period, with the right quadrants following closely behind.

The total #STR within each core quadrant, relative to the total #STR within storm 1 and storm 2, are shown on Fig. 4.11. Sixty seven percent (storm 1) to 79% (storm 2) of the total #STR are on the left side of the core center, 63% (storm 2) to 68% (storm 1) are on the back side of the core center, and approximately 50% (both storms) are found in the left back core quadrant alone. Of the 21 CG lightning strikes that occur every 10 minutes on average for storm 1, 12 are on the left side, and 17 are on the back side of the core center. Of the 11 CG lightning strikes that occur for storm 2, 9 are on the left side and 7 are on the back side of the core center.

The positions of CG lightning strikes relative to the core center are slightly different than the positions of CG lightning strikes relative to the storm center. For example, there is a 40-60% drop in the total #STR within the right back core quadrant, and a 40-60% rise in the total #STR within the left front core quadrant, when compared to the total #STR in the same storm quadrants. These differences can be partially attributed to the fact that the center of the precipitation core is preferentially located in the right back storm quadrant of both storms (see the numbers in bold on Table 4.1 and Table 4.2). Therefore, for both storms, the average size of the right back core quadrant is smaller than, and the left front core quadrant is larger than, the rest of the core quadrants. Even though there are these minor differences, whether we consider the positions of CG lightning strikes relative to the core center or to the storm center, the main trends are similar.

(b) Storms 3 and 4 on 30 July 1993

Fig. 4.12 shows the time history of CG lightning strikes (#STR in min^{-1}) for storm 3 and 4, as well as the relative contributions from the four core quadrants. The numerical data are listed in Tables 4.8 and 4.9, respectively. There is significant temporal variability in #STR within the core quadrants. CG lightning strikes tend to occur more frequently in the middle of the period. It is not apparent which core quadrant dominates storm 3, but the left front core quadrant has the greatest #STR throughout the life of storm 4.

The total #STR within each core quadrant, relative to the total #STR are shown on Fig. 4.13. Sixty one percent (108) to 71% (77) of the total #STR are on the left side of the core center for storm 3 and storm 4 respectively. These results are comparable to those for storm 1 and storm 2. Fifty six percent (99) and 29% (32) of the total #STR are on the back side of the core center for storm 3 and storm 4, respectively. The results for storms 1, 2, and 3 are similar. However, the #STR on the back side of the core center for storm 4 is much smaller because of the very large total #STR in the left front core quadrant. There is a better chance of having CG lightning strikes on the left side of the core center for storm 3 and storm 4, which is consistent with storm 1 and storm 2. Also, with the exception of storm 4, lightning

strikes occur mainly on the back side of the core center, in the left back core quadrant.

The positions of CG lightning strikes relative to the core center are different from the positions of CG lightning strikes relative to the storm center for all four storms. There is a 40-60% drop in the total #STR within the right back core quadrant, and a similar rise in the left front core quadrant. One explanation is that the center of the precipitation core is usually located within the right back storm quadrant. Therefore, the average size of the RBC is the smallest of the four core quadrants, while the LFC is the largest.

4.5 Number of lightning strikes as a function of rainfall rate

(a) Storms 1 and 2 on 19 August 1992

One of the objectives of these case studies is to explore the relationship between lightning strike frequency and rainfall rate. To investigate this issue, it is convenient to sort the data into different intervals of rainfall rate. Since the CAPPI maps show rainfall in intervals that double with increasing intensity, it is appropriate to follow this convention. The rainfall rate intervals selected are: 2-4 mm h^{-1}, 4-8 mm h^{-1}, 8-16 mm h^{-1}, 16-32 mm h^{-1}, 32-64 mm h^{-1} and 64-128 mm h^{-1}. In addition, the intervals of 0-0.25 mm h^{-1} and 0.25-2 mm h^{-1} are used. For each of these rainfall rate intervals, the number of lightning strikes are counted for the entire observing period.

The results are presented in pie diagrams shown in Fig. 4.14. All contributions are expressed in percentage values of the total number of lightning strikes accumulated within the observing period. The results show that CG lightning strikes occur throughout the range of precipitation rates. However, it tends to be bounded by 0.25 mm h^{-1} rainfall rate contour. Very few CG lightning strikes occur within the 0-0.25 mm h^{-1} rainfall rate interval. For storms 1 and 2, the greatest percentage of CG lightning strikes occur in the 0.25-2 mm h^{-1} range (60% of the total for storm 1 and 54% for storm 2). As the rainfall rate increases, the number of lightning strikes

decreases. The reason is obvious. Both storms have large areas of low rainfall rates. For example, the 0.25-2 mm/hr range covers approximately 75% of storm 1 and storm 2 (see Table 4.10 and Table 4.11). Conversely, only <1% covers the >64 mm h^{-1} range.

The area biases are removed by area-weighting the total #STR for each rainfall rate interval (see Appendix A). The results when adjusted for area are shown in Fig. 4.14c and 4.14d. The main results show that the 0.25-2 mm h^{-1} interval contributes only 6% for storm 1 and 5% for storm 2 (down from 60% and 54% before weighting). The percentage of strikes within each of the ranges between 2 and 64 mm h^{-1} are similar (~15%) for both storms. The percentage of strikes within the 0-0.25 and 64-128 mm h^{-1} intervals are more variable. Most CG lightning strikes occur within the area bounded by the 2 mm h^{-1} contour.

(b) Storms 3 and 4 on 30 July 1993

Pie diagrams show the percentage values of #STR within different rainfall rate intervals for storms 3 and 4 (Fig. 4.15). As for storm 1 and storm 2, CG lightning strikes discharge throughout the entire range of rainfall rates for storms 3 and 4. A vast majority (90-95%) of CG lightning strikes for the four storms are bounded by the detectable precipitation region (>0.25 mm h^{-1}). For storm 3 and storm 4, the greatest percentage of CG lightning strikes occurs in the 0.25-2 mm h^{-1}: 39% of the total for storm 3 and 42% for storm 4. The 0.25-2 mm h^{-1} range covers approximately 65% of the areal extent of storm 3 and storm 4.

The area biases are removed by weighting the total #STR within the maximum rain rate intervals. The weighted data are shown on Fig. 4.15c and 4.15d. The results are similar to those of storms 1 and 2. The 0.25-2 mm h^{-1} rainfall rate interval contributes only 5% for both storms 3 and 4. Also, all the listed rainfall rate intervals (within the 2-64 mm h^{-1} range) contribute roughly the same at about 15%. For both storms 3 and 4, the majority of CG lightning strikes (i.e. > 50%) occur where the rainfall rate exceeds 2 mm h^{-1}, when adjusting for areal biases. This agrees with the results for storms 1 and 2 of the previous section.

4.6 Temporal correlation of rainfall and lightning

(a) Storms 1 and 2 on 19 August 1992

Two radar parameters often used for severe storm forecasting in Alberta are the maximum height of the 40 dBz reflectivity (denoted by H) and the maximum rainfall rate R above 2 km (for example Fig. 4.4). The R value is obtained using the Marshall-Palmer relationship ($Z = 200R^{1.6}$). As pointed out before, the Z-R conversion becomes problematic in heavy convective rain and hail (Xin and Larochelle, 1997). To estimate the peak values of R and H from the radar maps some objective "extrapolation" is needed at some time steps. The procedure used to specify R and H is given in the Appendix.

Fig. 4.16 compares the timing of lightning strikes with the evolution of H and R for storm 1. The numerical values are also listed in Table 4.14. In the first 2 hours, the maximum height H of the 40 dBz reflectivity increases from 7 to 10.5 km, while the maximum rainfall rate R intensifies from 40 to 80 mm h^{-1}. This rapid growth in rainfall has no immediate impact on the number of lightning strikes (#STR), which oscillates around 1 min^{-1}. However, from 2 to 3.5 h, #STR increases dramatically from 0.5 to 5 min^{-1}.

Fig. 4.17 compares the radar observations with the number of lightning strikes for storm 2 (see also Table 4.15). In the first hour of the observing period, the increase in #STR coincides with increasing H and R. Thereafter, the upward and downward fluctuations in H do not coincide with those in #STR. Similarly, changes in R and #STR are not correlated.

The Correlation Coefficient (CC) of #STR versus H, and #STR versus R with various time delays is computed. For a given time delay of Δt, H at time t is correlated with #STR at time $t+\Delta t$ for all times t. For delay times of less than 40 minutes, H and #STR are negatively correlated for storm 1 (Fig. 4.18a). However, with a delay of 80 minutes, the correlation coefficient between H and #STR becomes about +0.6. Similarly, R is uncorrelated with #STR for time delays less than 1 hour.

The best correlation of +0.4 occurs for a delay of 100 min. The findings for storm 2 are similar (Fig. 4.18b). Significant positive correlation occurs only for a delay of 70-100 min.

(b) Storms 3 and 4 on 30 July 1993

The analyses for storm 3 and storm 4 are depicted in Figs. 4.19 and 4.20. In both cases, the maximum height of the 40 dBz reflectivity is deep, varying between 10 and 12 km for most of the storms' lifetime. The 12 km level for H, coincides with the tropopause for that day. Also R remains fairly uniform, ranging from 60 to 100 mm h^{-1}. These high values suggest the occurrence of large hail, which was observed from both storm cells. More variability is indicated in the number of lightning strikes. The correlation between radar and lightning parameters is weak for both storms.

Both storms 3 and 4 have positive CC's between #STR and R for delay times of 0-20 minutes (Fig. 21). A 20 minute delay is still within the typical convective timescale of cumulus development. There is also positive correlation between #STR and H for a delay of 0-30 min. The highest CC value is +0.6 for a 30 min delay.

4.7. Displacement of lightning strikes from precipitation core center

(a) Storms 1 and 2 on 19 August 1992

The last issue investigated is the possible relationship between the average distance of CG lightning strikes from the center of the precipitation core and the precipitation core intensity. For a given 10 minute time interval the horizontal distance of each lightning strike location is estimated from the center of the rainfall rate maximum R above 2 km. Averaging over the 10 min interval, the average distance RD is estimated.

Fig. 4.22 shows the time histories of RD (in km) and R (in mm/h) for storms 1 and 2. Short-lived fluctuations of RD are evident in both storms. A few of the larger fluctuations coincide with a suspiciously small number of CG lightning strikes within the 10 min time interval (e.g. at 0220 UTC for Storm 2). On average, CG lightning strikes for both storms occur within about 15 km of the precipitation core defined by R.

(b) Storms 3 and 4 on 30 July 1993

Fig. 4.23 shows the time histories of RD (in km) and R (in mm/h) for storms 3 and 4. The curves indicate an increase in RD toward the middle of the storms' life times, followed by a decrease in RD near the end of the period. However, short-lived fluctuations in RD tend to dominate the pattern for both storms. RD values for storms 3 and 4, are roughly double those found for storms 1 and 2. Some of the large values of RD for storms 3 and 4 occur when there are fewer than 4 CG lightning strikes recorded in 10 minutes. This may skew the average distance for those intervals.

4.8 Conclusions

CG lightning strike observations are analyzed for four severe Alberta hailstorms. Lightning activity varies significantly throughout the lifetime of the four storms; this is consistent with Rogers and Sakellariou's (1986) study. They found that peaks in the precipitation rate were separated by about 30-40 minutes.

The spatial distribution of lightning strikes within the radar echo region of individual superstorms is far from uniform. About 60-85% of the lightning strikes occur on the upshear side (i.e. on the southwest side of the northeast moving storms). Of the four storm quadrants, the left back quadrant tends to have the most lightning strikes. The right front quadrant usually has the fewest lightning strikes. These findings agree well with those reported by Williams (1985).

Most of the CG lightning strikes for storms 1, 2, and 4 occur in the left back core quadrant. Storm 4 has approximately 25% less #STR on the back side of the core, and 25% more on the left side of the core center compared to the other 3 storms. The finding that CG lightning strikes tend to occur in the left back core quadrant is similar to the results reported by Keighton et al. (1991).

Most CG lightning strikes occur outside the precipitation core in the rainfall rate interval 0.25-2 mm h^{-1}. A similar finding was made by Rust et al. (1981), who found that few lightning sources were in high reflectivity cores. When removing area biases, a larger fraction of CG lightning strikes per area are found to occur in the precipitation core compared to the weakest precipitation. This is consistent with Holle et al.'s (1994) results. They found that there were more CG lightning strikes per unit area of the precipitation core than in the remainder of the storm area.

For the two storms on 30 July 1993, lightning strike frequency is correlated with radar-derived rainfall parameters with an optimal delay of about 10-30 minutes. This agrees with the notion that the coupling of precipitation and lightning parameters should occur within a period of 30 minutes, which is the time span of a typical thunderstorm cell. The two storms on 19 August 1992 do not indicate that precipitation growth is followed by an increase in the number of lightning strikes for delay times less than an hour. However, lightning tends to be correlated with the precipitation recorded 90 minutes earlier. A similar finding was reported by Rutledge and MacGorman (1988).

CG lightning strikes occur mostly within 15 km of the center of the precipitation core for storms 1 and 2, and within 30 km for storms 3 and 4. This is consistent with the study of MacGorman and Nielsen (1991). They found that lightning strikes were usually located within about 20 km of the center of the radar reflectivity core.

5. SUMMARY AND CONCLUSIONS

This thesis presents an investigation of the spatial and temporal distributions of cloud-to-ground (CG) lightning strikes associated with summer thunderstorms in Alberta. It consists of two major parts. The first part documents the summertime CG lightning climatology for Alberta, and examines how spatial and temporal distributions of summer CG lightning strikes are affected by geographical and meteorological properties. The second part contains detailed case studies of four severe thunderstorms. Here the focus is on relating the location and timing of CG lightning strikes relative to the precipitation structure.

The lightning climatology is based on the CG lightning data recorded by the Alberta Forest Service lightning detection network during 1984 to 1995. 1104 days of lightning data (12 years × 92 days year^{-1}) are analyzed. The main findings can be summarized as follows:

- CG lightning strike frequency in Alberta varies significantly on an interannual, intraseasonal and daily basis. Most lightning occurs in July, with August and June in second and third place. There is large day-to-day variability in the number of CG lightning strikes. Overall, CG lightning strike frequency gradually increases during June and the first week of July, peaks in the last week of July, and then decreases during August.

- In Alberta, hourly CG lightning strike frequency increases during the afternoon, peaks at about 1900 MDT, and decreases during the rest of the evening and into the early morning hours.

- Average summertime CG lightning strikes are not uniformly distributed throughout Alberta. Large CG lightning strike densities and lightning day counts are located over western Alberta, particularly in the Edson-Rocky Mountain House corridor. High lightning strike positions tend to occur in clusters, within about 200 km of the Continental Divide.

- The average spatial distribution of summer CG lightning strikes is related closely to topography. The frequency of lightning increases in elevated (and northeast-facing sloped areas) near the foothills in west-central Alberta. The lightning strike frequency decreases in flat and low areas (towards the north and east). Orographic lift, caused by upslope wind, produces storms over higher terrain. This occurs frequently near the foothills, partly because of the mountain-plain circulation.

- The average spatial distribution of summer CG lightning strikes is also influenced by latitudinal changes in sunlight availability, and vegetation and water cover. Lightning activity increases towards the south due to more sunlight hours. Urban areas do not impact lightning activity significantly. Similarly, lake-breeze effects on lightning are unimportant in Alberta..

- There is movement in the average peak of CG lightning strike frequency as a function of distance from the Continental Divide in Alberta. From 15-24 MDT the primary peak in CG lightning strikes moves away from the Continental Divide with a speed of about 15 km h^{-1}..

- CG lightning activity varies intraseasonally in Alberta. Lightning activity intensifies as the surface warms during June and July. Lightning activity also shifts north and east during June and July following the northward movement of the storm track. August indicates a retreat of lightning activity away from the north, east, and southeast.

In the second part of this thesis we analyze four long-lived hailstorms. The focus of the case studies is to analyze the relationship between CG lightning strikes and the precipitation structure. The results are summarized in point form as follows:

- The number of CG lightning strikes (#STR) per minute varies significantly throughout the lifetime of the four storms. There are half-hour periods of very intense lightning activity, interspersed with periods of only a few lightning strikes.

- The spatial distribution of the CG lightning strikes within the radar echo region is not uniform. Of the four storm quadrants, the left back quadrant tends to have the most lightning strikes. The right front usually has the fewest lightning strikes.

- Most of the CG lightning strikes occur in the left back core quadrant. This is evident in three of the four storms.

- Most CG lightning strikes occur just outside the precipitation core. However, when removing the area biases, a larger fraction of CG lightning strikes are found to occur in the precipitation core than in the weakest rainfall rate.

- CG lightning frequency tends to lag peaks in precipitation intensity. For the two storms on 30 July 1993 the lightning strike frequency is correlated with radar-derived rainfall parameters with an optimal delay of about 10-30 minutes. The two storms on 19 August 1992 indicate that precipitation development is followed by an increase in the number of lightning strikes 90 minutes later.

- CG lightning strikes occur mostly within 15 km of the center of the precipitation core for the two storms on 19 August 1992, and within 30 km for the two storms on 30 July 1993.

The conclusions above are obtained for four long-lived hailstorms of supercell structure. It is conceivable that the results are not valid for multicell storms or for short-lived airmass thunderstorms. Further research is needed to determine how lightning is related to precipitation in those types of convective storms that are less severe.

Appendix A: Weighting Method

The following notation is introduced:

$(t,t+\Delta t)$	is the time interval from t to $t+\Delta t$
$(R,R+\Delta R)$	is the rainfall rate interval ranging from R to $R+\Delta R$
$A(R,t)$	is the total area that has a rainfall rate within $(R,R+\Delta R)$ during the time interval $(t,t+\Delta t)$
$\Sigma A(t)$	is the total storm area during $(t,t+\Delta t)$
$w(R,t)$	is the fraction of the area that receives a rainfall rate within $(R,R+\Delta R)$ during $(t,t+\Delta t)$
$S(R,t)$	is the total number of lightning strikes that occur within the area $A(R,t)$ during $(t,t+\Delta t)$
$P(R)$	is the total number of lightning strikes that occur when the observed rainfall rate lies within the interval $(R,R+\Delta R)$ accumulated over the entire observing period $(0,T)$
$Q(R)$	is the total number of lightning strikes that occur when the observed rainfall rate lies within the interval $(R,R+\Delta R)$ accumulated over the entire observing period $(0,T)$ after removing the area bias
$Q^*(R)$	is the scaled $Q(R)$ such that P equals Q^*

The following formula are used for determining $w(R,t)$, $P(R)$, and $Q(R)$:

$$w(R,t) = A(R,t)/\Sigma A(t)$$

$$P(R) = \int S(R,t)\, dt$$

$$Q(R) = \int [S(R,t)/w(R,t)]\, dt$$

$$Q^*(R) = [Q(R) \int P(R)\, dR / \int Q(R)\, dR]$$

The integration is done over the interval $(0,T)$.

Appendix B: Estimation of R and H

The CAPPI map of maximum rainfall above 2 km shows different colors for discrete rainfall rate intervals (0.25-2 mm h^{-1}, 2-4 mm h^{-1}, 4-8 mm h^{-1}, 8-16 mm h^{-1}, 16-32 mm h^{-1}, 32-64 mm h^{-1}, and >64 mm h^{-1}). To estimate R, the maximum rainfall rate, we use the following procedure:

1. Find the highest rainfall rate interval within which the peak value lies. We denote this interval (R_i, R_{i+1}).
2. Estimate the area weight w_i by taking the ratio of the pixel count versus the highest pixel count in column
3. Compute R using a weighted mean of R_i and R_{i+1}

$$R = (1-w_i) R_i + w_i R_{i+1}.$$

For R_i = 64 mm h^{-1}, we use R_{i+1} = 96 mm h^{-1}

The severe storm map displays the maximum height of 40 dBz by using different colors for discrete height intervals (5.5-8.5 km, 8.5-10.5 km, 10.5-12 km, and >12 km). To estimate the peak value H we use the following procedure:

1. Find the highest height interval within which the peak value lies. We denote this interval (H_i, H_{i+1}).
2. Estimate the area weight v_i by taking the ratio of the pixel count versus the highest pixel count in column
3. Compute R using a weighted mean of H_i and H_{i+1}.

$$H = (1-v_i) H_i + v_i H_{i+1}.$$

For H_i = 12 km, we use H_{i+1} = 13 km.

REFERENCES

Anderson, K., 1991: Models to predict lightning occurrence and frequency over Alberta, Masters thesis, Univ. of Alberta, 2-12.

Berger, K., 1977: Lightning; *the earth flash*, Vol. 1. Academic Press, New York, NY, Chapter 5., 119-190.

Biswas, K.R., and P.V. Hobbs, 1990: Lightning over the Gulf Stream. *Geophys. Res. Letters*, **17**, 941-943.

Brook, M., and T. Ogawa, 1977: Lightning; *the cloud discharge*, Vol 1. Academic Press, New York, NY, Chapter 6., 191-230.

Chagnon, S.A., Jr., and R.G. Semonin, 1979: Impact of man upon local and regional weather. *Rev. Geophys. Space. Phys.* **17**, 1891-1900.

Clodman, S., and W. Chisholm, 1996: Lightning flash climatology in the southern Great Lakes region. *Atmos.-Ocean*, **34**, 345-377.

Cotton, W.R., 1990: *Storms*, Vol. 1. 1st ed. ASTeR Press, Fort Collins, CO, 47-53.

--------, and R.A. Anthes, 1989: *Storm and cloud dynamics*, Vol. 44. Academic Press Inc., San Diego, CA, 564-577.

Court, A., and J.F. Griffiths, 1986: Thunderstorm climatology. *Thunderstorms: A social, scientific and technological documentary.* 2nd ed. University of Oklaholma Press, Vol. 2, pp. 11-52.

Deibert, R.J., 1977: Alberta Hail Project field program, Report No. 6, 92 pp.

Devore, J., and R. Peck, 1990: *Introductory statistics*. West Publishing Company, Los Angeles, CA, 356-391.

Goodman, S.J., and D.R. MacGorman, 1986: Cloud-to-ground lightning activity in mesoscale convective complexes. *Mo. Wea. Rev.*, **114**, 2320-2328.

Hane, C.E., 1986: Mesoscale meteorology and forecasting; *extratropical squall lines*. American Meteorological Society, Boston, 363 pp.

Hanuta, S., and S. LaDochy, 1989: Thunderstorm climatology based on lightning detector data, Manitoba, Canada. *Phys. Geog.* **10**, 101-119.

Hermann, B.D., M.A. Uman, R.D. Brantley, and E.P. Krider, 1976: Test of the principle of operation of the wideband magnetic direction finder for lightning return strokes. *J. Appl. Meteo.*, **15**, 402-405.

Holle, R.L., A.I. Watson, R.E. Lopez, D.R. MacGorman, and R. Ortiz, 1994: The life cycle of lightning and severe weather in a 3-4 June 1985 PRE-STORM mesoscale convective system. *Mo. Wea. Rev.*, **122**, 1798-1808.

Keighton, S.J., H.B. Bluestein, D.R. MacGorman, 1991: The evolution of a severe mesoscale convective system: cloud-to-ground lightning location and storm structure. *Mo. Wea. Rev.*, **119**, 1533-1556.

Krehbiel, P.R., M. Brook, R.L. Lhermitte, and C.L. Lennon, 1983: Proceedings in atmospheric electricity; *lightning charge structure in thunderstorms*. A. Deepak Publ., Hampton, Virginia, 408-410.

Krider, E.P., R.C. Noggle, A.E. Pifer,, and D.L. Vance, 1980: Lightning direction finding systems for forest fire detection. *Bull. Amer. Meteor. Soc.*, **61**, 980-986.

Lopez, R.E., and R.L. Holle, 1986: Diurnal and spatial variability of lightning activity in northeastern Colorado and central Florida during the summer. *Mon. Wea. Rev.*, **114**, 1288-1312.

MacGorman, D.R., and K.E. Nielsen, 1991: Cloud-to-ground lightning in a tornadic storm on 8 May 1986. *Mo. Wea. Rev.*, **119**, 1557-1574.

Mackerras, D., and M. Darveniza, 1994: Latitudinal variation of lightning occurrence characteristics. *J. Geophys, Res.*, **99**, 10,813-10,821.

Maier, L.M., E.P. Krider, and M.W. Maier, 1984: Average diurnal variation of summer lightning over the Florida peninsula. *Mo. Wea. Rev.*, **112**, 1134-1140.

Mason, B.J., 1976: In reply of a critique of precipitation theories of thunderstorm electrification by C. B. Moore. *Quar. J. Roy. Meteor. Soc.*, **102**, 219-225.

Moore, C.B., 1976: Reply (to B. J. Mason). Quart. J. Roy. Meteor. Soc., **102**, 225-240.

--------, and B. Vonnegut, 1977: Lightning; *the thundercloud*, Vol. 1. Academic Press, New York, NY, Chapter 3., 51-98.

Orville, R.E., 1990: Winter lightning along the East Coast. *Geophys. Res. Letters*, **17**, 713-715.

--------, 1991: Annual summary: Lightning ground flash density in the contiguous United States - 1989. *Mon. Wea. Rev.*, **119**, 573-577.

--------, 1994: Cloud-to-Ground lightning flash characteristics in the contiguous United States: 1989-1991. *J. Geophys. Res.*, **99**, 10,833-10,841.

--------, and D.W. Spencer, 1979: Global lightning flash frequency. *Mon. Wea. Rev.*, **107**, 934-943.

--------, and R.W. Henderson, 1986: Global distribution of midnight lightning: September 1977 to August 1988. *Mon. Wea. Rev.*, **114**, 2640-2653.

Pakiam, J.E., and J. Maybank, 1975: The electrical characteristics of some severe hailstorms in Alberta, Canada. *J. Meteorol. Soc. Jpn*, **53**, 363-383.

Rabin, R.M., S. Stadler, P.J. Wetzel, D.J. Stensrud, and M. Gregory, 1990: Observed effects of landscape variability on convective clouds. *Bull. Amer. Meteor. Soc.*, **71**, 272-280.

Ray, P.S., D.R. MacGorman, and W.D. Rust, 1987: Lightning location relative to storm structure in a supercell storm and a multicell storm. *J. Geophys. Res.*, **92**, 5713-5724.

Reuter, G.W., and N. Aktary, 1995: Convective and symmetric instabilities and their effects on precipitation: seasonal variations on central Alberta during 1990 and 1991. *Mon. Wea. Rev.*, **123**, 153-162.

--------, and R. Beubien, 1996: Radar observations of snow formation in a warm pre-frontal snowband. *Atmos. – Ocean.*, **34**, 605-626.

Rogers, R.R., and N.K. Sakellariou 1986: Precipitation production in three Alberta thunderstorms. *Atmos. – Ocean.*, **24**, 293 pp.

Rust, W.D., W.L. Taylor, and D.R. MacGorman, 1981: Research on electrical properties of severe thunderstorms in the Great Plains. *Bull. Am. Meteorol. Soc.*, **62**, 1286-1293.

Rutledge, S.A., and D.R. MacGorman, 1988: Cloud-to-ground lightning activity on the 10-11 June 1985 mesoscale convective system observed during the Oklahoma PRE-STORM project. *Mo. Wea. Rev.*, **116**, 1393-1408.

Schonland, B.F.J., 1953: *Atmospheric electricity*. 2nd ed. John Wiley and Sons, New York, NY, 80-82.

Smith, S.B., and M.K. Yau, 1993: The cause of severe convective outbreaks in Alberta. Part I: A comparison of a severe outbreak with two nonsevere events. *Mon. Wea. Rev.*, **121**, 1099-1125.

Summers, R., and A. Paul, 1970: Weather and Climate; *Some climatological characteristics of hailfall in central Alberta*. Methuen, Toronto, 193-211.

Uman, M.A., 1971: *Understanding lightning*. Bek Technical Publications Inc., Carnegie, PA, 166 pp.

Vonnegut, B., 1963: Some facts and speculations concerning the origin and role of thunderstorm electricity. *Met. Monogr.*, **5**, 224-241.

Williams, E.R., 1985: Large-scale charge separation in thunderclouds. *J. Geophys. Res.*, **90**, 6013-6025.

Wojtiw, L., 1977: Climatology of hailstorms in central Alberta. *The Albertan Geographer*, Univ. of Alberta, **13**, 15-30.

Wojtiw, L., 1986: *A bibliography of weather modification and related topics conducted in Alberta*. Alberta Research Council, Edmonton, Alberta, 1-53.

Xin, L., and G.W. Reuter, 1996: Numerical simulation of the effects of mesoscale convergence on convective rainshowers. *Mon. Wea. Rev.*, **124**, 2828-2842.

----, and ------, 1998: VVP technique applied to an Alberta storm. *J. Atmos. Oceanic Technol.*, **15**, 587-592.

----, G.W. Reuter, and B. Larochelle, 1997: Reflectivity-rain rate relationships for convective rainshowers in Edmonton. *Atmos. – Ocean.*, **35**, 513-521.

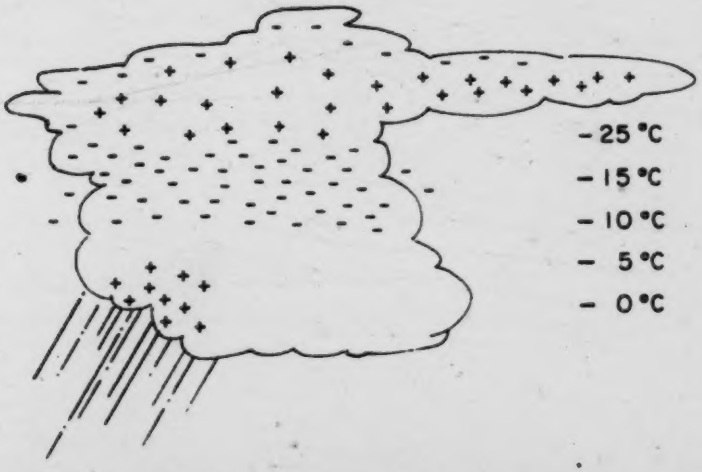

FIG. 1.1. The top of the storm is positively charged with the exception of a thin layer of negative charge right at the cloud top. Centered near -15°C is a layer of negative charge. Positive charge of a mature thunderstorm is frequently found near cloud base in rain shafts (after Cotton, 1990).

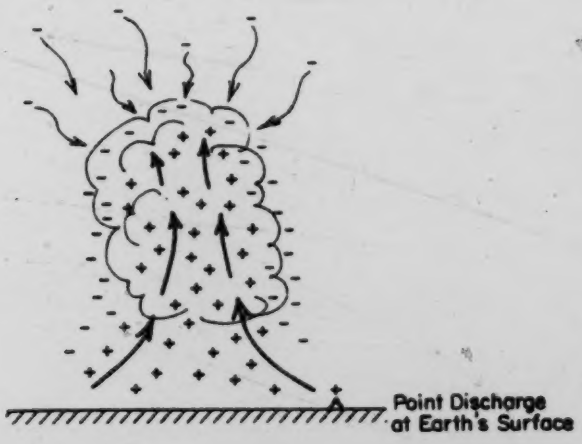

FIG. 1.2. Illustration of the convective charging theory. Positive ions are swept aloft, where they attract negative ions at the cloud boundaries. Downdrafts at the cloud edges sweep the negative ions downward where they induce point discharge at the Earth's surface supplying more positive ions (after Cotton, 1990).

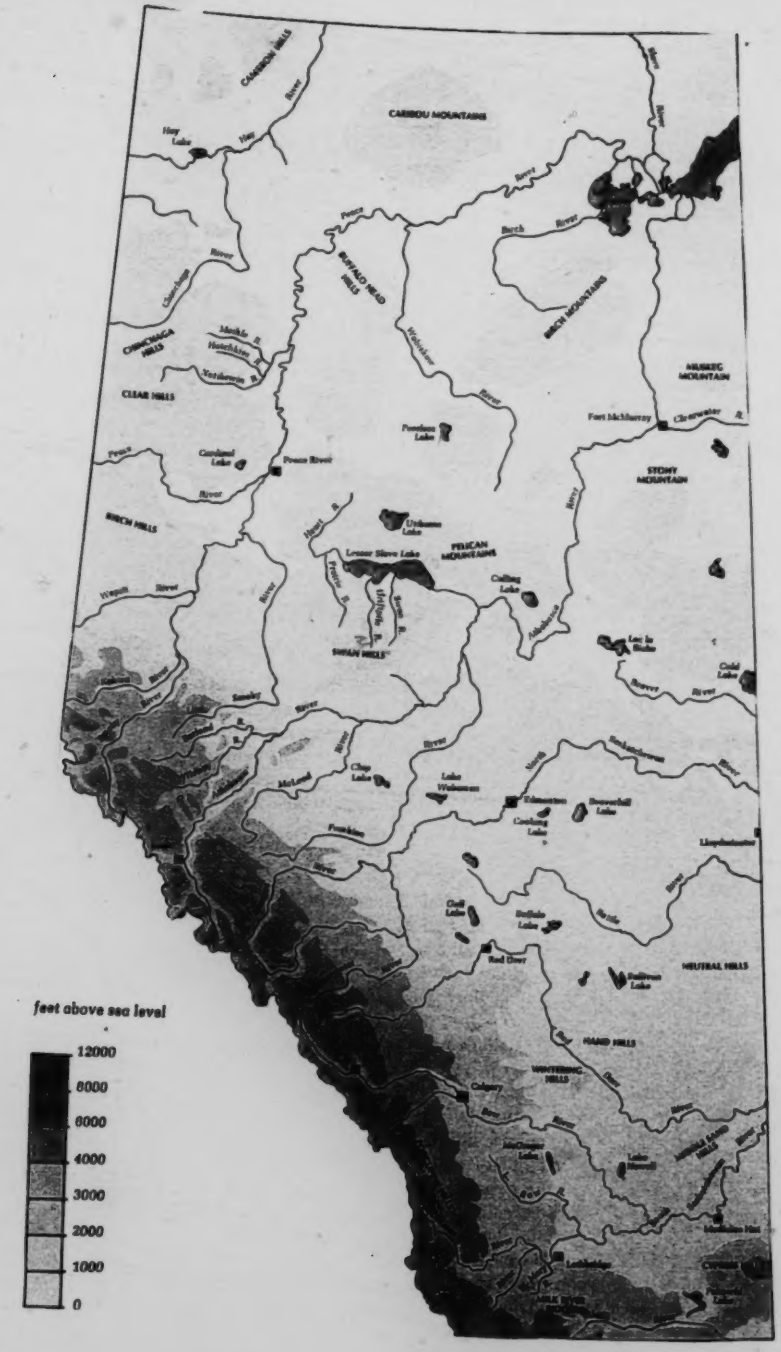

FIG. 1.3. Topographical map for Alberta contoured every 1000 feet (300 m) up to 4000 feet. Lakes and rivers are also indicated.

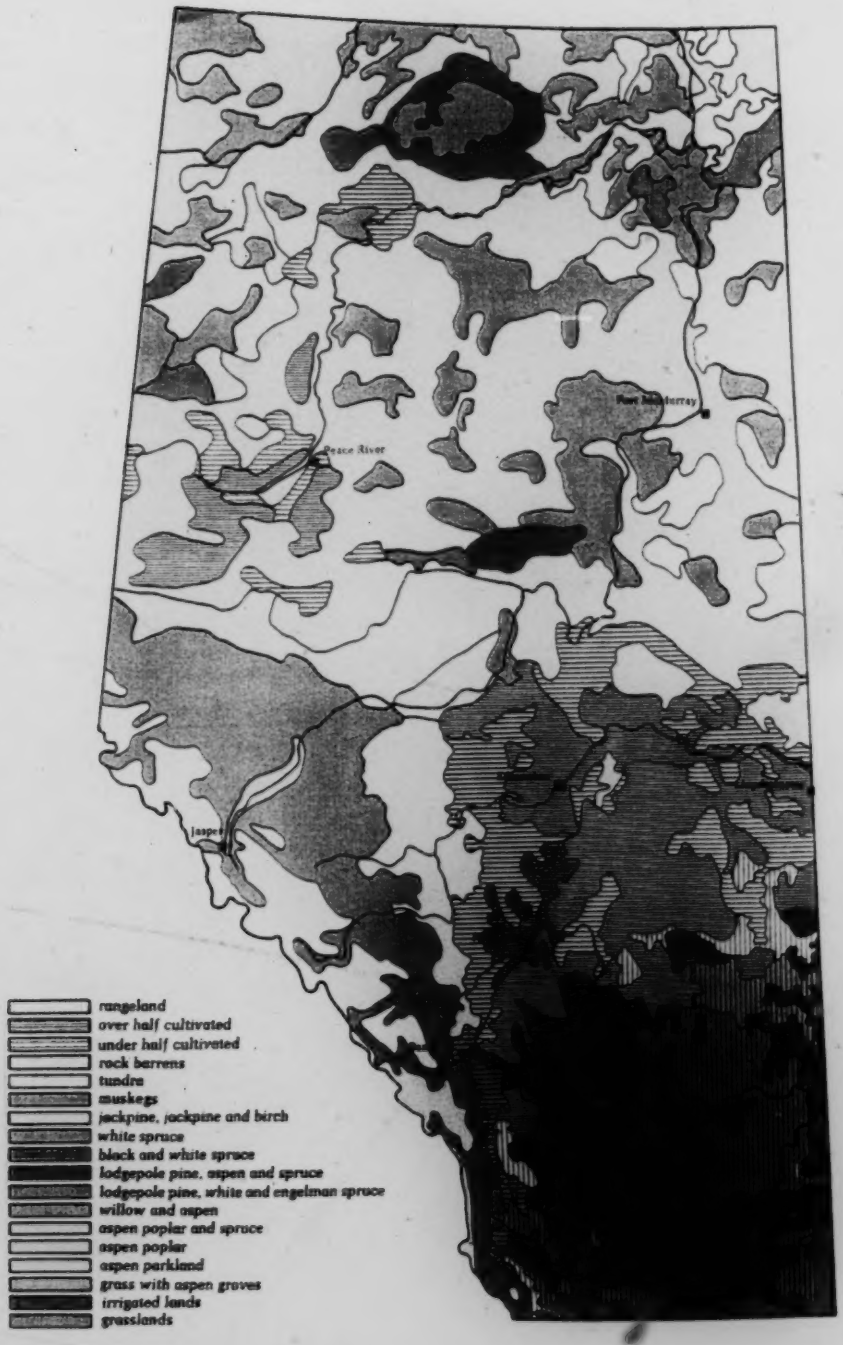

FIG. 1.4. Map of vegetation types for Alberta.

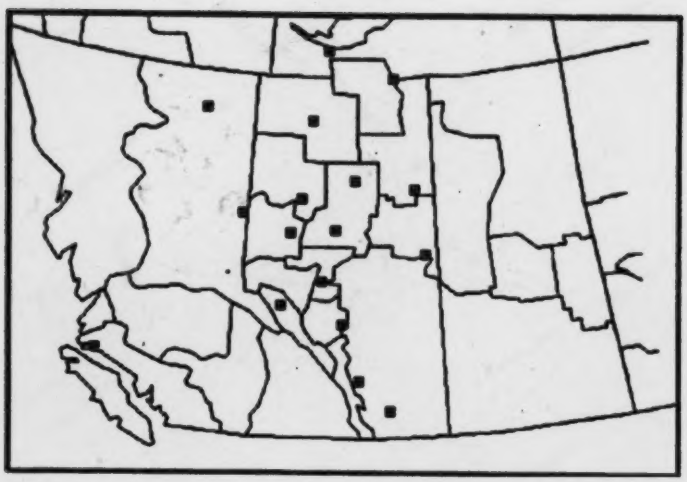

FIG. 2.1. The Alberta Forest Service's LLP lightning detection network consists of 16 lightning direction finders.

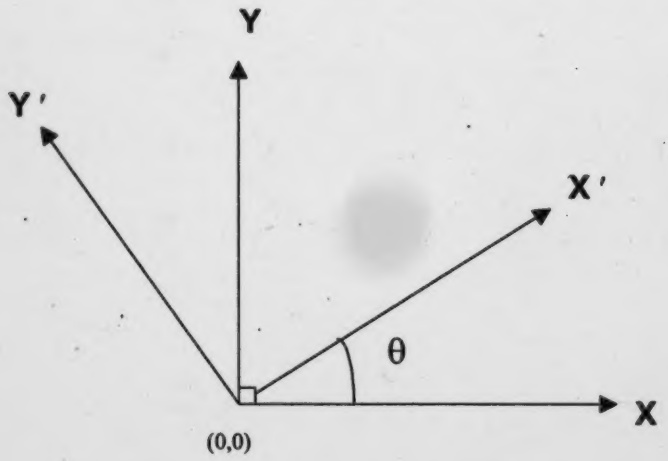

FIG. 2.2. Transforming x-y coordinate system to an x '-y ' coordinate system by rotating around the z-axis (0,0) with an angle θ.

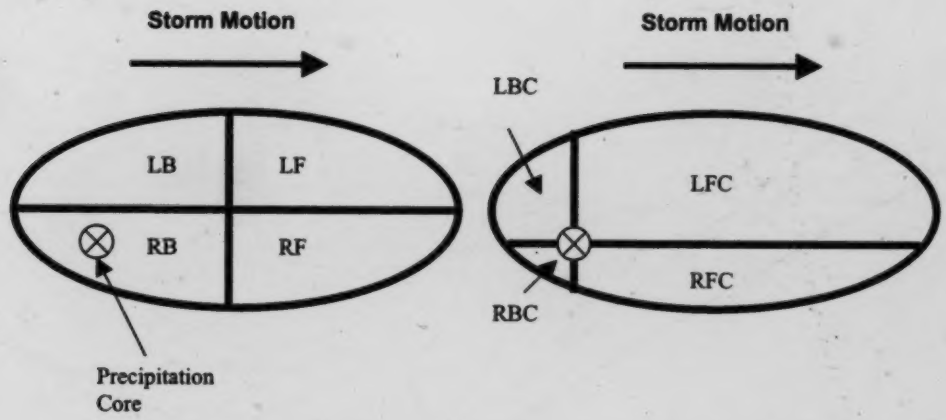

FIG. 2.3. The supercell storm of elliptical form is divided into quadrants relative to the storm center (left) and relative to the precipitation core center (right). The storm motion is in the direction of the major axis of the ellipse. LB(C) is left back, LF(C) is left front, RB(C) is right back, and RF(C) is right front.

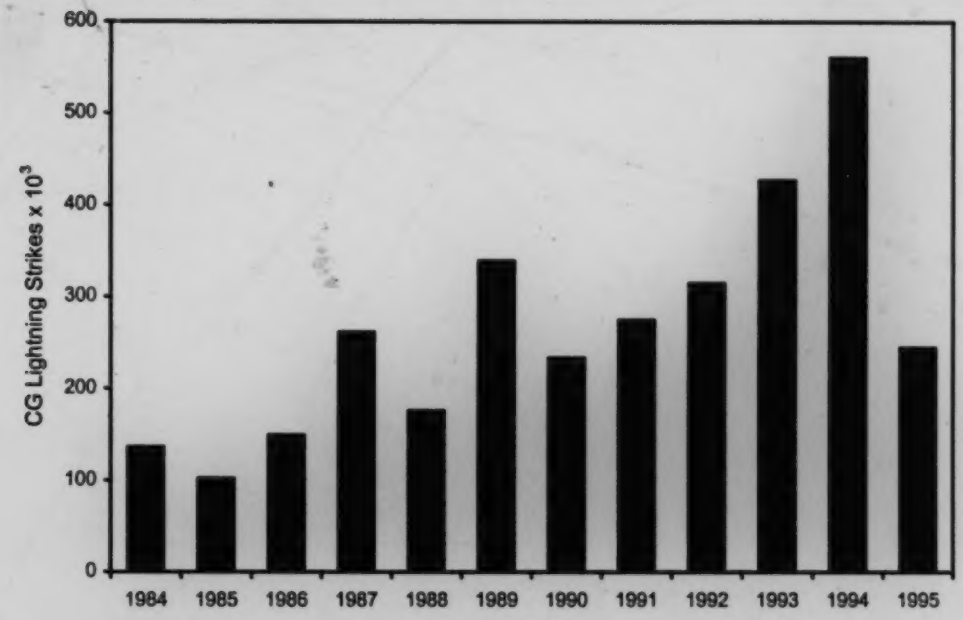

FIG. 3.1. Summertime CG lightning strike totals over Alberta from 1984-95.

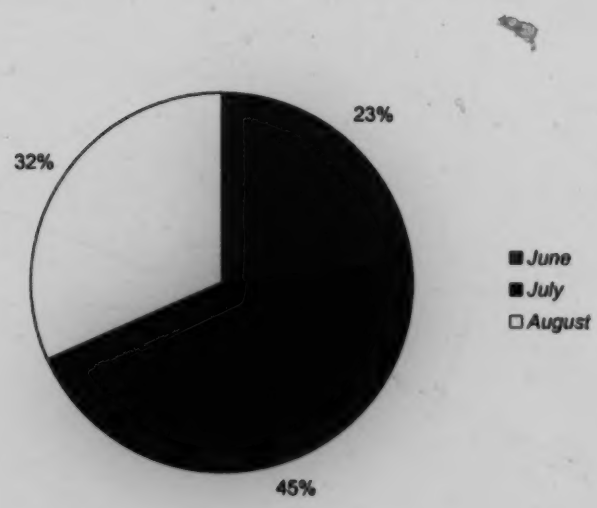

FIG. 3.2. Average percentages of CG lightning strikes that occur in June, July, and August, with respect to the summer total.

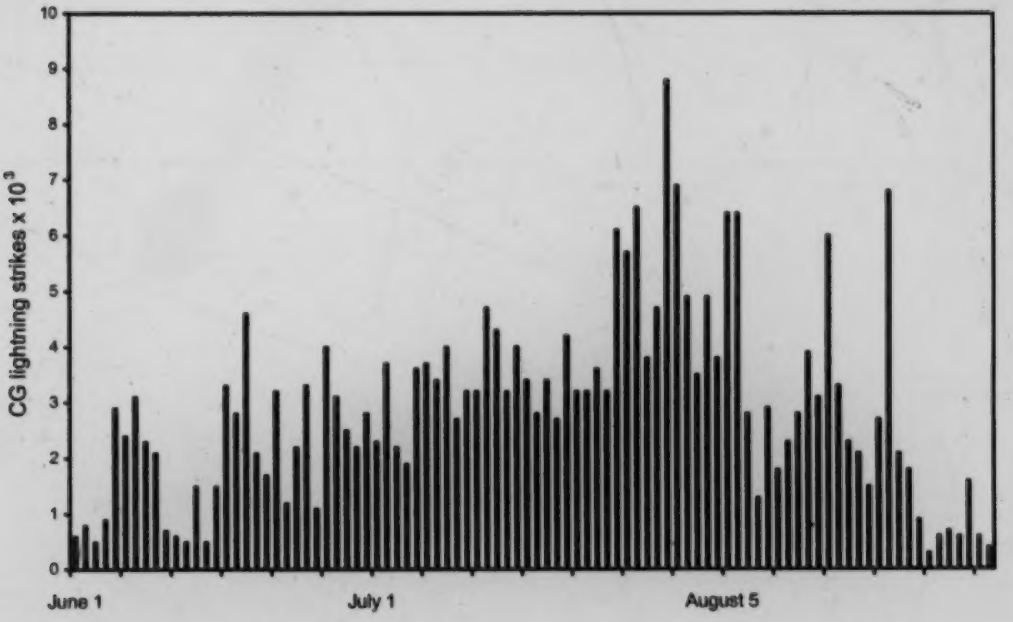

FIG. 3.3. Average CG lightning strikes per day.

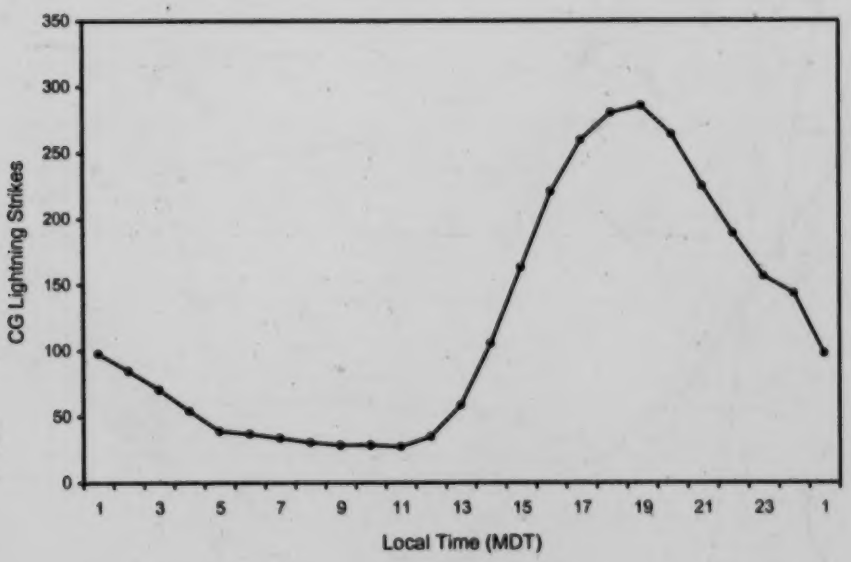

FIG. 3.4. Average diurnal cycle of CG lightning strikes.

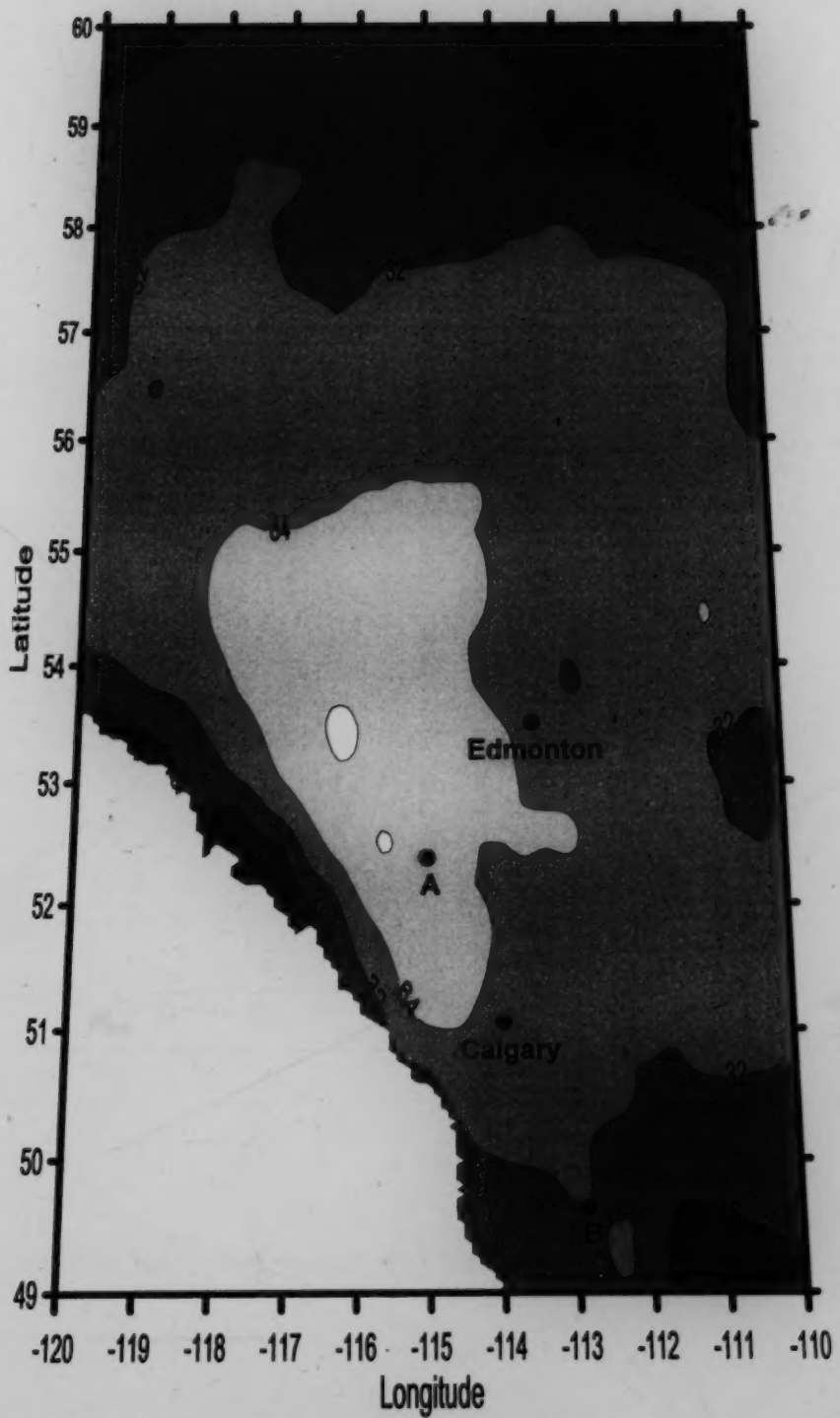

FIG. 3.5. Average summer CG lightning strike density [strikes per 10 km squared].

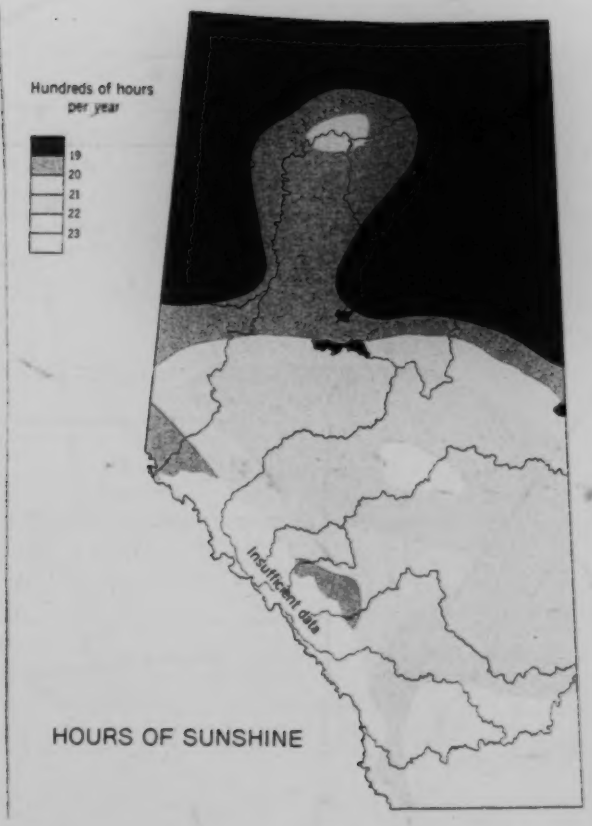

FIG. 3.6. Average annual hours (× 100) of sunshine, from 1931-60.

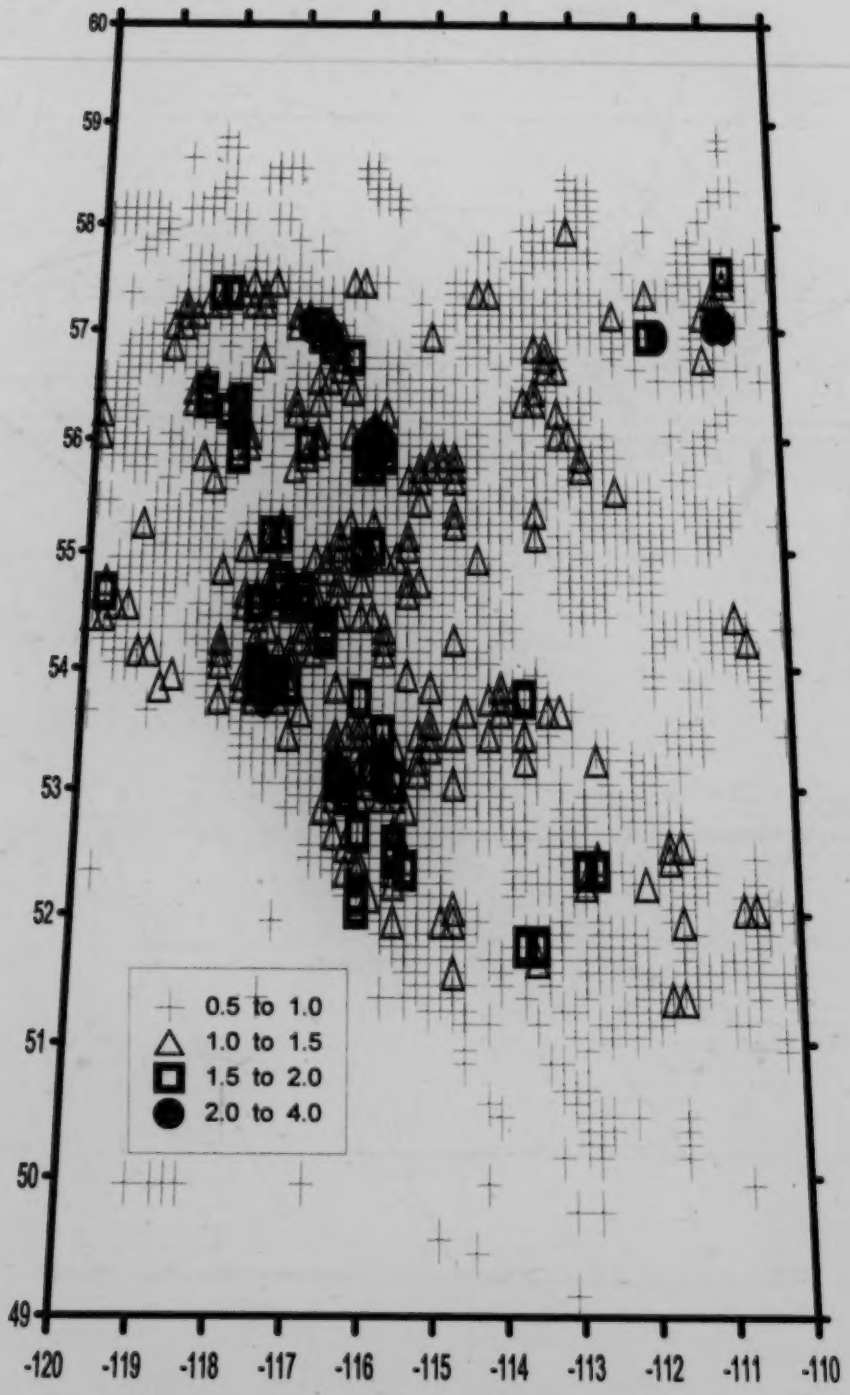

FIG. 3.7. Total 1984-95 summer high CG lightning strike positions [strikes per km squared].

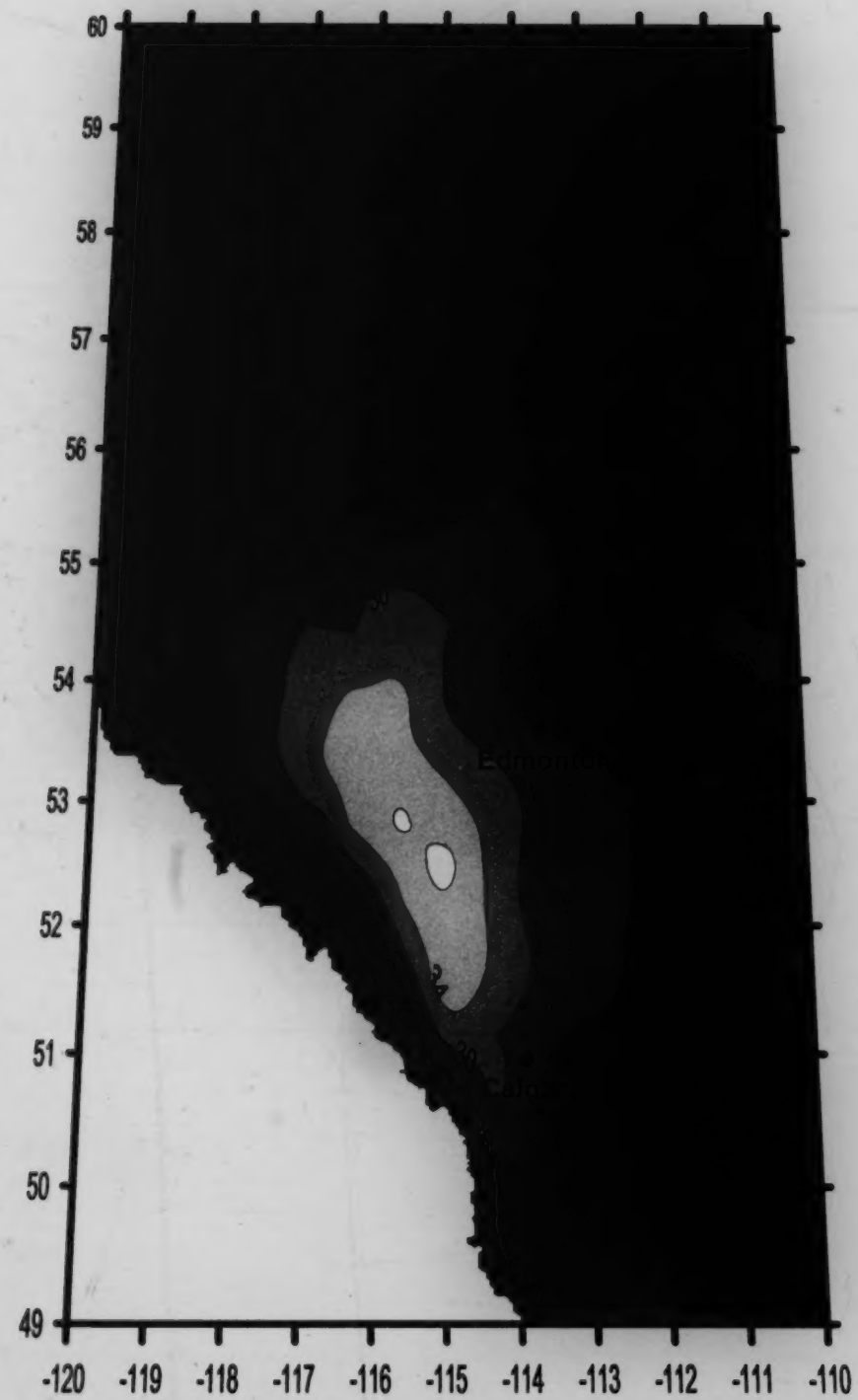

FIG. 3.8. Average summer lightning day count [lightning days per km squared].

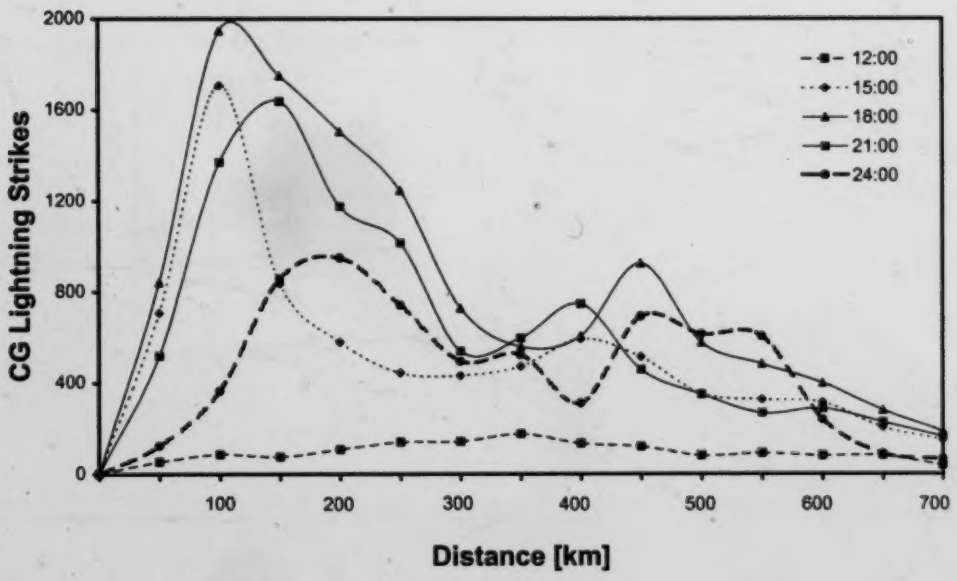

FIG. 3.9. CG lightning strikes from 12-24 MDT, in three hour intervals, as a function of the distance from the Continental Divide in km.

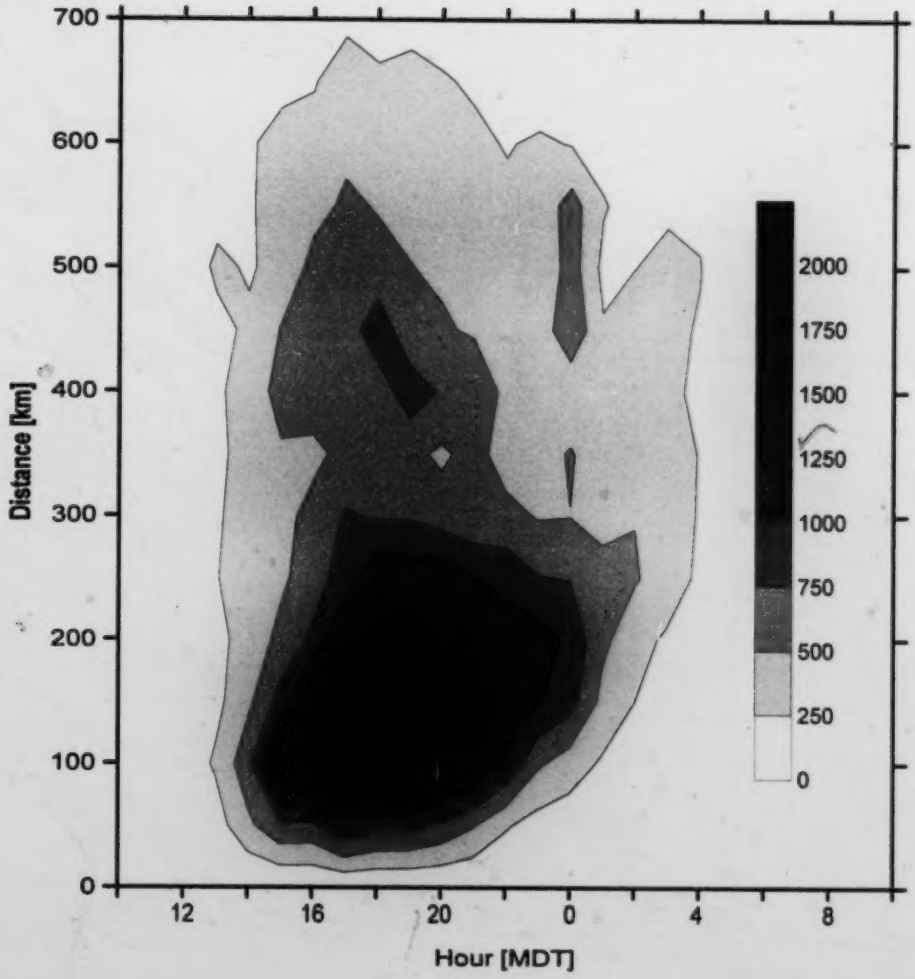

Figure 3.10. Contour plot of summertime CG lightning strikes as a function of time of day [MDT] and distance from the continental divide [km].

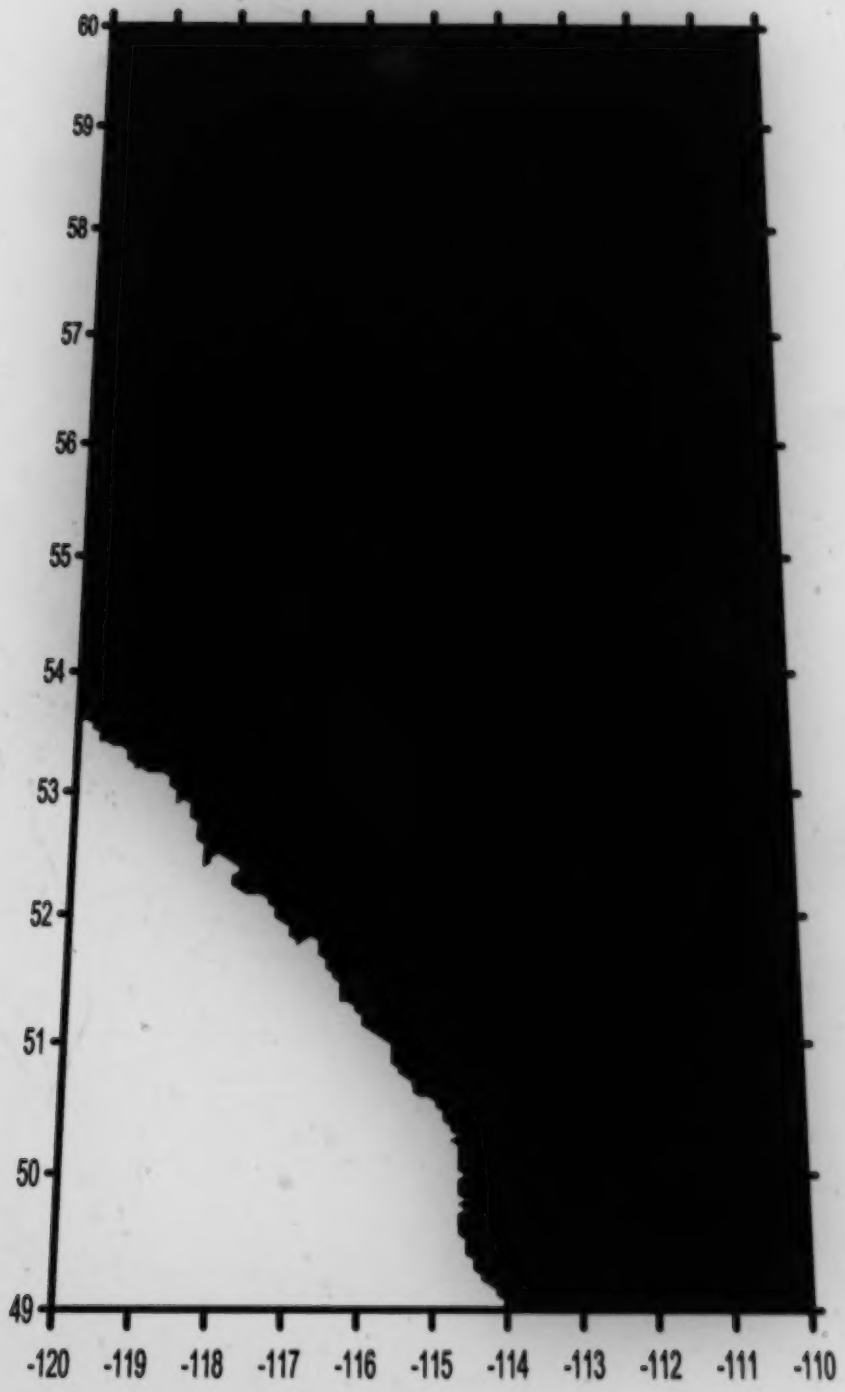

FIG. 3.11. Average June 1-15 lightning strike density.

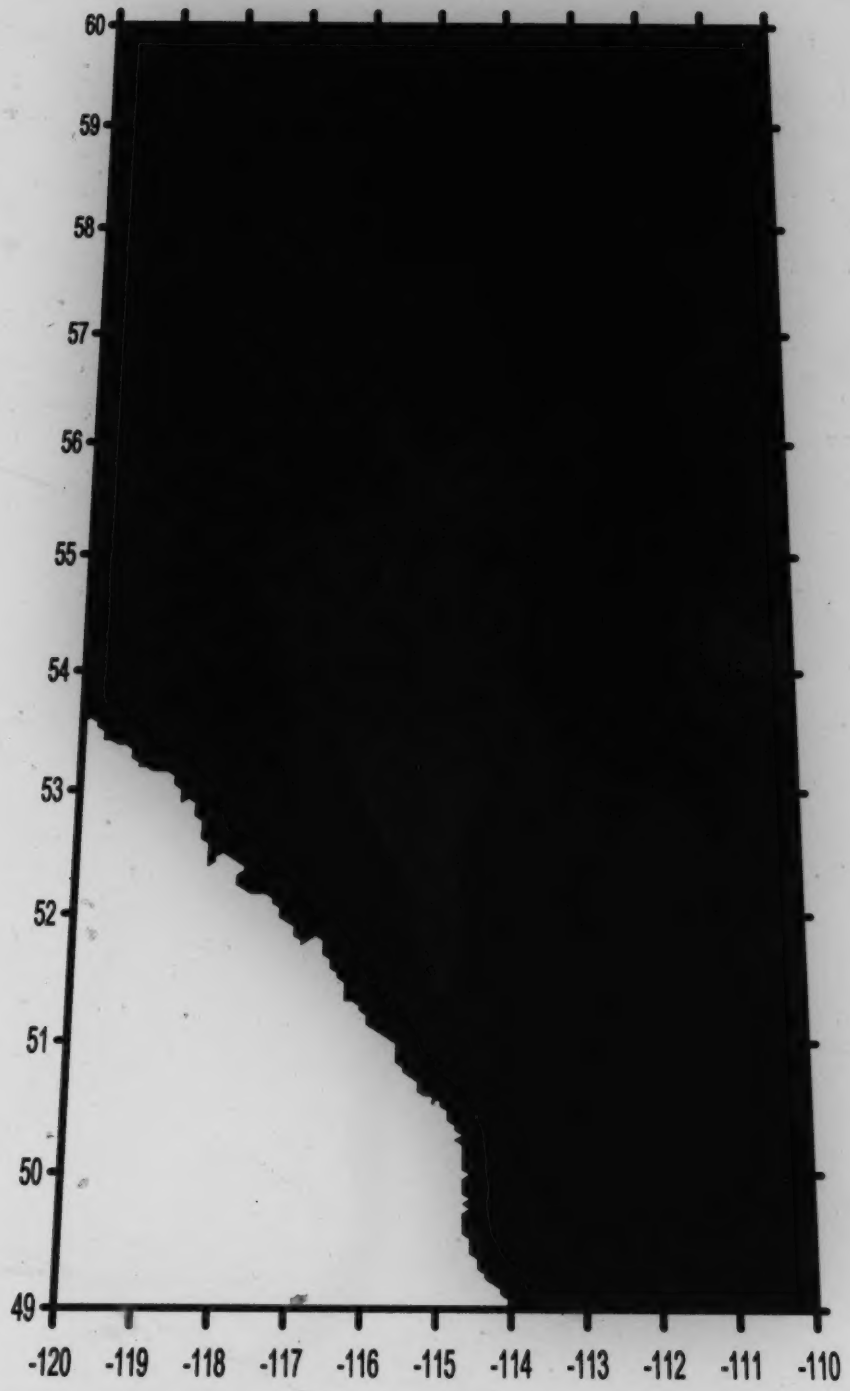

FIG. 3.12. Average June 16-30 lightning strike density.

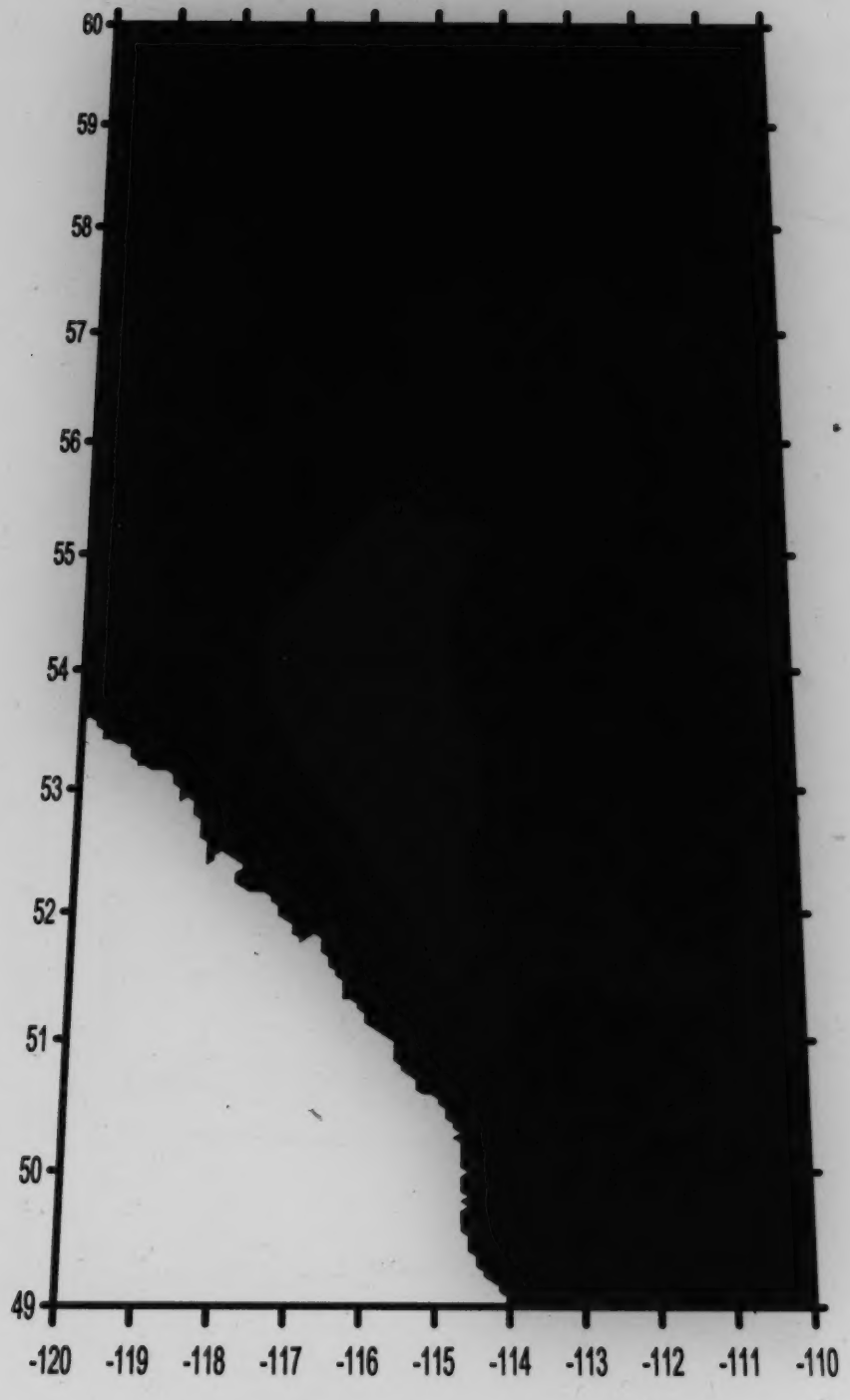

FIG. 3.13. Average July 1-15 lightning strike density.

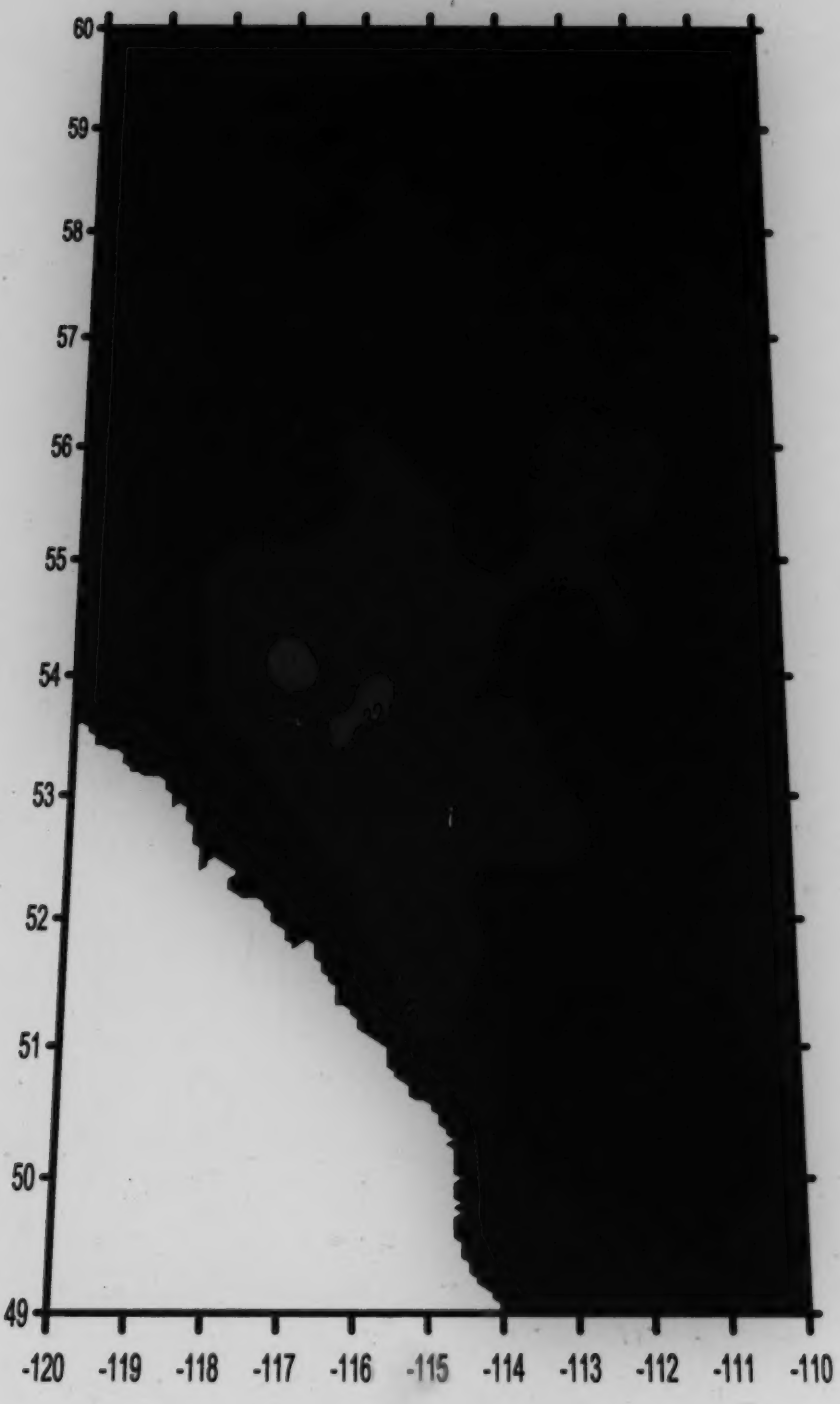

FIG. 3.14. Average July 16-31 lightning strike density.

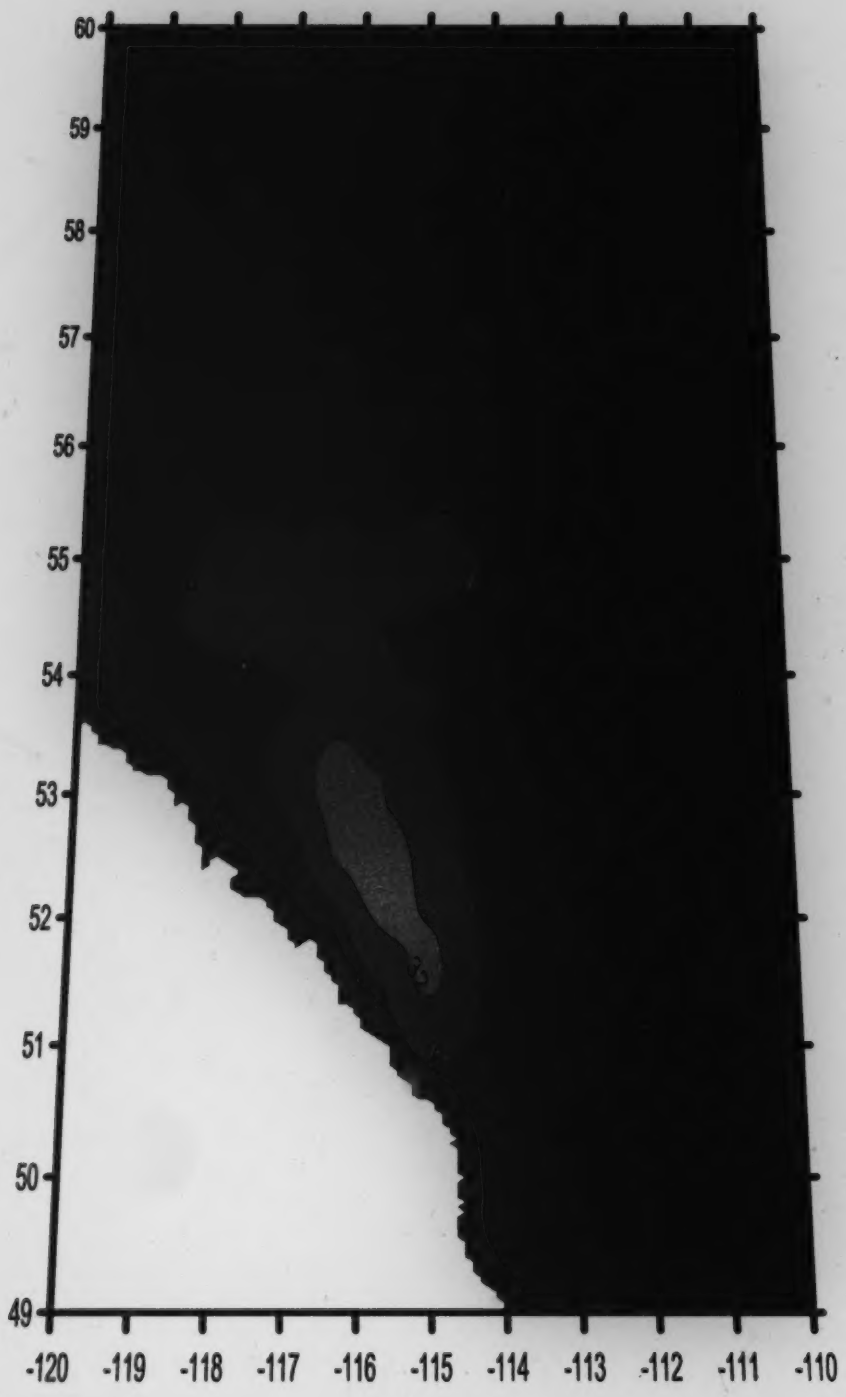

FIG. 3.15. Average August 1-15 lightning strike density.

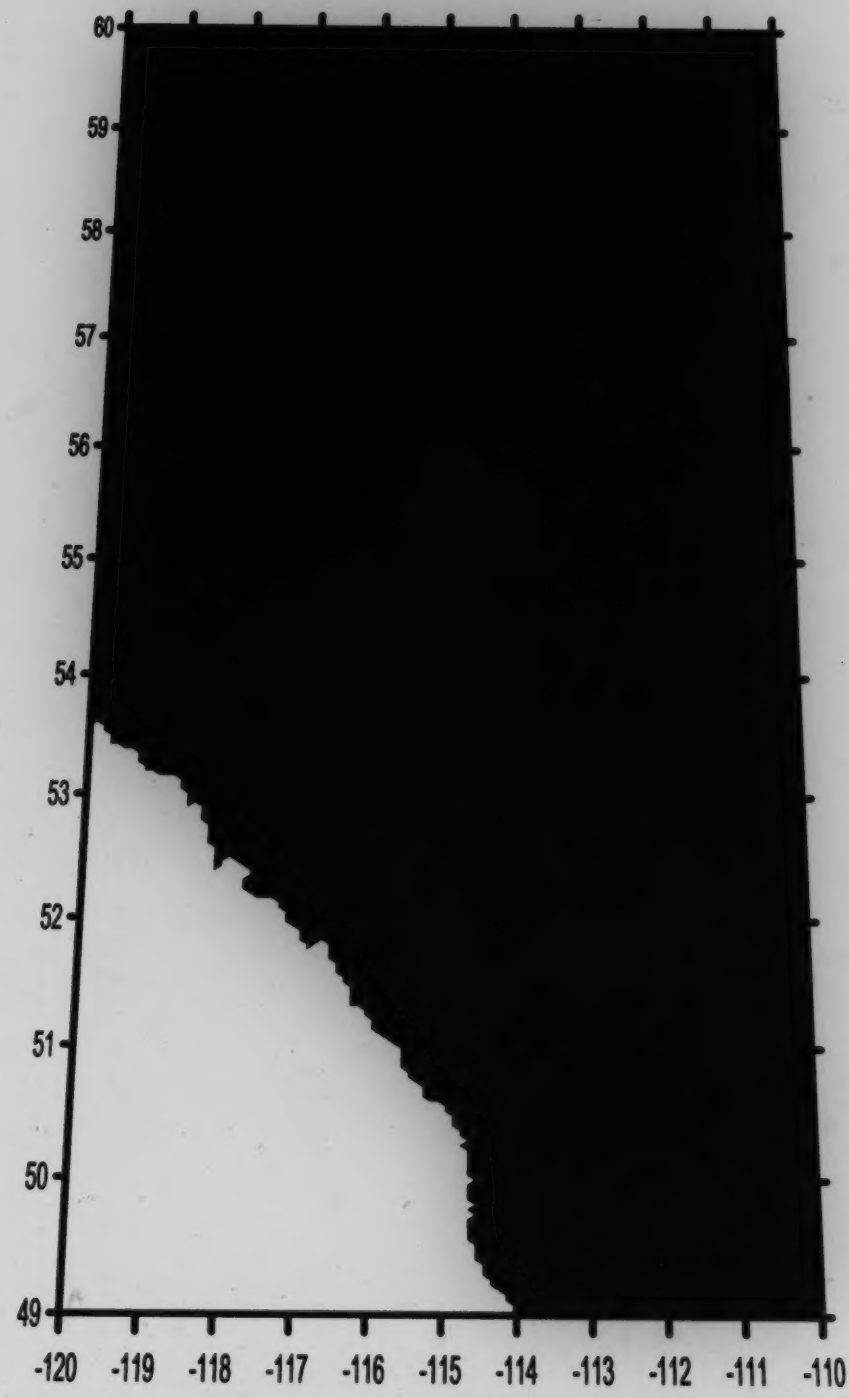

FIG. 3.16. Average August 16-31 lightning strike density.

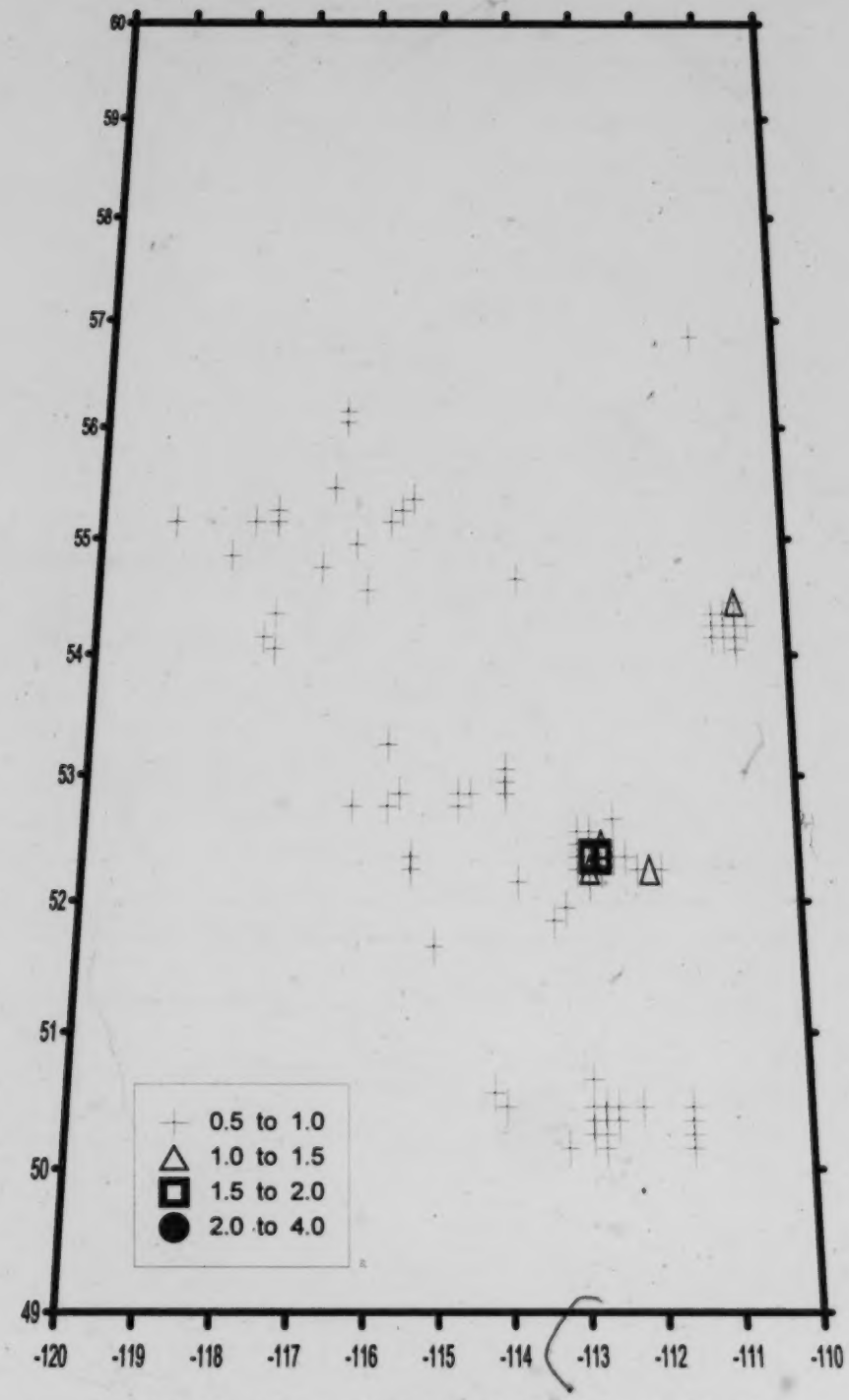

FIG 3.17. June 1-15 high lightning strike positions.

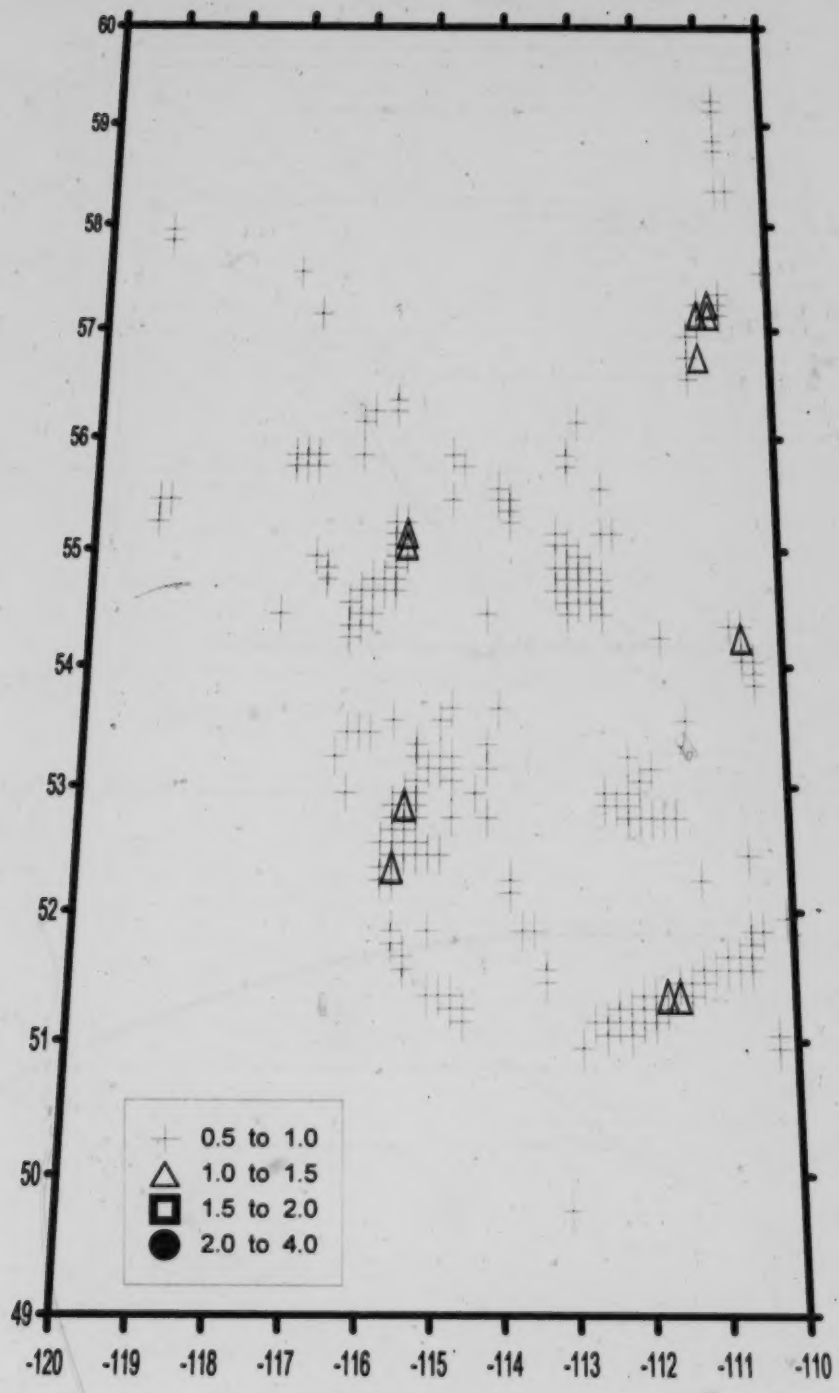

FIG. 3.18. June 16-30 high lightning strike positions.

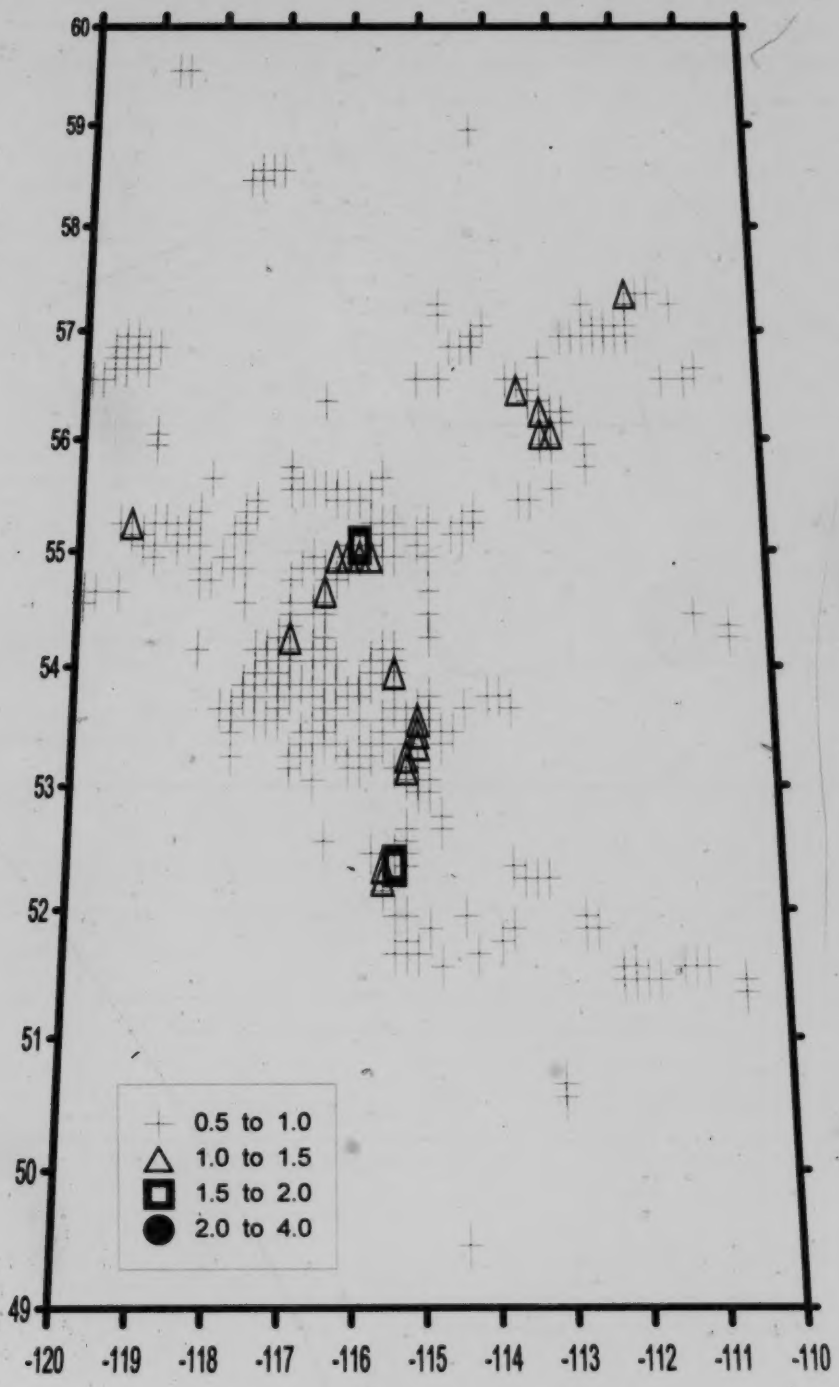

FIG. 3.19. July 1-15 high lightning strike positions.

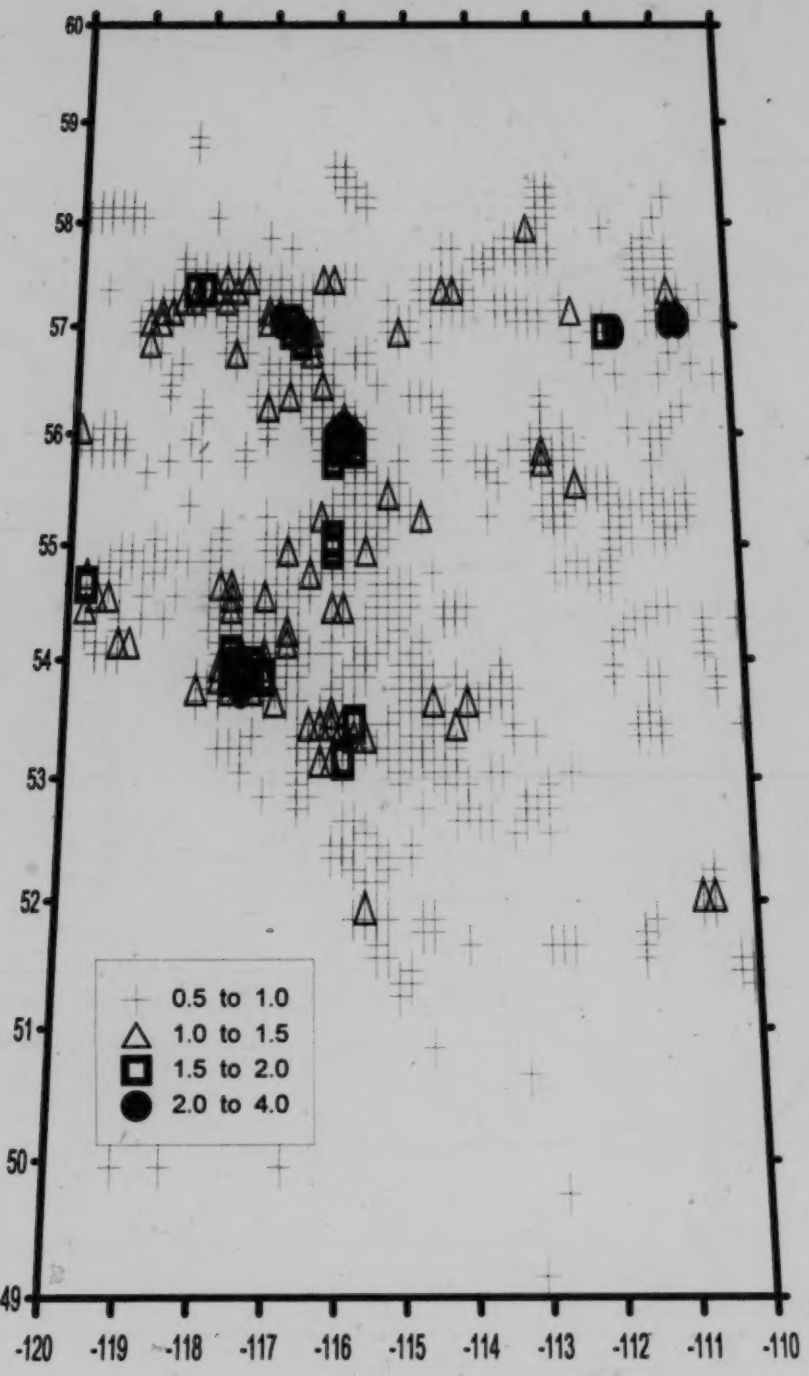

FIG. 3.20. July 16-31 high lightning strike positions.

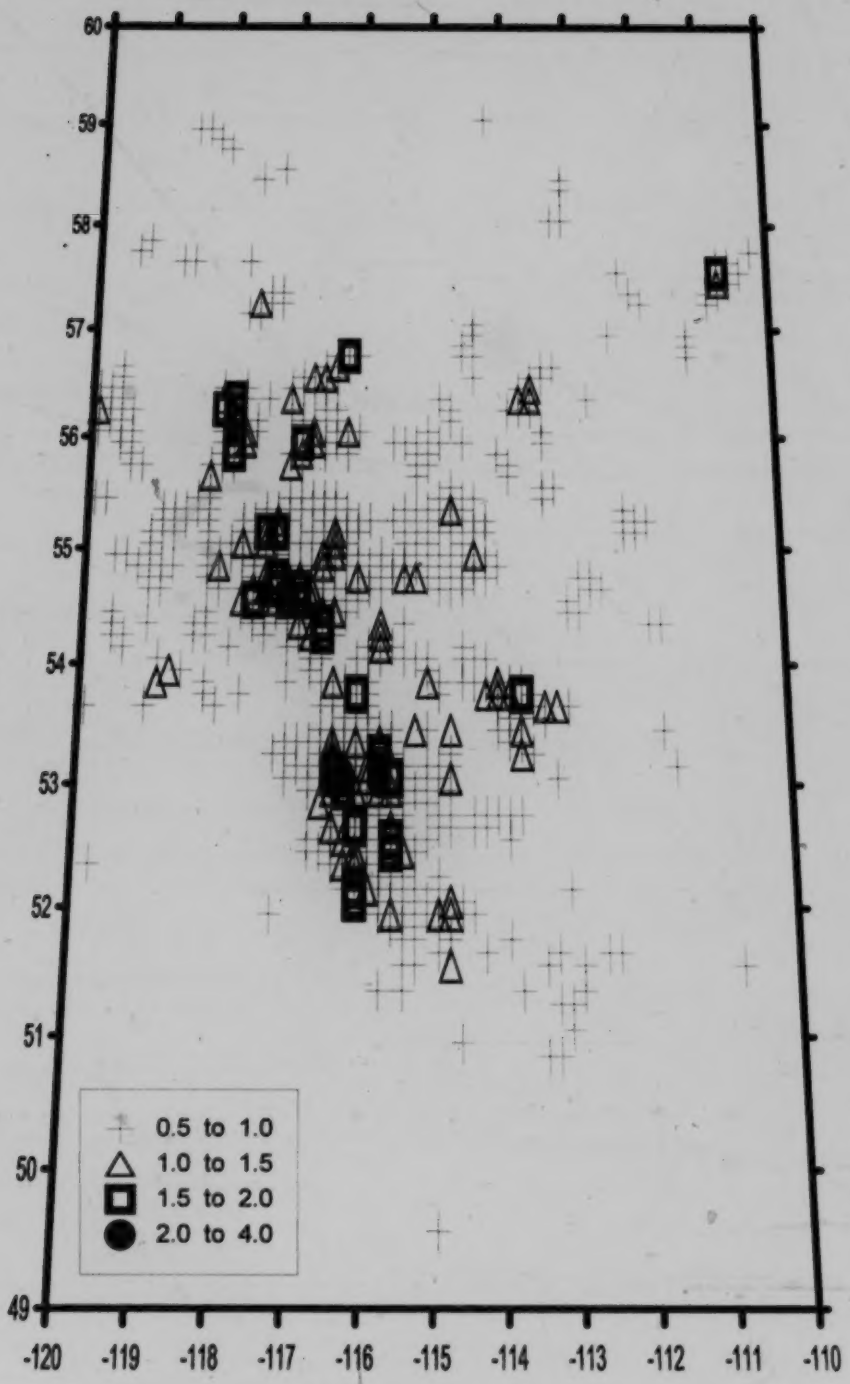

FIG. 3.21. August 1-15 high lightning strike positions.

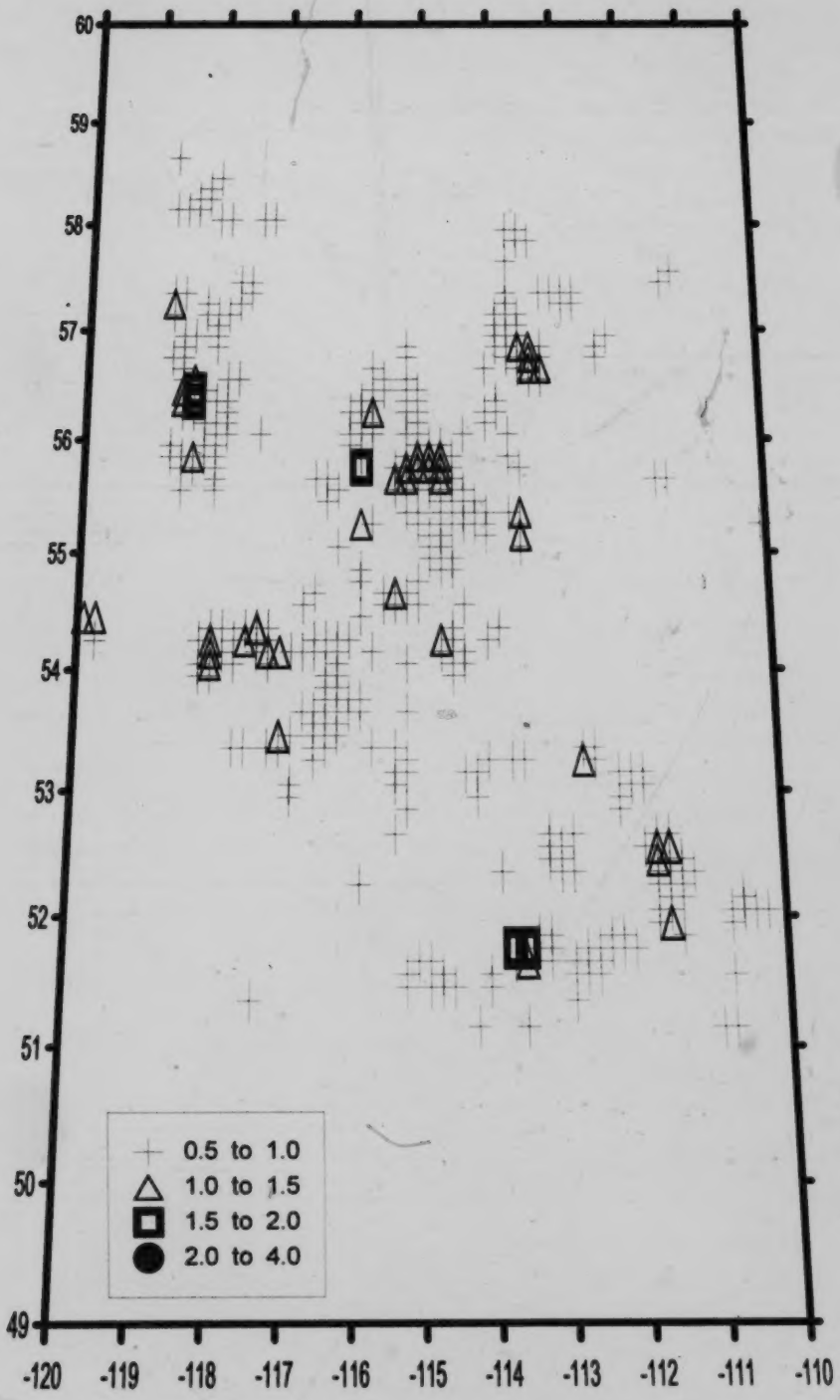

FIG. 3.22. August 16-31 high lightning strike positions.

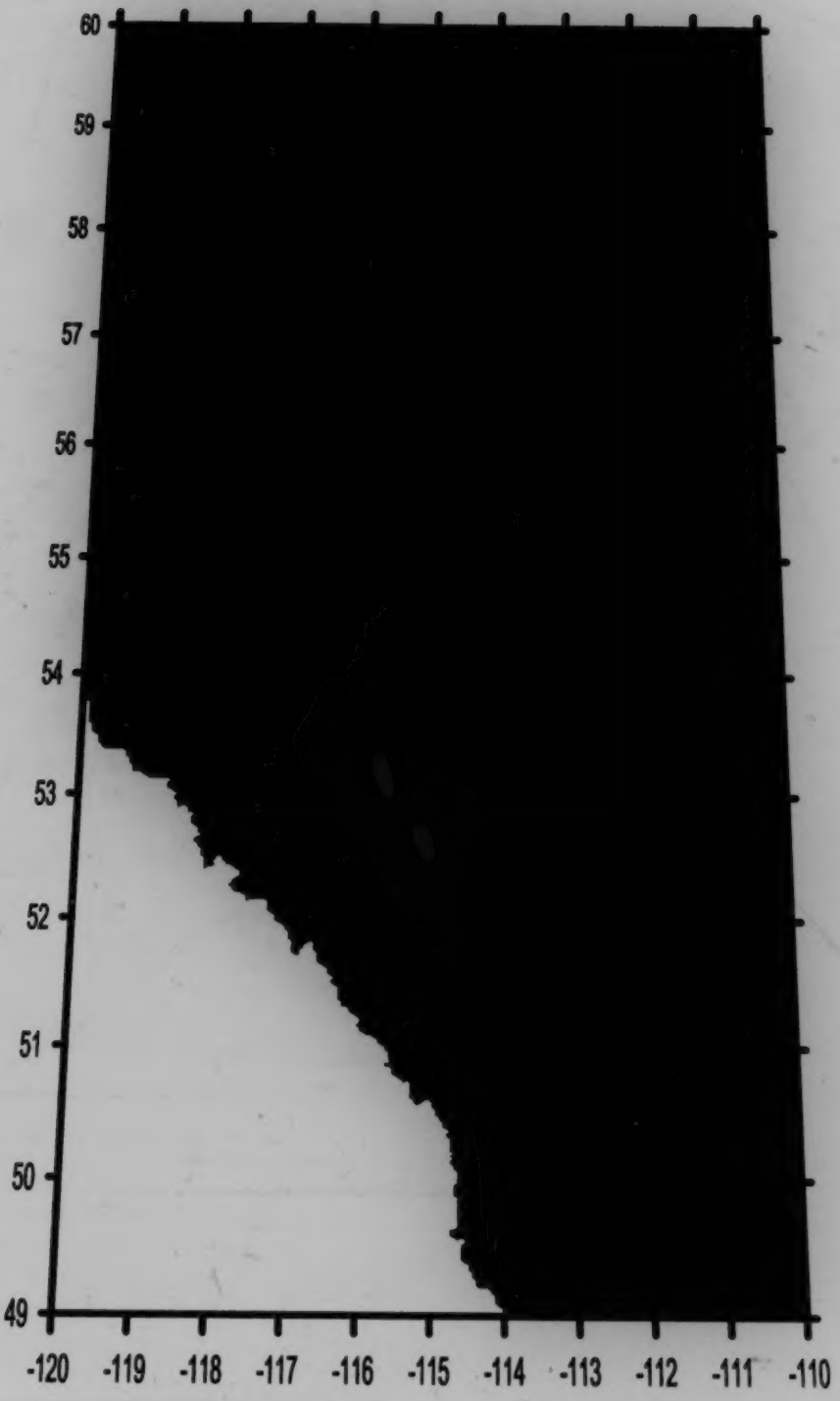

FIG. 3.23. Average June 1-15 lightning day count.

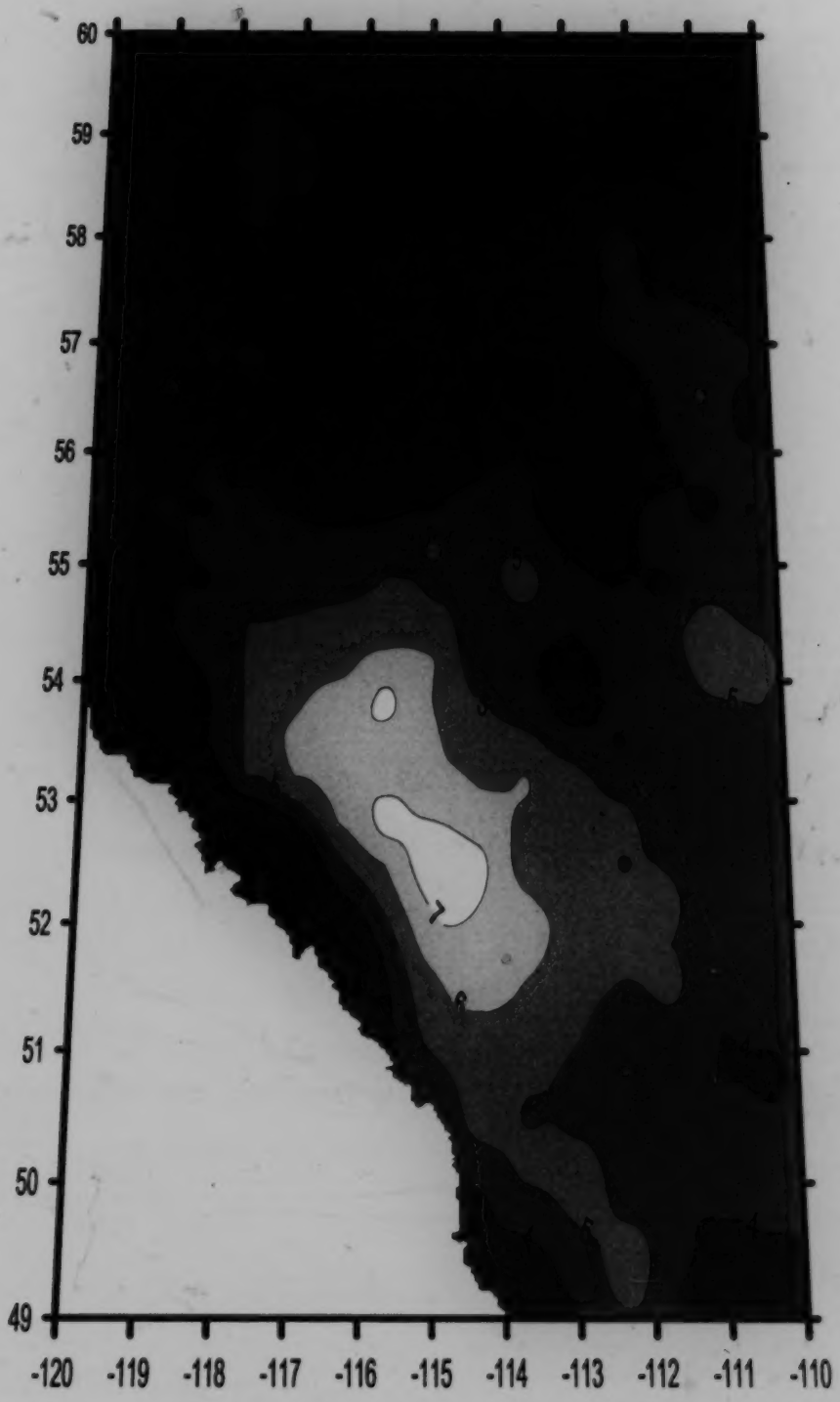

FIG. 3.24. Average June 16-30 lightning day count.

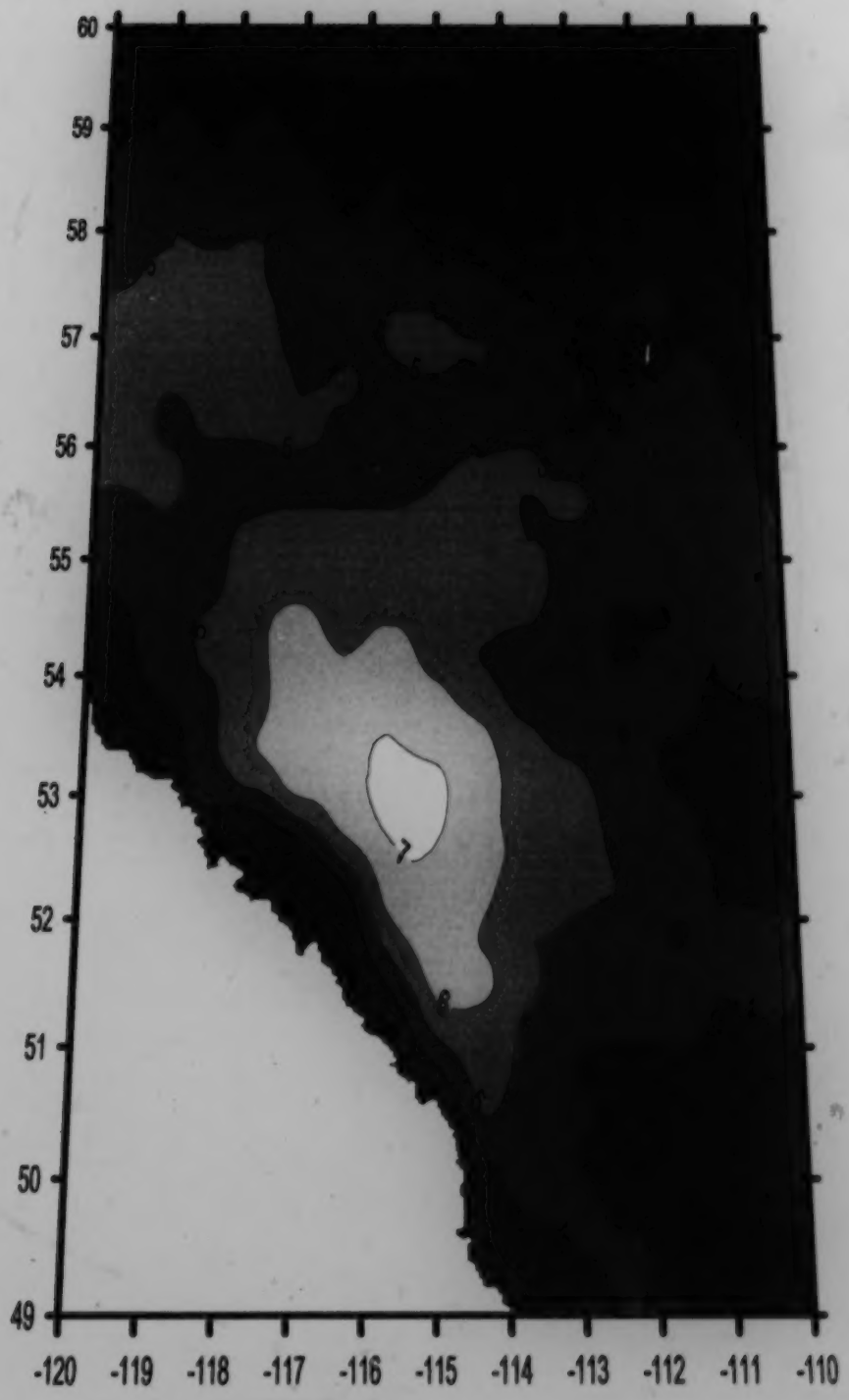

FIG. 3.25. Average July 1-15 lightning day count.

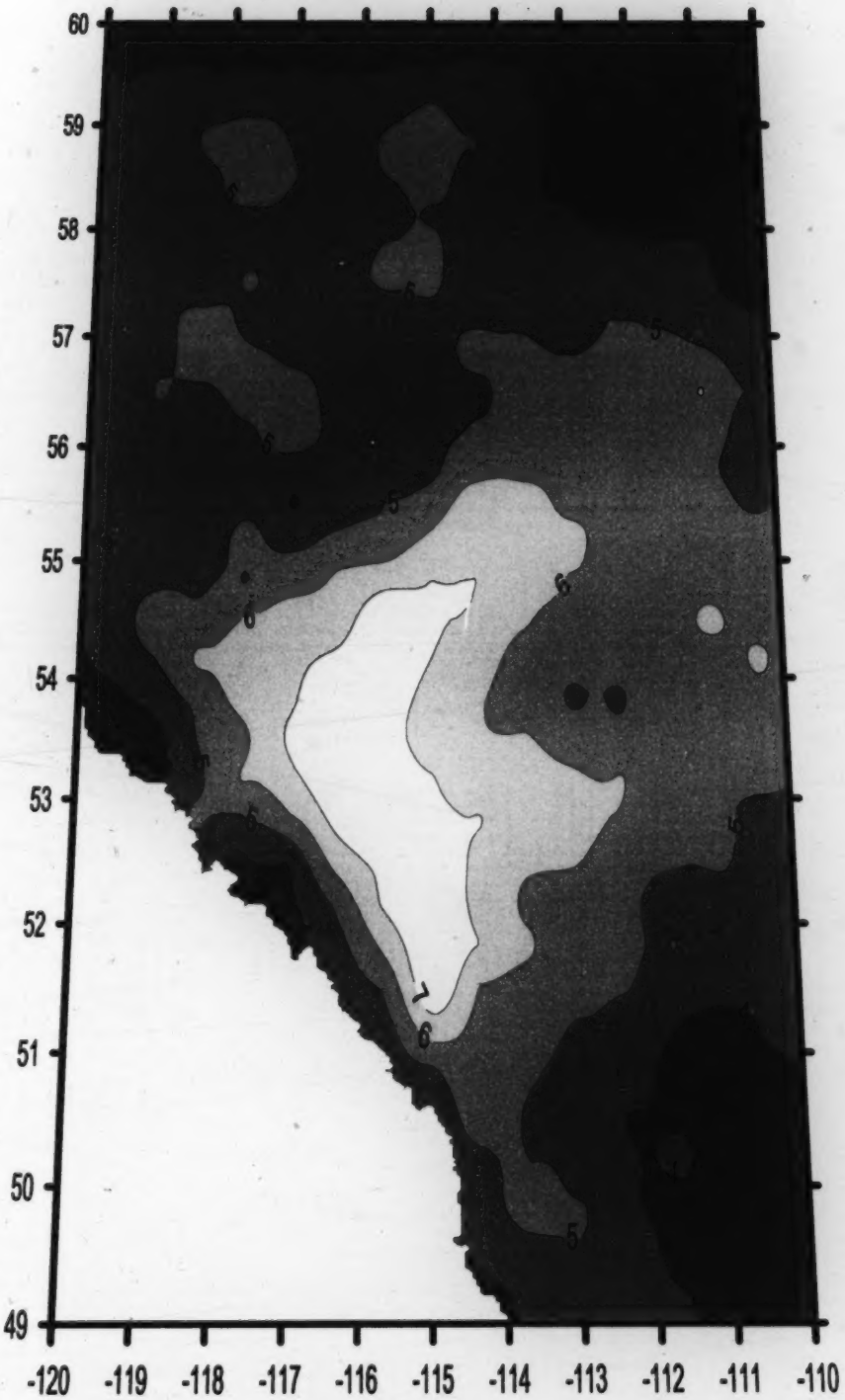

FIG. 3.26. Average July 16-31 lightning day count.

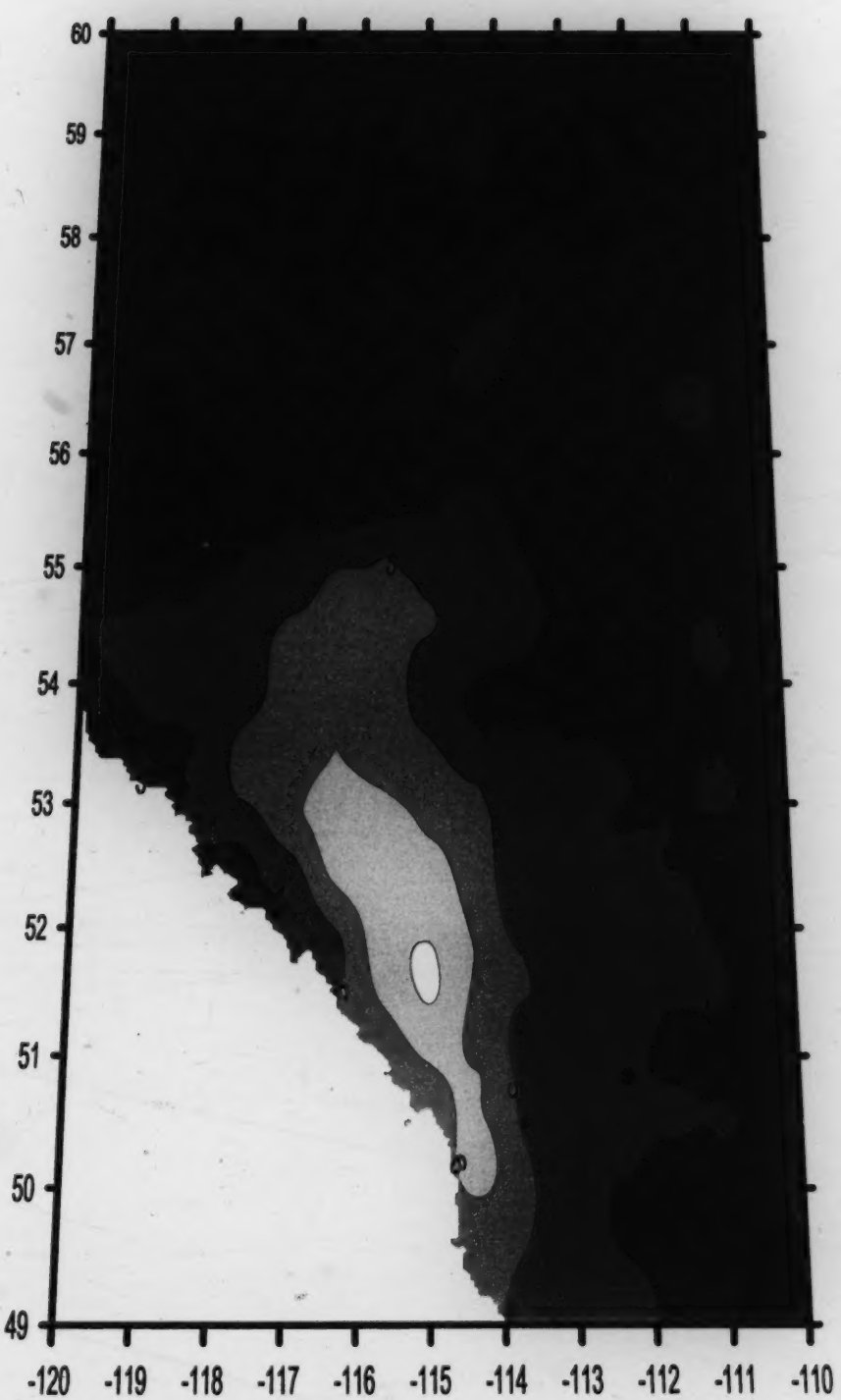

FIG. 3.27. Average August 1-15 lightning day count.

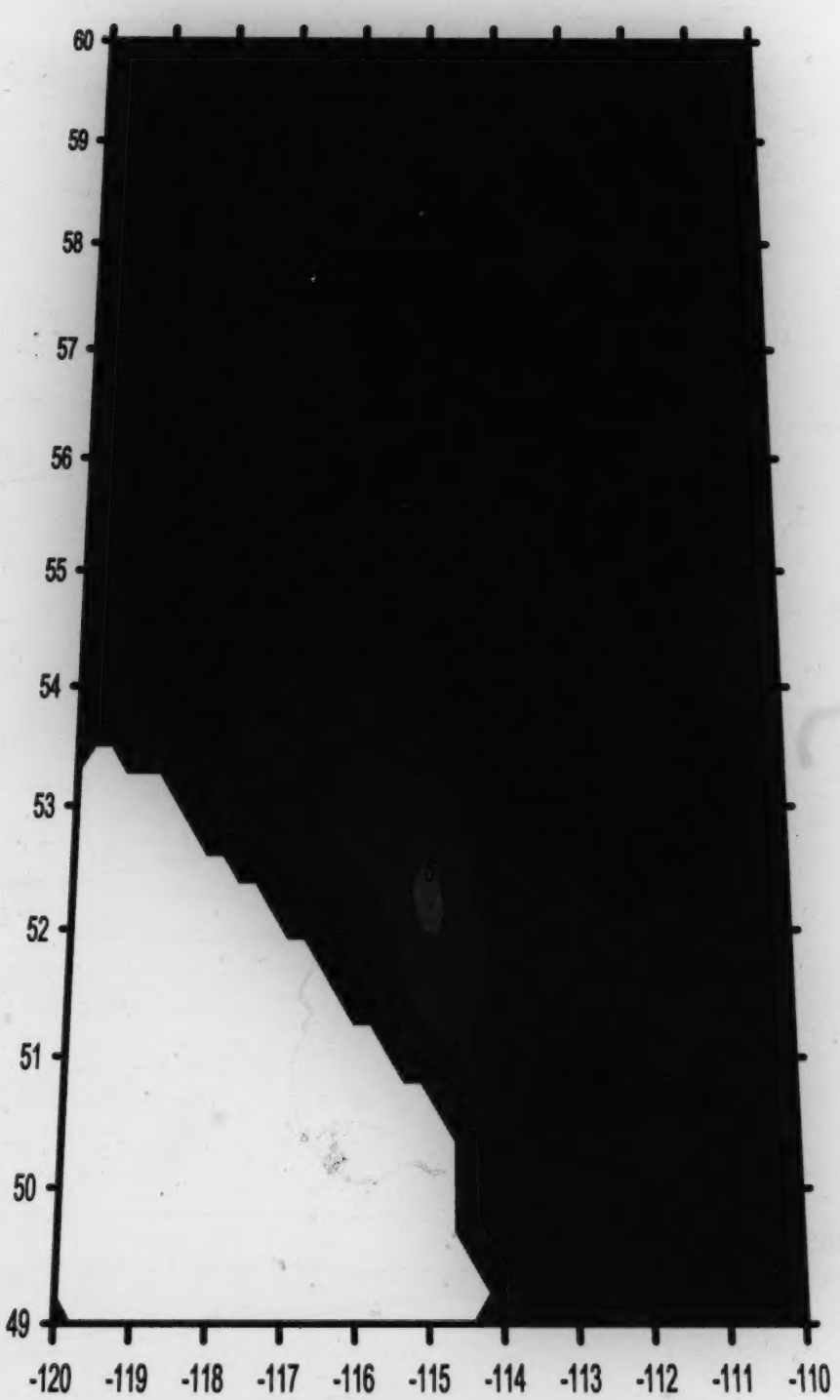

FIG. 3.28. Average August 16-31 lightning day count.

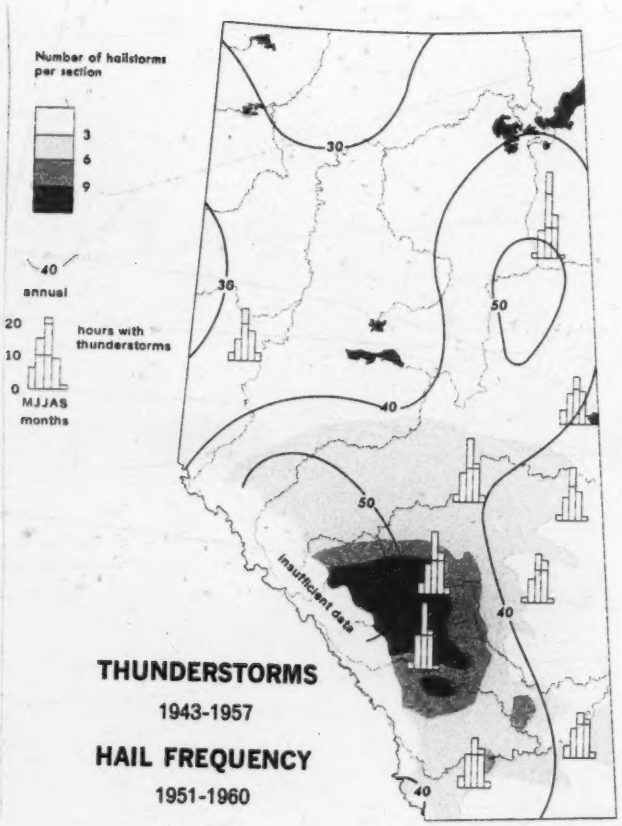

FIG. 3.29. Average annual hailstorm frequency, from 1943-57, shown with a grey-scale. Average annual thunderstorm hours depicted with labeled contours.

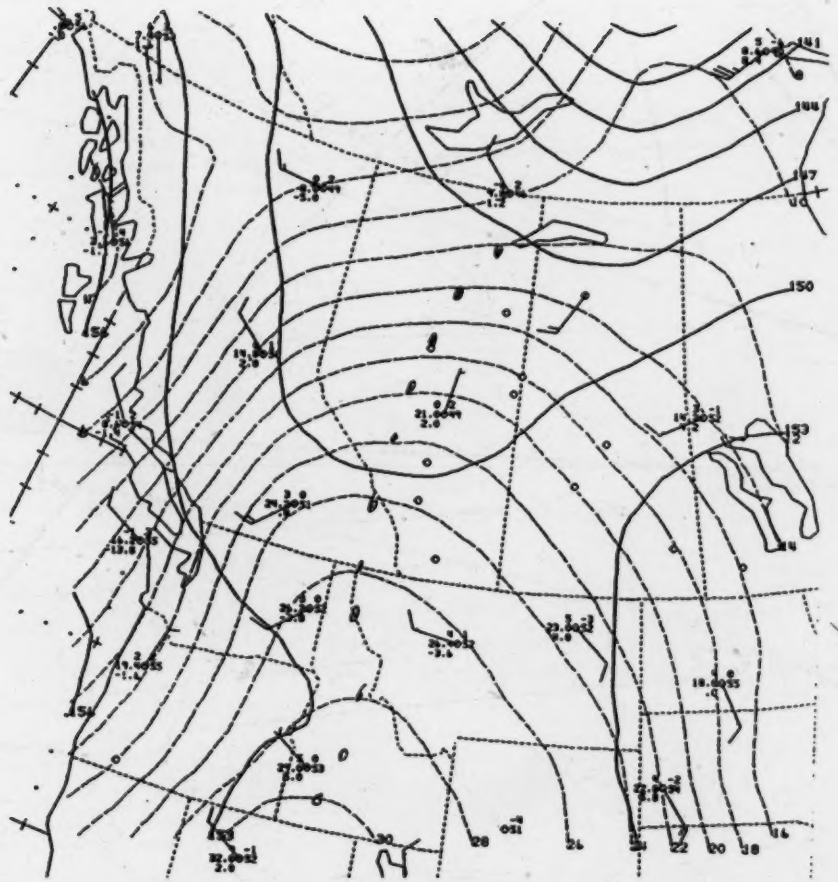

FIG. 4.1. The 850 mb analysis at 0000 UTC on 19 August 1992. Solid lines are geopotential height contours in decametres while dashed lines are isotherms in °C. Wind barbs are in knots. A short windbarb is 5 knots, and a long wind barb is 10 knots (analysis by Environment Canada).

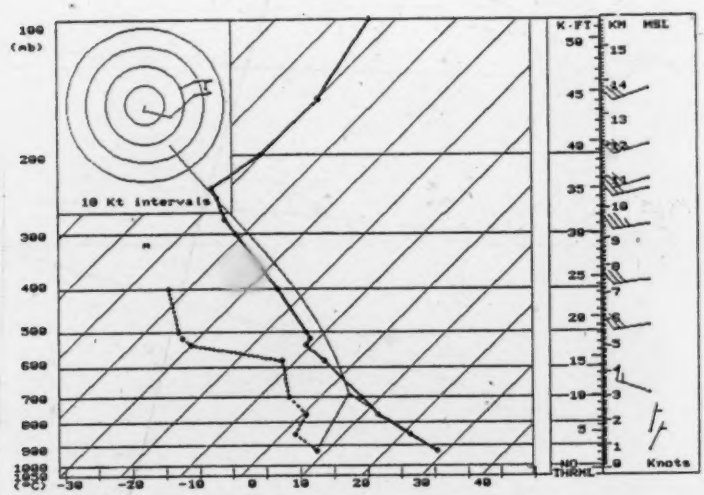

FIG. 4.2. Sounding recorded at Stony Plain at 0000 UTC on 19 August 1992. The solid line depicts temperature and the dashed line depicts the dewpoint.

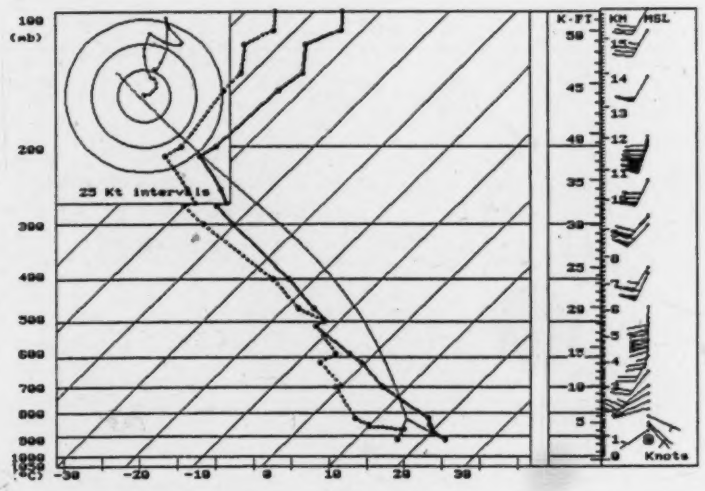

FIG. 4.3. Sounding recorded at Stony Plain at 0000 UTC on 30 July 1993. The solid line depicts temperature and the dashed line depicts the dewpoint.

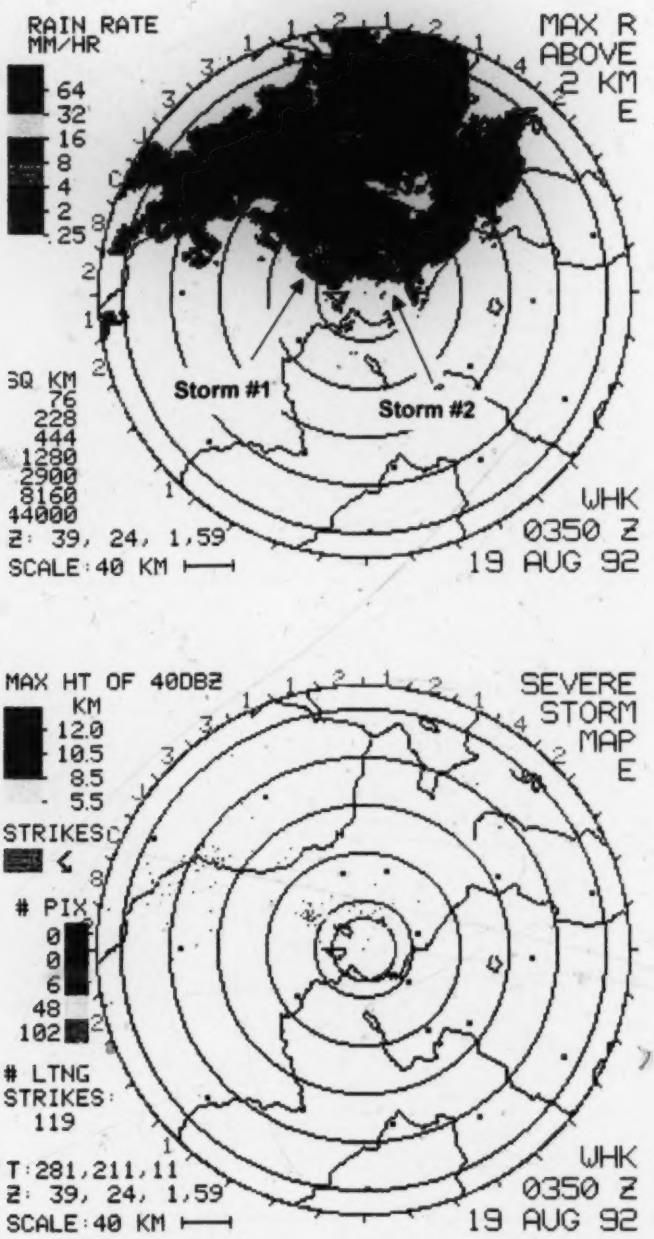

FIG. 4.4. Radar observations sampled by Carvel radar at 0350 UTC on 19 August 1992. The top map shows the maximum rainfall rate [mm h^{-1}] above 2 km from the ground. The Severe Storm Map (bottom) displays the maximum height [km] of the 40 dBz radar reflectivity factor. The locations of the CG lightning strikes are also shown.

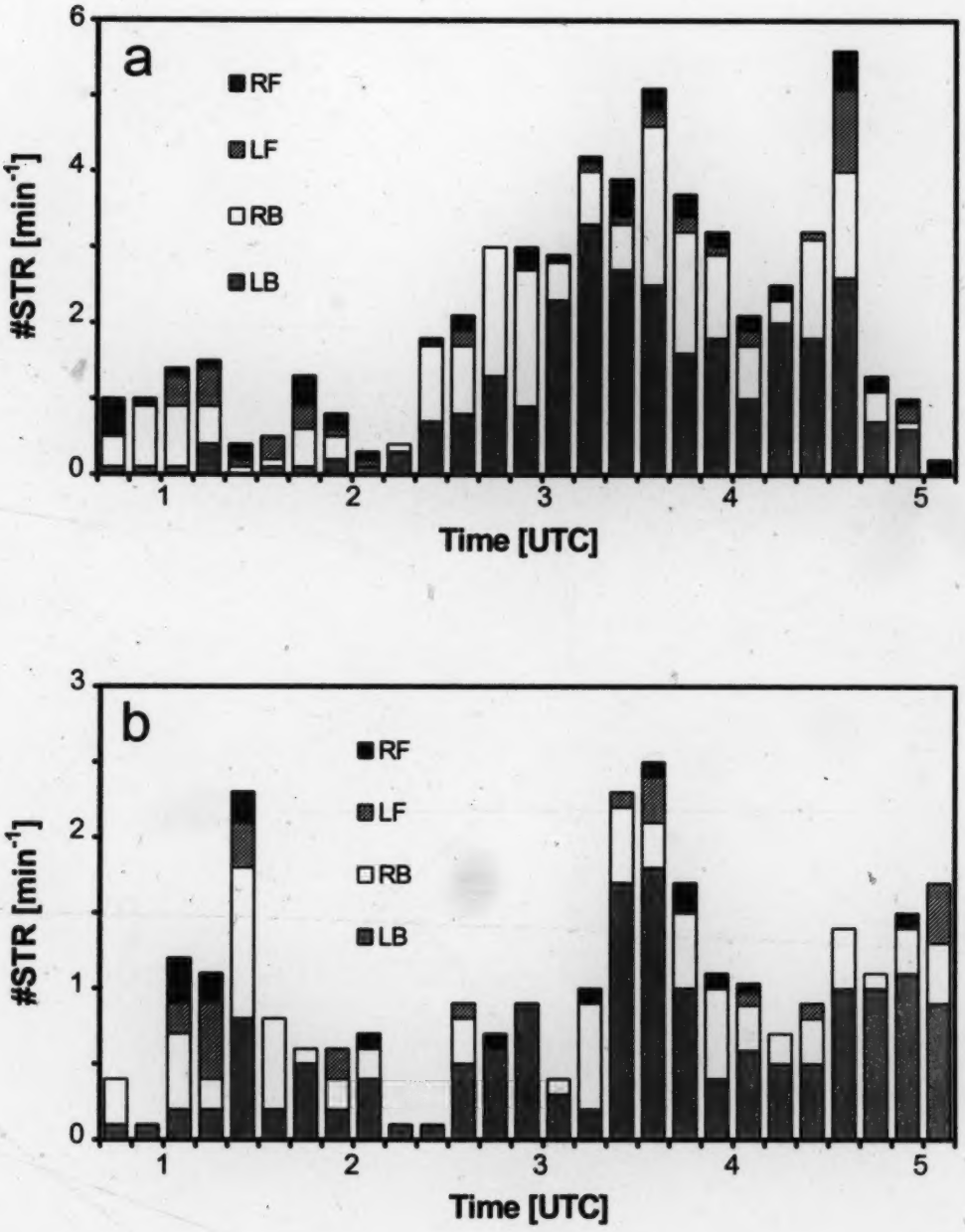

FIG. 4.5. Time history of number of lightning strikes #STR per minute within each of the four quadrants (Right Front, Left Front, Right Back, and Left Back) for (a) storm 1 and (b) storm 2 on 19 August 1992.

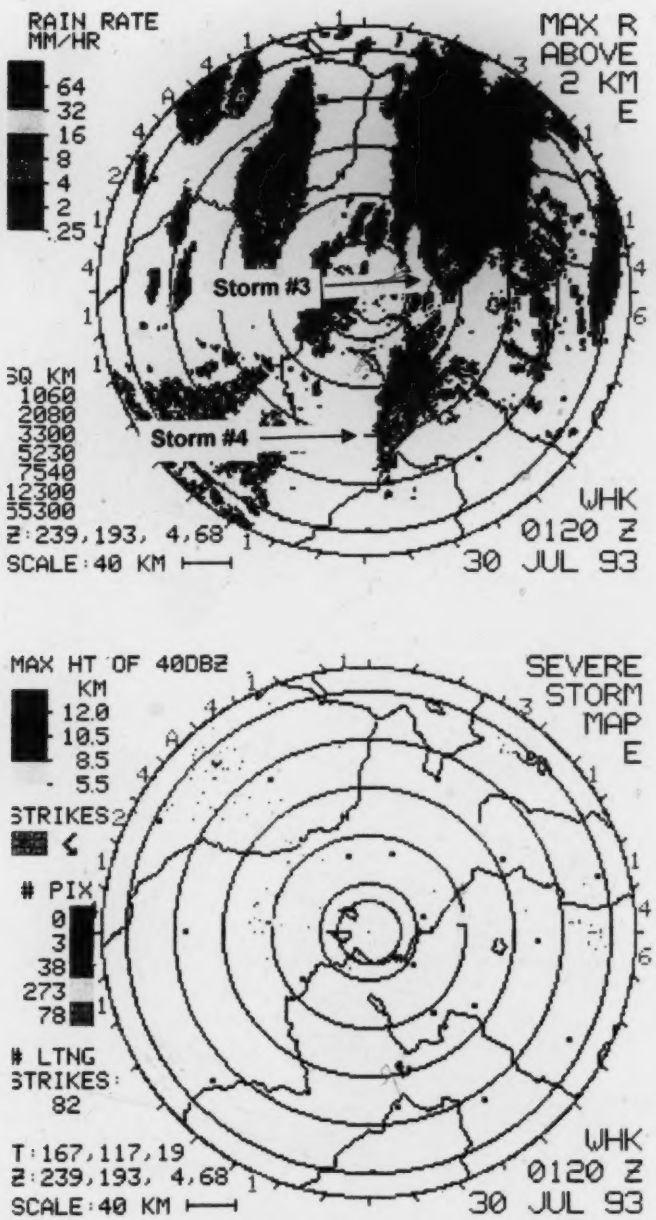

FIG. 4.6. Radar observations sampled by Carvel radar at 0120 UTC on 30 July 1993. The top map shows the maximum rainfall rate [mm h^{-1}] above 2 km from the ground. The Severe Storm Map (bottom) displays the maximum height [km] of the 40 dBz radar reflectivity factor. The locations of the CG lightning strikes are also shown.

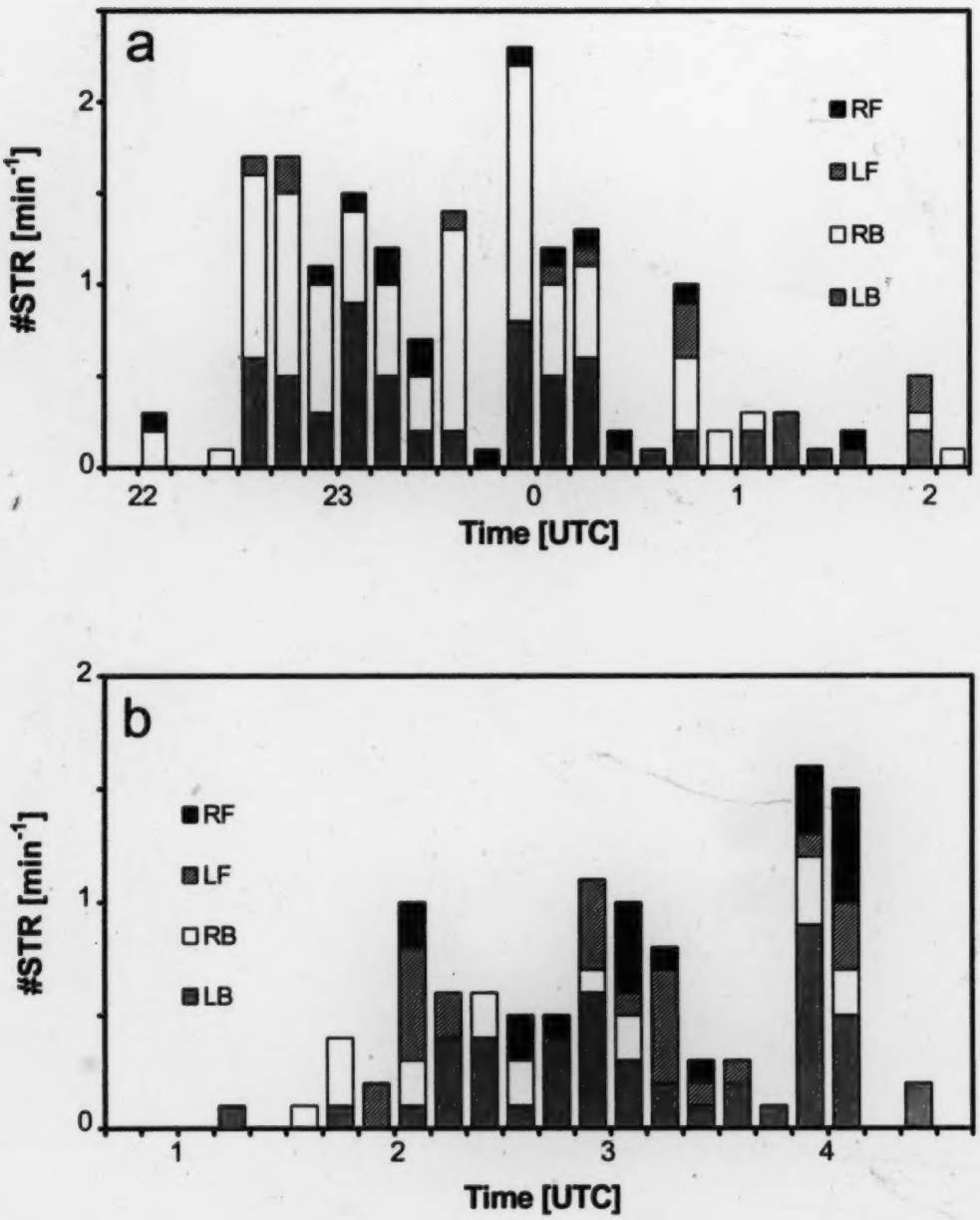

FIG. 4.7. Time history of number of lightning strikes #STR per minute within each of the four quadrants (Right Front, Left Front, Right Back, and Left Back) for (a) storm 3 and (b) storm 4 on 30 July 1993.

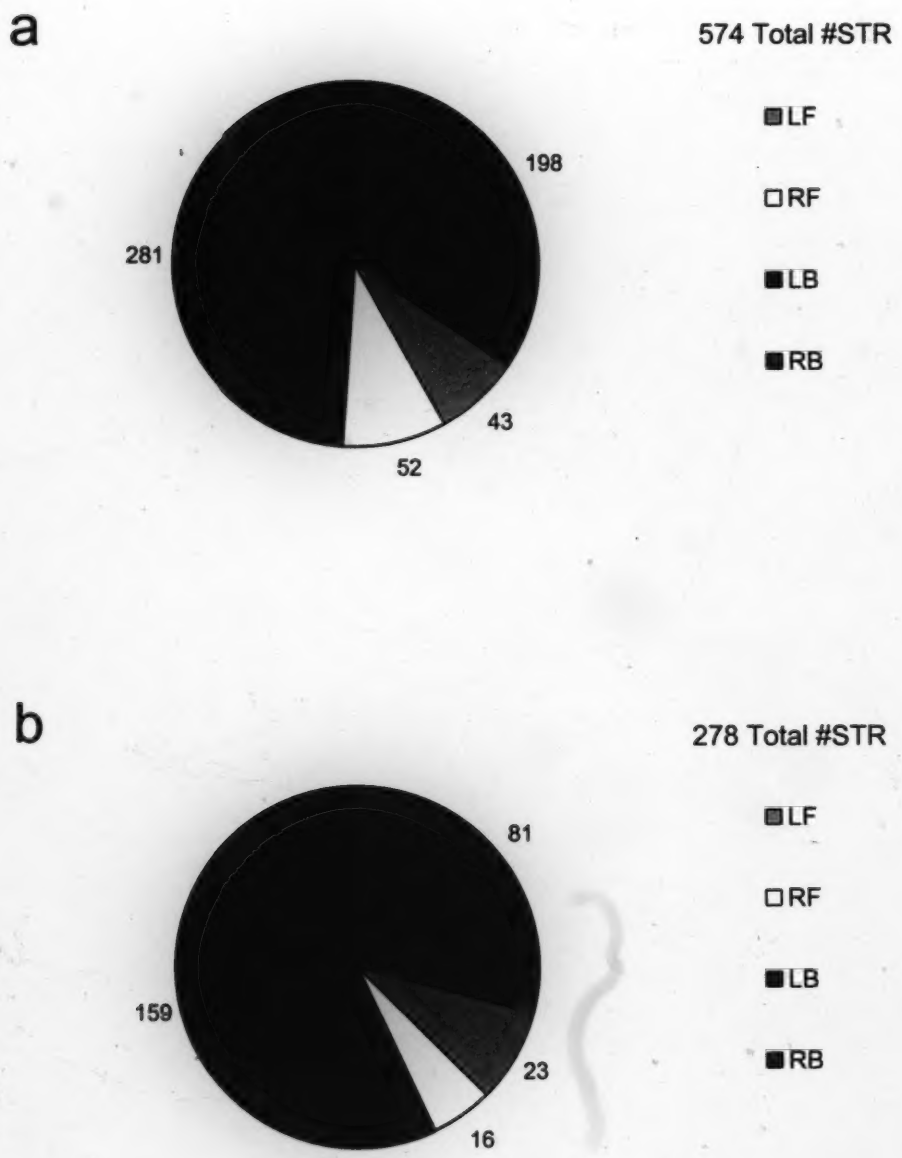

FIG. 4.8. Accumulated number of lightning strikes #STR in each quadrant for (a) storm 1 and (b) storm 2.

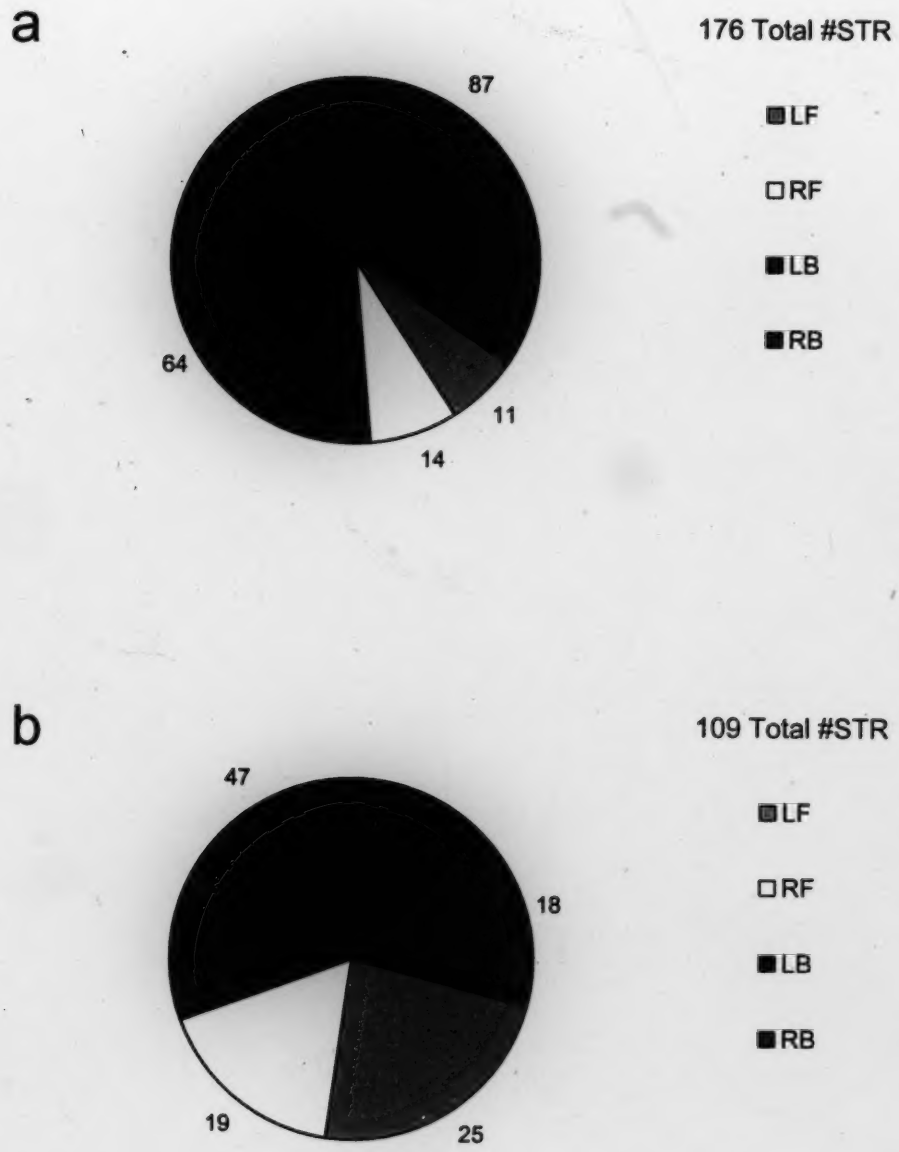

FIG. 4.9. Accumulated number of lightning strikes #STR in each quadrant for (a) storm 3 and (b) storm 4.

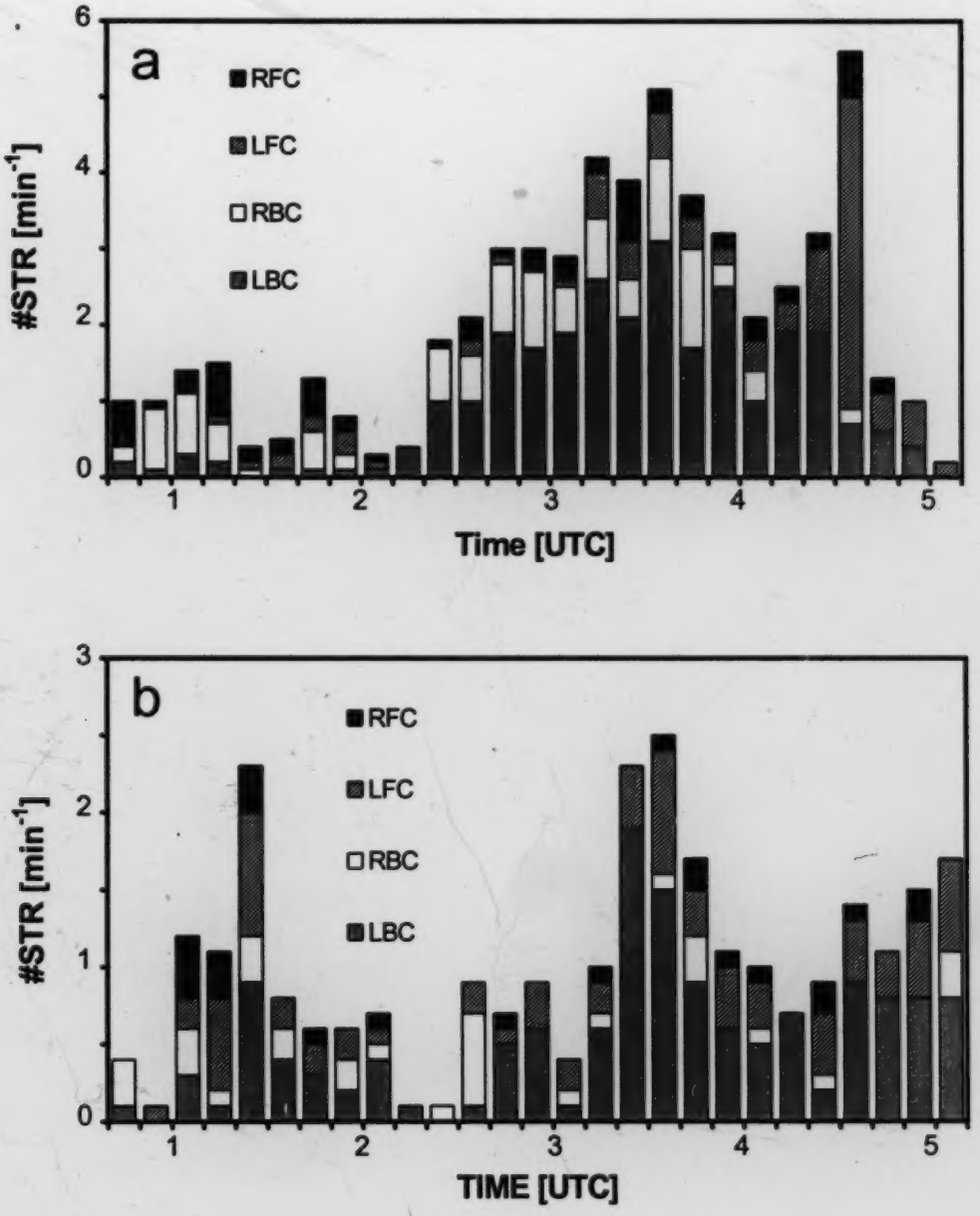

FIG. 4.10. Time history of number of lightning strikes #STR per minute within each of the four quadrants (Right Front Core, Left Front Core, Right Back Core, and Left Back Core) for (a) storm 1 and (b) storm 2 on 19 August 1992.

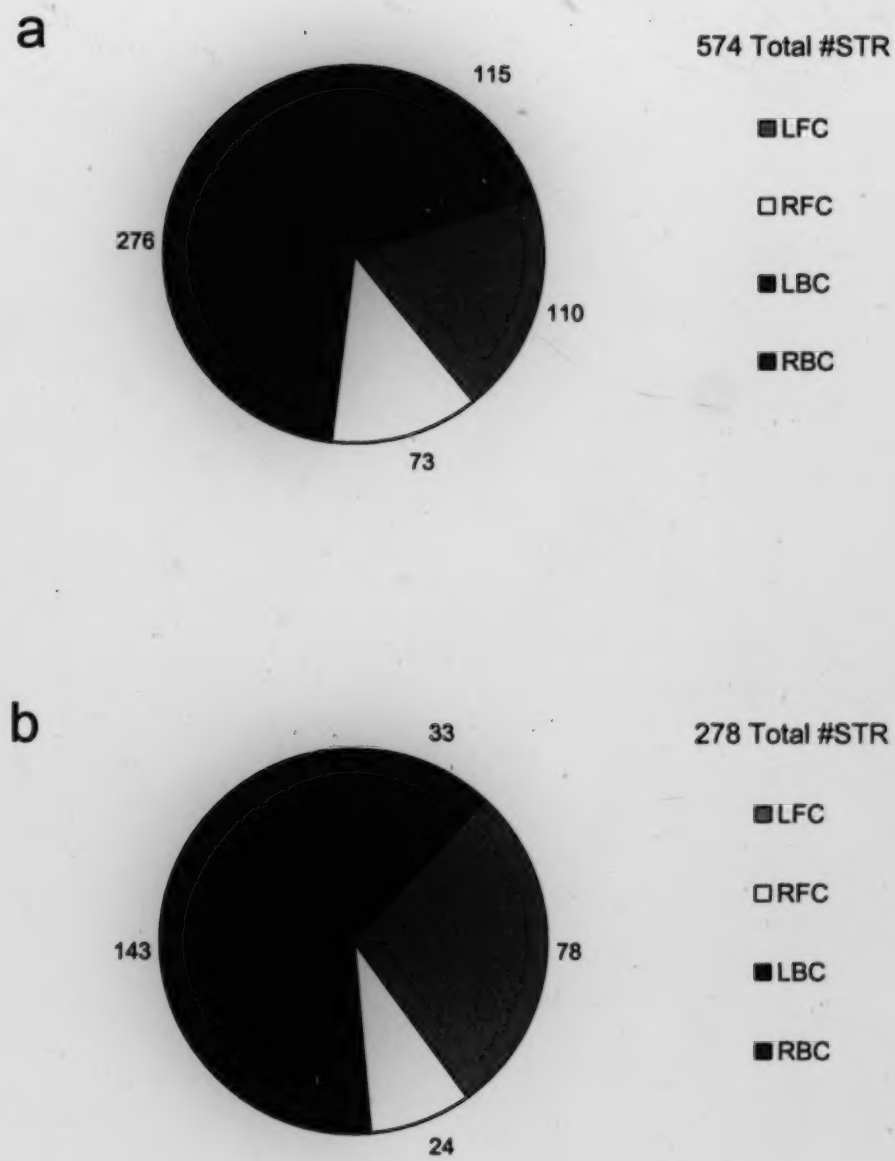

FIG. 4.11. Accumulated number of lightning strikes #STR in each core quadrant for (a) storm 1 and (b) storm 2.

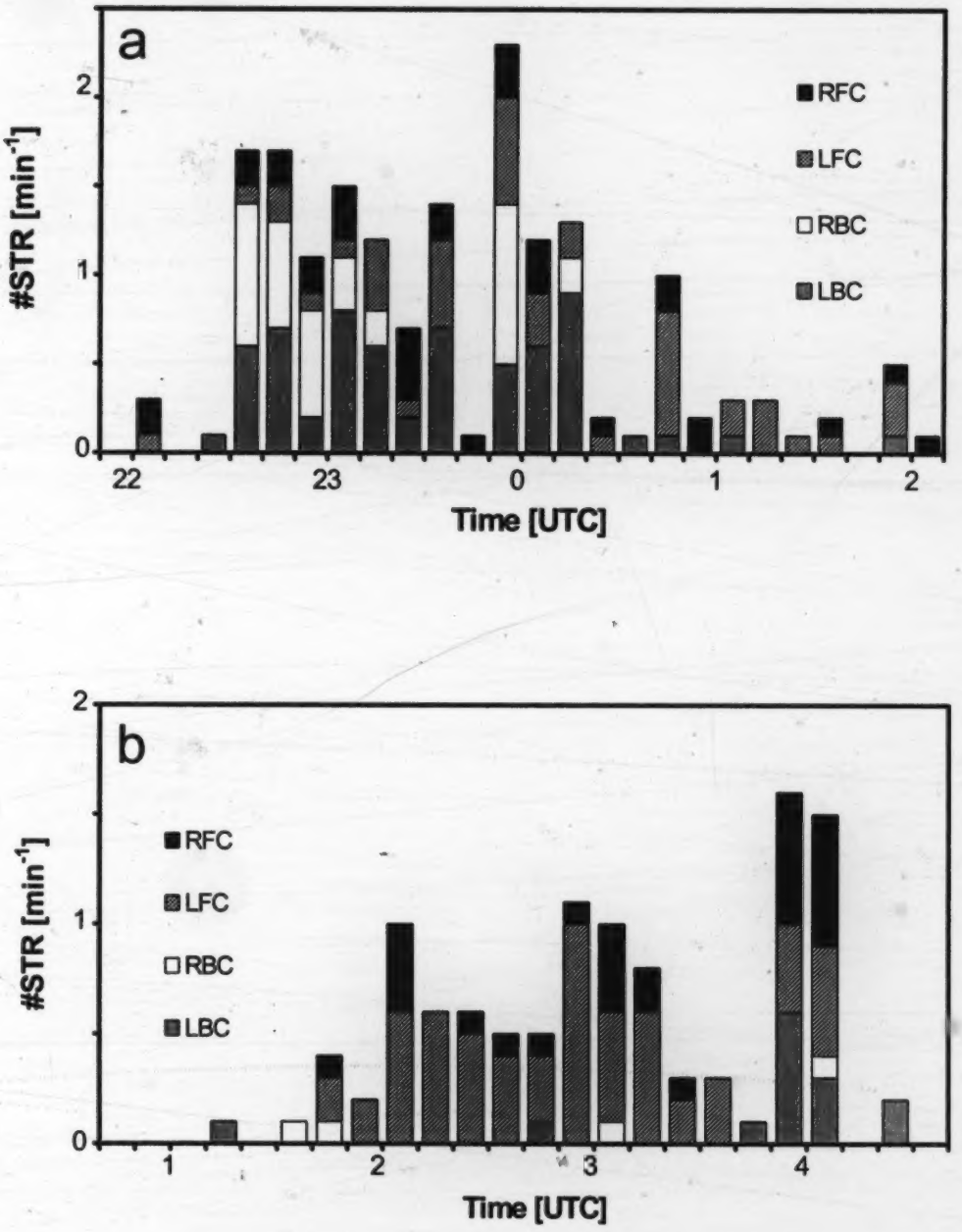

FIG. 4.12. Time history of number of lightning strikes #STR per minute within each of the four quadrants (Right Front Core, Left Front Core, Right Back Core, and Left Back Core) for (a) storm 3 and (b) storm 4 on 30 July 1993.

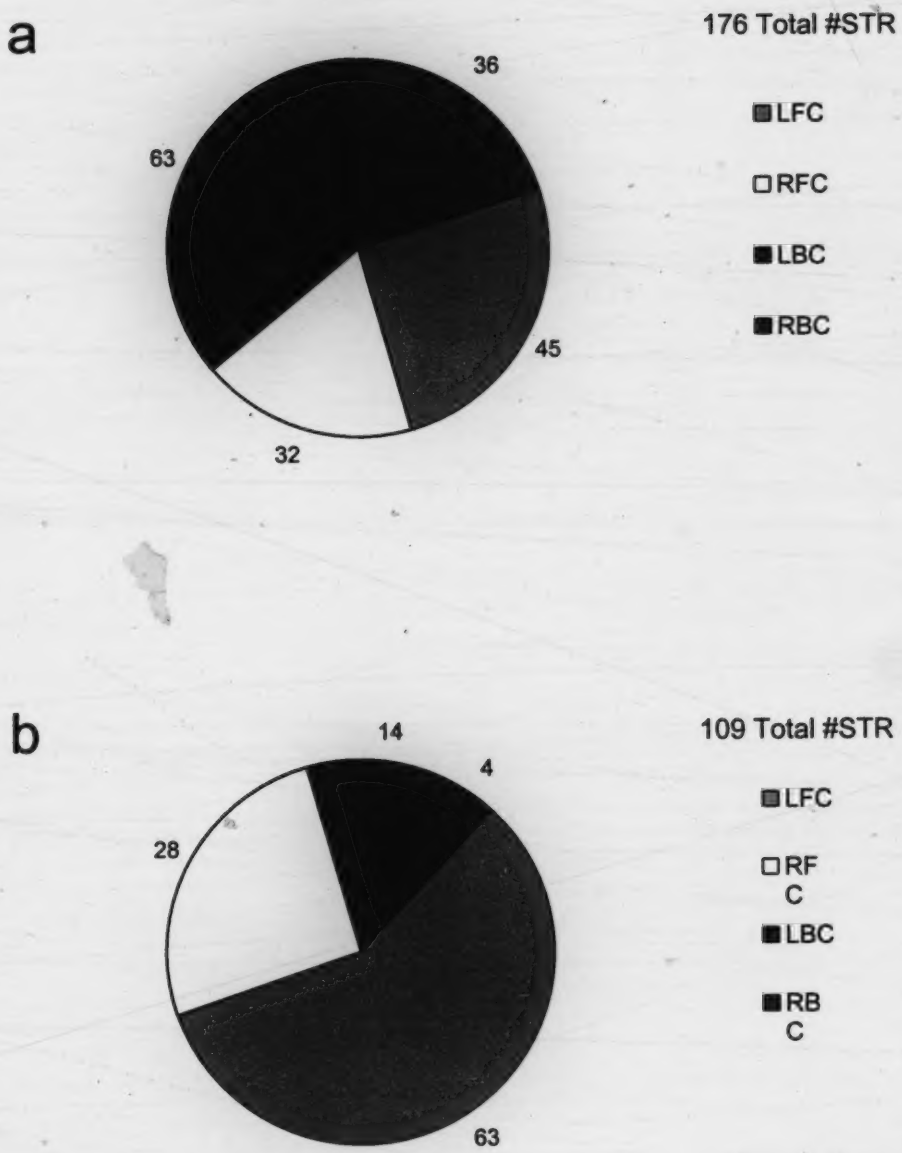

FIG. 4.13. Accumulated number of lightning strikes in each core quadrant for storm 3 (a) and storm 4 (b).

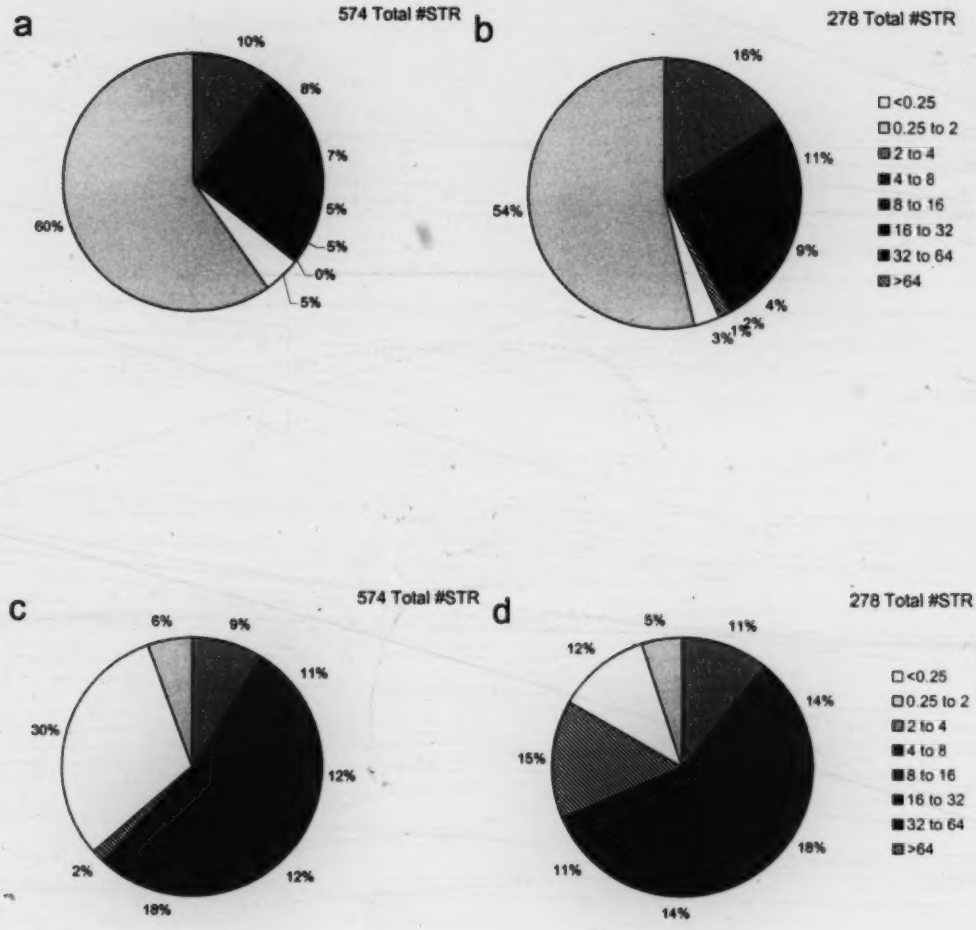

FIG. 4.14. Percentage values of CG lightning strikes for different rainfall rate intervals in mm h^{-1} for (a) storm 1 and (b) storm 2, and adjusted for area for (c) storm 1 and (d) storm 2.

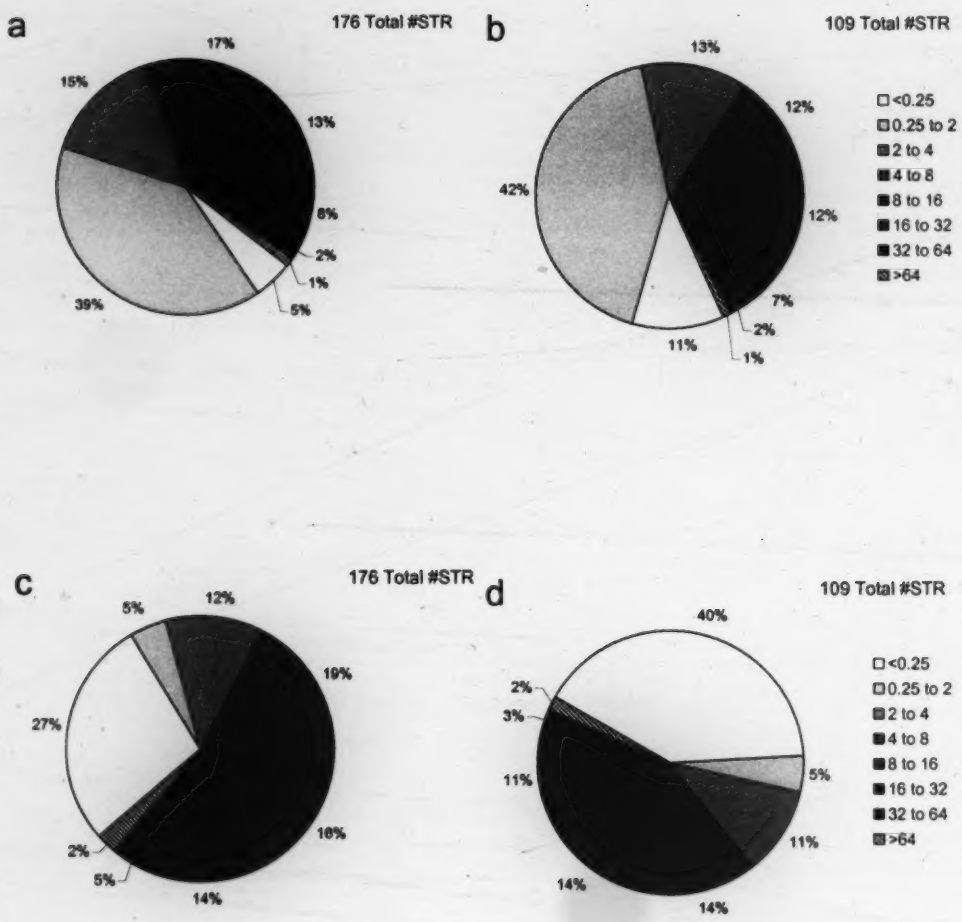

FIG. 4.15. Percentage values of CG lightning strikes for different rainfall rate intervals in mm h^{-1} for (a) storm 3 and (b) storm 4, and adjusted for area for (c) storm 3 and (d) storm 4.

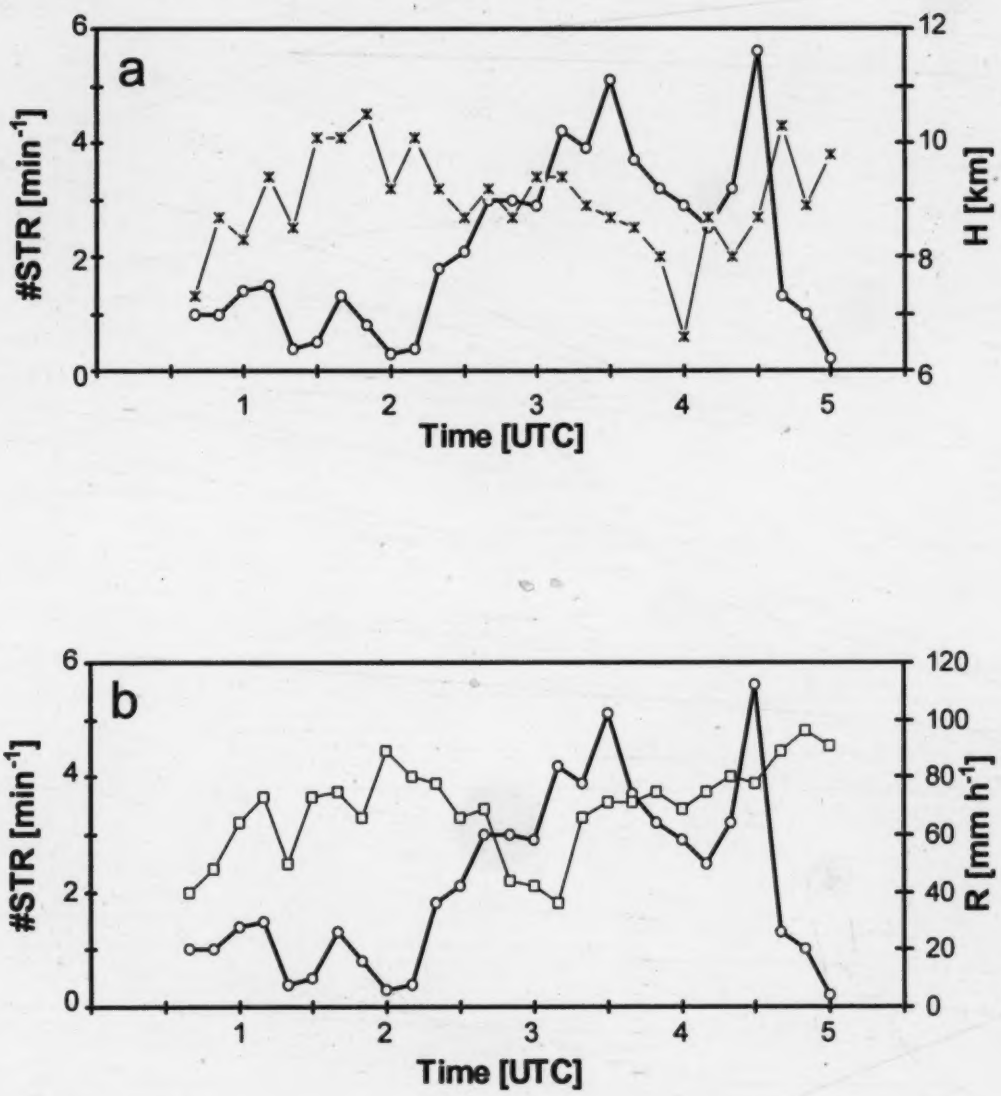

FIG. 4.16. Number of lightning strikes #STR (circles) compared with (a) maximum 40 dBz height H in km (crosses), and (b) maximum rainfall rate R in mm h^{-1} (squares) for storm 1.

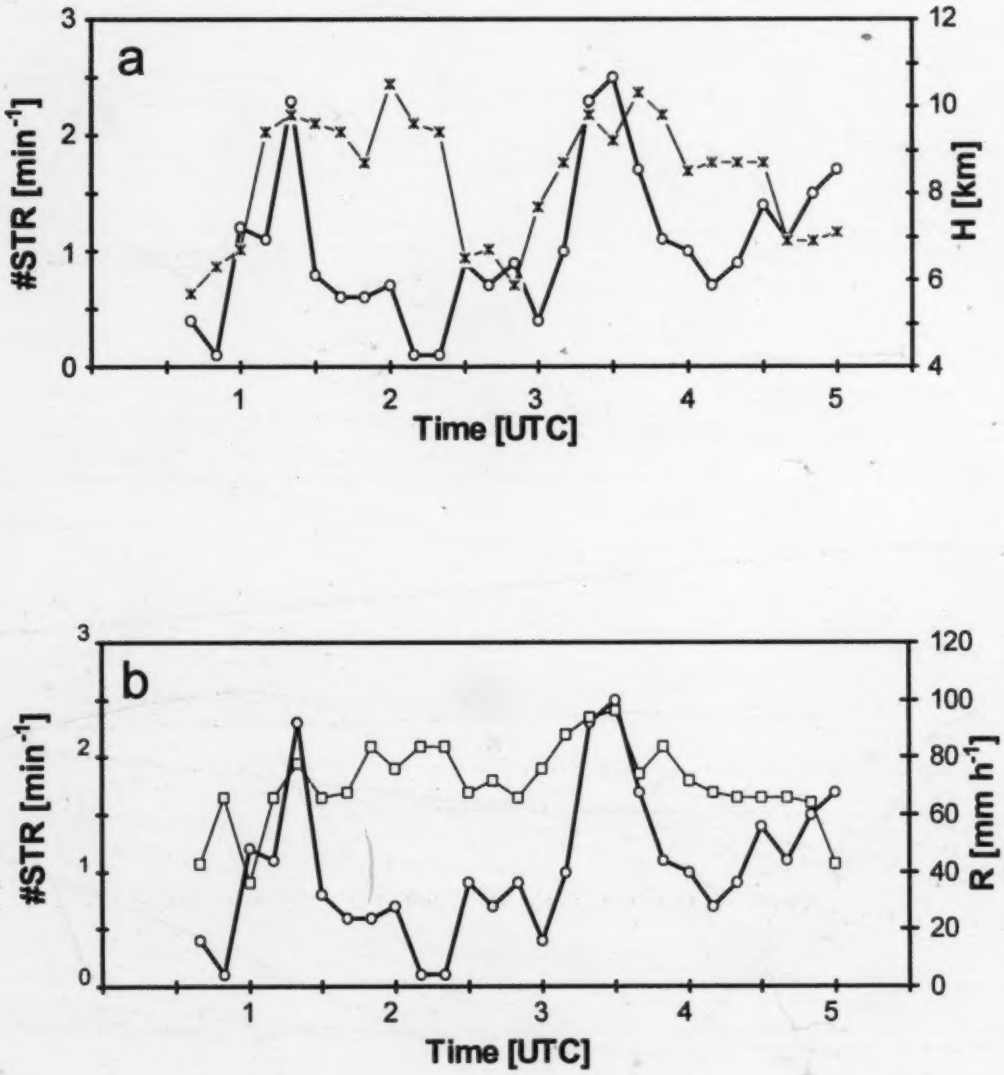

FIG. 4.17. Number of lightning strikes #STR (circles) compared with (a) maximum 40 dBz height H in km (crosses), and (b) maximum rainfall rate R in mm h^{-1} (squares) for storm 2.

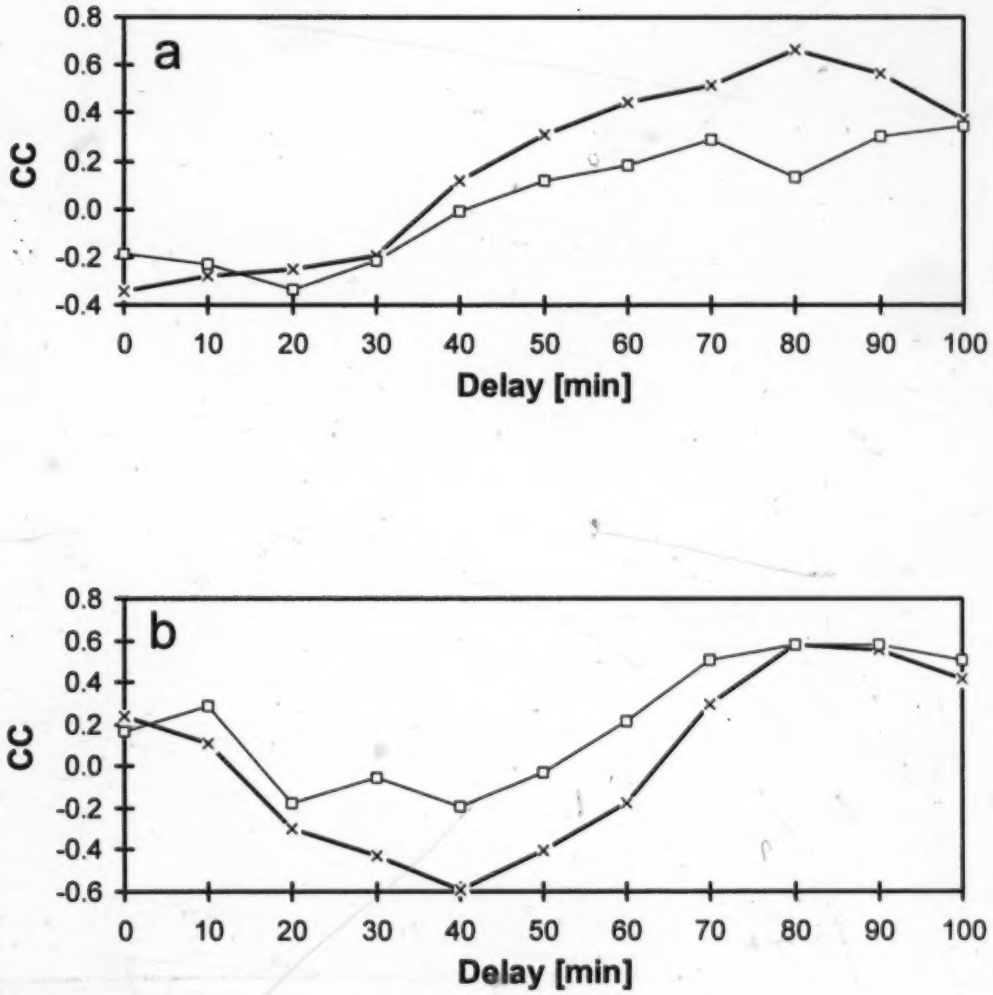

FIG. 4.18. Correlation coefficient (CC) plotted versus time delay of lightning strikes with maximum 40 dBz height H in km (crosses) and maximum rainfall rate in mm h^{-1} (squares) for (a) storm 1, and (b) storm 2 of 19 August 1992.

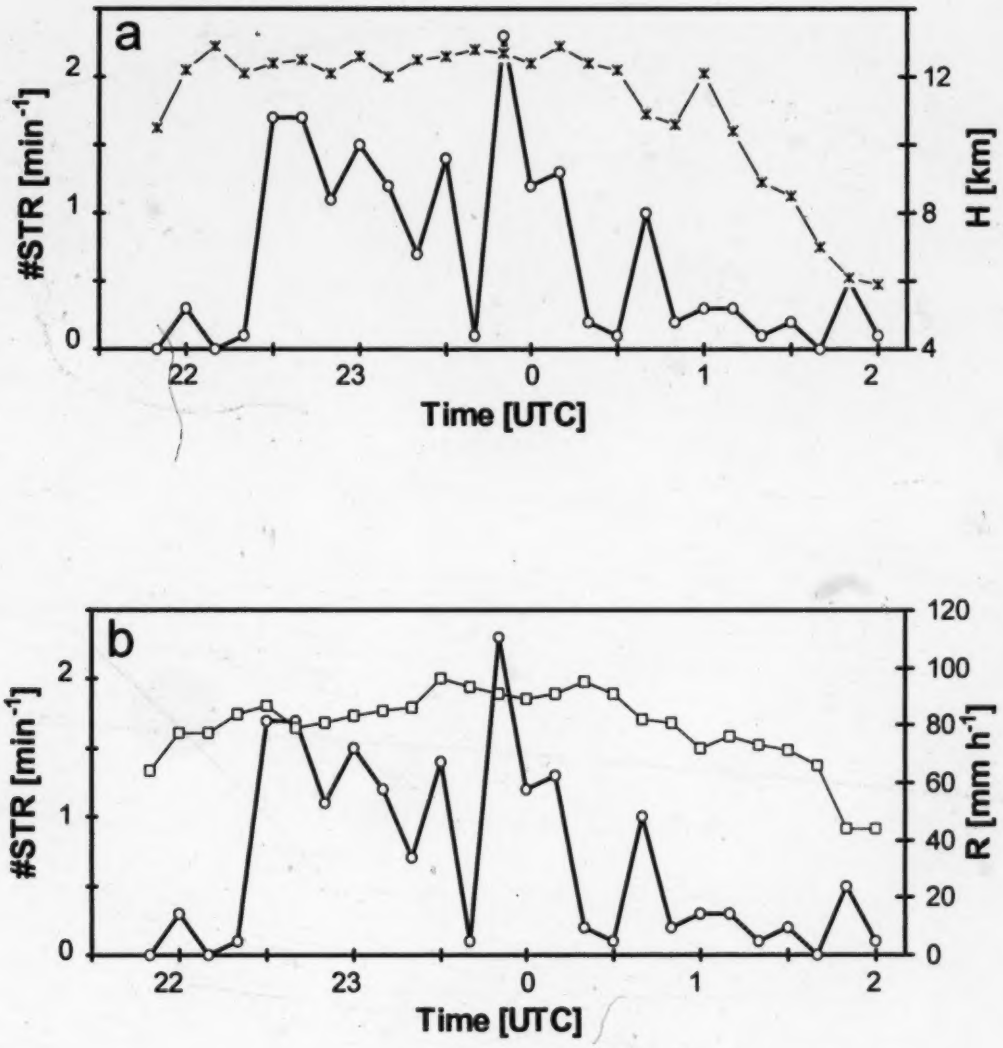

FIG. 4.19. Number of lightning strikes #STR (circles) compared with (a) maximum 40 dBz height H in km (crosses), and (b) maximum rainfall rate R in mm h^{-1} (squares) for storm 3.

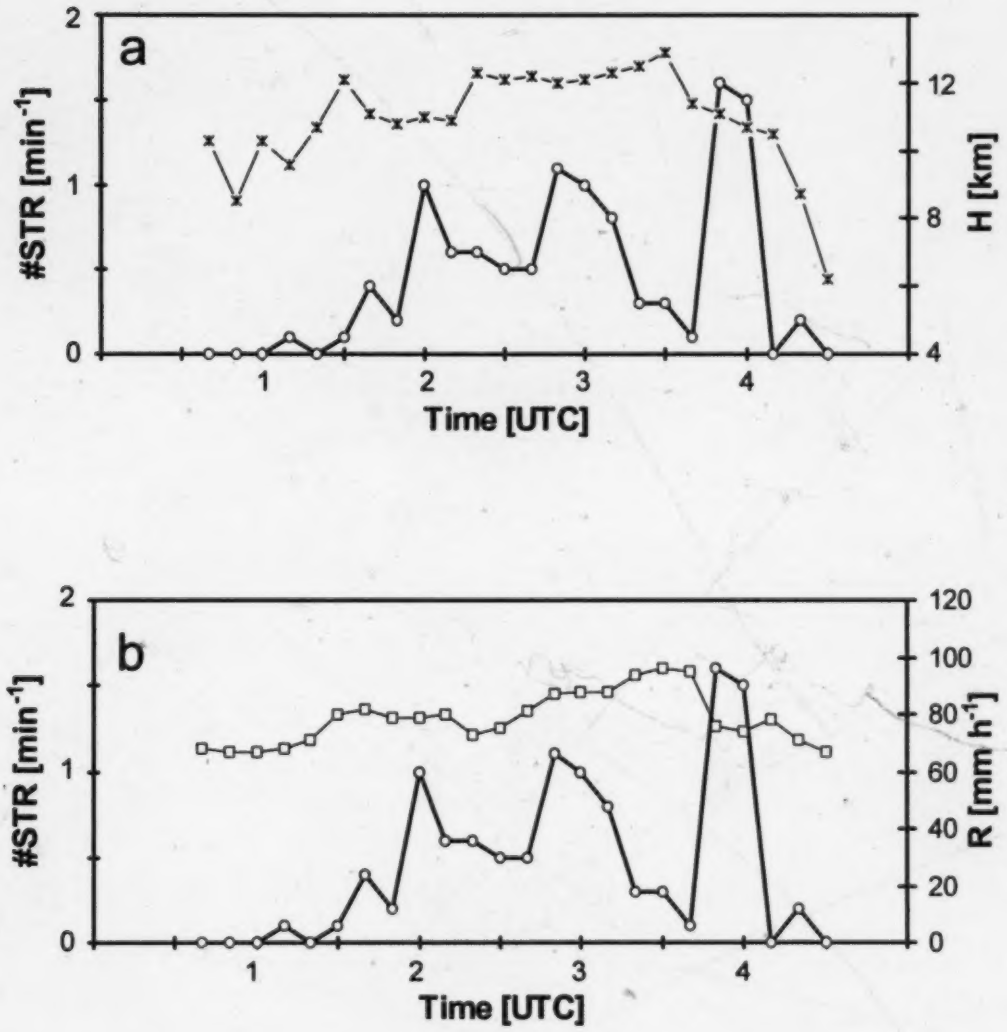

FIG. 4.20. Number of lightning strikes #STR (circles) compared with (a) maximum 40 dBz height H in km (crosses), and (b) maximum rainfall rate R in mm h^{-1} (squares) for storm 4.

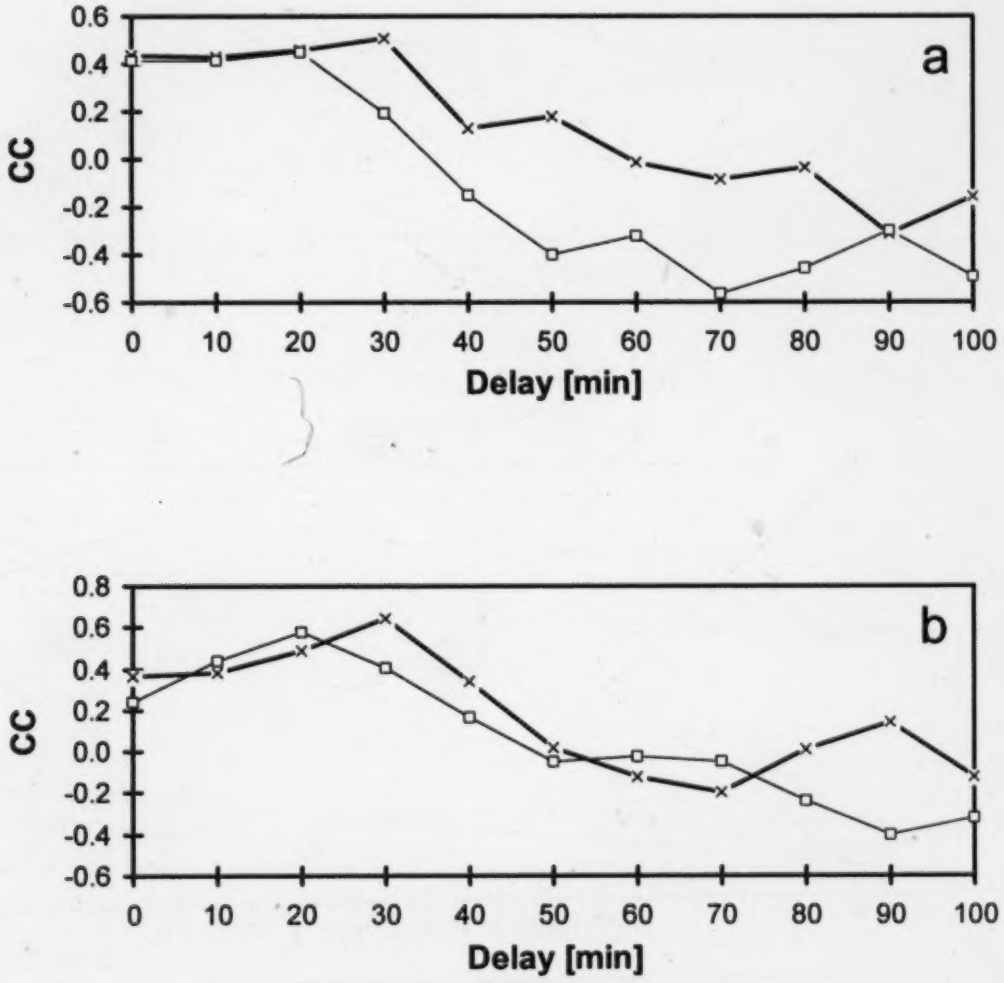

FIG. 4.21. Correlation coefficient (CC) plotted versus time delay of lightning strikes with maximum 40 dBz height H in km (crosses) and maximum rainfall rate in mm h^{-1} (squares) for (a) storm 3, and (b) storm 4 of 30 July 1993.

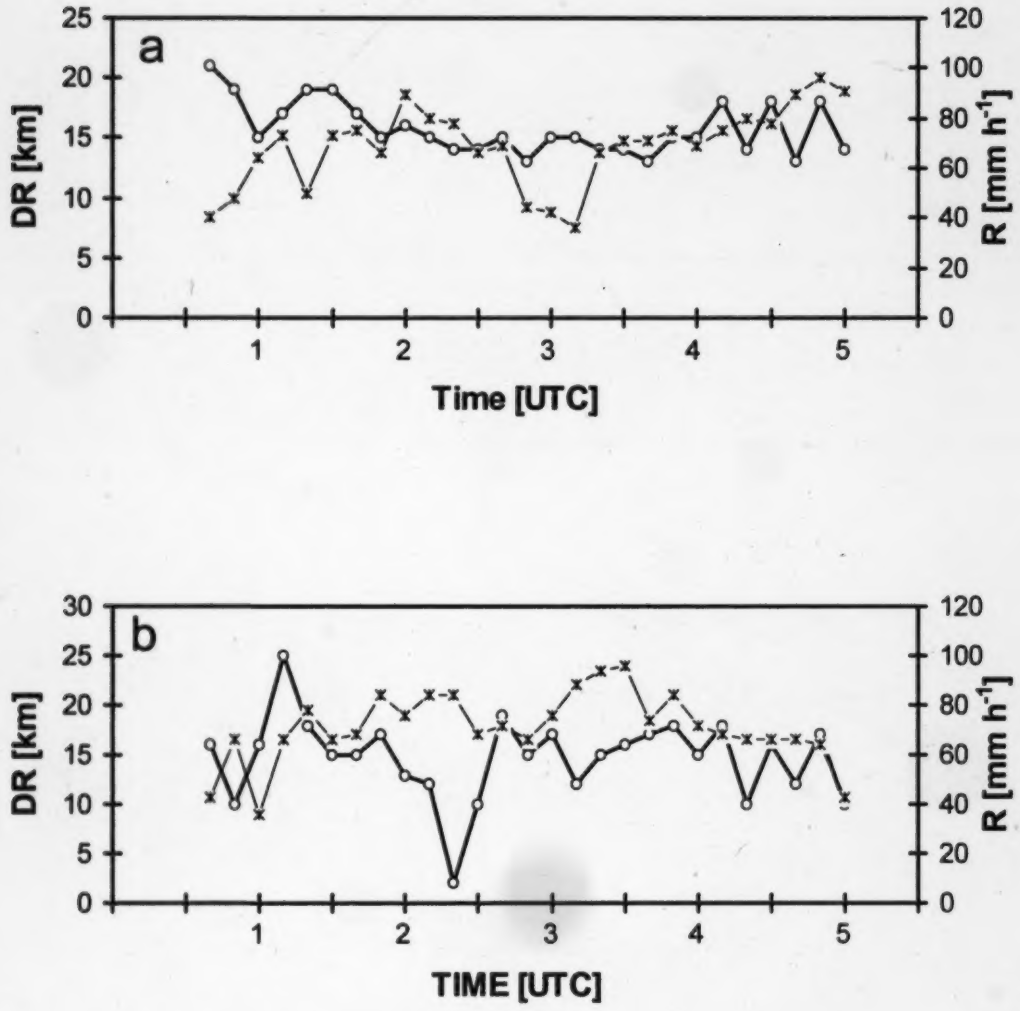

FIG. 4.22. Time histories of distance of lightning from rainfall maximum in km (DR in circles) and rainfall rate in mm h^{-1} (R in crosses) for (a) storm 1 and (b) storm 2.

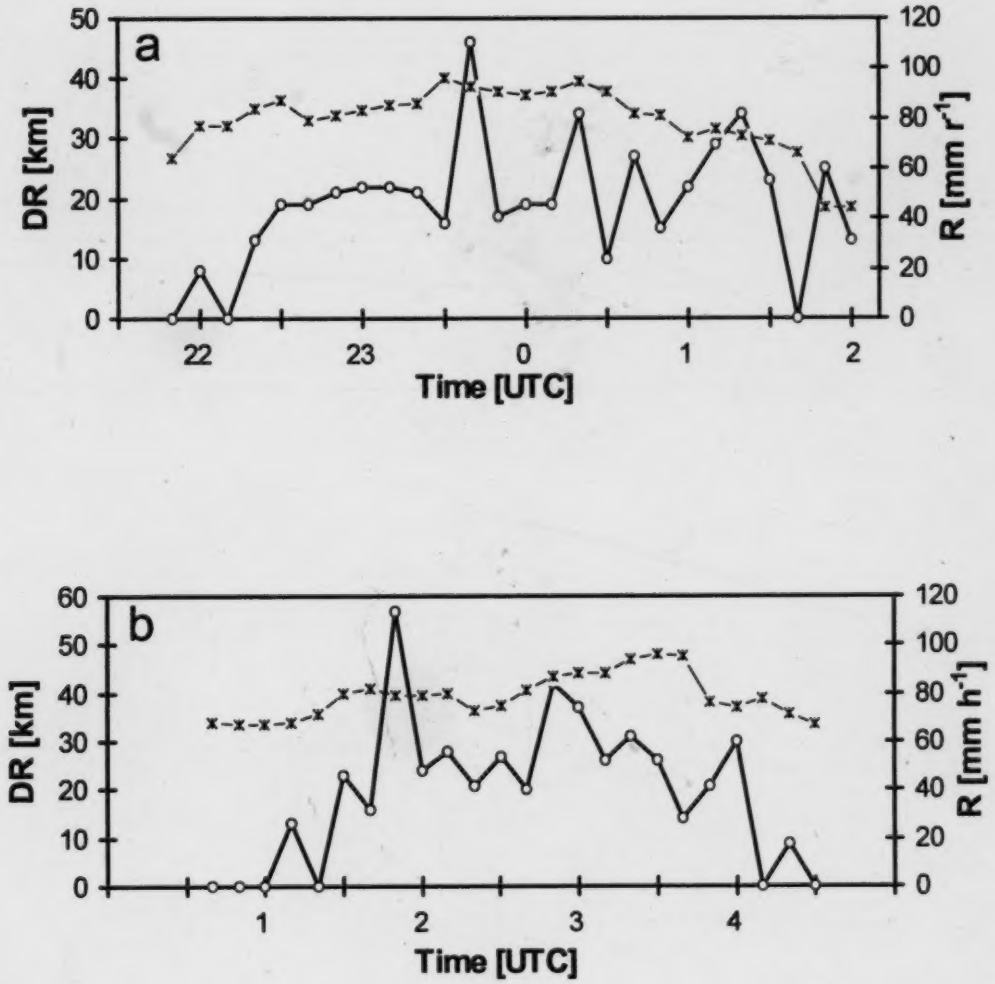

FIG. 4.23. Time histories of distance of lightning from rainfall maximum in km (DR in circles) and rainfall rate in mm h^{-1} (R in crosses) for (a) storm 3 and (b) storm 4.

Table 3.1. 1984-95 average strike count over Alberta. Data are in units of thousands of strikes.

	June	July	August	Total
1984	27.7	35.8	73.6	137.1
1985	26.6	36.1	40.0	102.7
1986	51.2	64.1	34.5	149.8
1987	41.0	188.1	32.6	261.7
1988	87.2	47.5	41.6	176.2
1989	50.5	174.6	114.1	339.2
1990	64.0	105.6	64.3	233.9
1991	67.7	97.6	109.8	275.3
1992	64.4	141.6	109.3	315.3
1993	71.4	215.6	140.7	427.7
1994	82.5	255.9	222.9	561.3
1995	105.6	101.4	38.3	245.3
Avg	61.7	122.0	85.1	268.8

Table 3.2. Two regions used to analyze the impact of vegetation coverage on CG lightning strike density [strikes $(10\ km)^{-2}$].

	Region A	Region B
Location close to:	Rocky Mountain House	Lethbridge
(lat, long)	(52.4°N,114.9°E)	(49.6°N,112.8°E)
Altitude [m]	930	1000
Distance from Continental Divide [km]	120	110
Vegetation coverage	uncultivated forests	grasslands
Lightning strike density [strikes $(10\ km)^{-2}$]	64-128	16-32

Table 3.3. Average June, July, and, August temperatures in °C and precipitation in mm, for Lethbridge, Edmonton Municipal Airport, and Fort Vermillion. The periods of observations are shown in brackets.

		Lethbridge (1938-90)	Edmonton Mun. (1937-90)	Fort Vermillion (1908-85)
Temp [°C]	June	15.8	15.6	15.0
	July	18.4	17.5	16.9
	August	17.8	16.6	15.0
Precip [mm]	June	66.3	79.9	47.1
	July	45.3	94.3	64.4
	August	42.9	67.0	54.7

Table 3.4. Average percentage of CG lightning strikes that occur in June, July, and August, with respect to the summer total, for Alberta, Manitoba, and southern Ontario. Percentage of strikes that occur in the morning (0-12 Local Time), and afternoon and evening (12-24), with respect to the daily total, are also shown.

	Alberta	Manitoba	Ontario
Years of Data	12	1	3
Area of Coverage	663 741	652 600	90 000
Summer Avg # Strikes	268 800	68 800	162 000
% June	23	15	30
% July	45	45	50
% August	32	40	20
% 0-12 [LT]	20	35	29
% 12-24 [LT]	80	65	71

Table 4.1. Number of lightning strikes #STR within storm quadrants and number of lightning strikes #STR within storm as a function of time, for storm 1. Averages and totals are also included. Numbers in bold indicate the location of the precipitation core center.

Time	LF	RF	LB	RB	Storm
0:40	0	5	**1**	4	10
0:50	0	1	**1**	8	10
1:00	4	1	**1**	8	14
1:10	5	1	**4**	5	15
1:20	1	2	**0**	1	4
1:30	3	0	1	**1**	5
1:40	3	4	1	**5**	13
1:50	1	2	2	**3**	8
2:00	1	1	1	**0**	3
2:10	0	0	3	**1**	4
2:20	0	1	7	**10**	18
2:30	2	2	8	**9**	21
2:40	0	0	13	**17**	30
2:50	0	3	9	**18**	30
3:00	0	1	**23**	5	29
3:10	1	1	33	**7**	42
3:20	1	5	**27**	6	39
3:30	2	3	25	**21**	51
3:40	2	3	16	**16**	37
3:50	1	2	18	**11**	32
4:00	2	2	10	**7**	21
4:10	0	2	20	**3**	25
4:20	1	0	18	**13**	32
4:30	11	5	26	**14**	56
4:40	0	2	7	**4**	13
4:50	2	1	6	**1**	10
5:00	0	2	0	**0**	2
Average	2	2	10	7	21
Total	43	52	281	198	[illegible]

Table 4.2. Number of strikes #STR within storm quadrants and number of strikes #STR within storm as a function of time, for storm 2. Averages and totals are also included. Numbers in bold indicate the location of the precipitation core center.

Time	LF	RF	LB	RB	Storm
0:40	0	0	1	3	4
0:50	0	0	1	0	1
1:00	2	3	2	5	12
1:10	5	2	2	2	11
1:20	3	2	8	10	23
1:30	0	0	2	6	8
1:40	0	0	5	1	6
1:50	2	0	2	2	6
2:00	0	1	4	2	7
2:10	0	0	1	0	1
2:20	0	0	1	0	1
2:30	1	0	5	3	9
2:40	0	1	6	0	7
2:50	0	0	9	0	9
3:00	0	0	3	1	4
3:10	0	1	2	7	10
3:20	1	0	17	5	23
3:30	3	1	18	3	25
3:40	0	2	10	5	17
3:50	0	1	4	6	11
4:00	1	1	6	3	11
4:10	0	0	5	2	7
4:20	1	0	5	3	9
4:30	0	0	10	4	14
4:40	0	0	10	1	11
4:50	0	1	11	3	15
5:00	4	0	9	4	17
Average	1	1	6	3	11
Total	23	16	159	81	279

Table 4.3. Number of strikes #STR within storm quadrants and number of strikes #STR within storm as a function of time, for storm 3. Averages and totals are also included. Numbers in bold indicate the location of the precipitation core center.

Time	LF	RF	LB	RB	Storm
21:50	0	0	0	**0**	0
22:00	0	1	0	**2**	3
22:10	0	0	0	**0**	0
22:20	0	0	0	**1**	1
22:30	1	0	6	**10**	17
22:40	2	0	5	**10**	17
22:50	0	1	3	**7**	11
23:00	0	1	9	**5**	15
23:10	0	2	5	**5**	12
23:20	0	2	2	**3**	7
23:30	1	0	2	**11**	14
23:40	0	1	0	**0**	1
23:50	0	1	8	**14**	23
0:00	1	1	5	**5**	12
0:10	1	1	6	**5**	13
0:20	0	1	1	**0**	2
0:30	0	0	1	**0**	1
0:40	3	1	2	**4**	10
0:50	0	0	0	**2**	2
1:00	0	0	2	**1**	3
1:10	0	0	3	**0**	3
1:20	0	0	1	**0**	1
1:30	0	1	1	**0**	2
1:40	0	0	0	**0**	0
1:50	2	0	2	**1**	5
2:00	0	0	0	**1**	1
Average	0	1	2	**3**	7
Total	11	14	64	**87**	177

Table 4.4. Number of strikes #STR within storm quadrants and number of strikes #STR within storm as a function of time, for storm 4. Averages and totals are also included. Numbers in bold indicate the location of the precipitation core center.

Time	LF	RF	LB	RB	Storm
0:40	0	0	0	**0**	0
0:50	0	0	0	**0**	0
1:00	0	0	0	**0**	0
1:10	0	0	1	**0**	1
1:20	0	0	0	**0**	0
1:30	0	0	0	**1**	1
1:40	0	0	**1**	3	4
1:50	2	0	0	**0**	2
2:00	5	2	**1**	2	10
2:10	2	0	4	**0**	6
2:20	0	0	4	**2**	6
2:30	0	2	1	**2**	5
2:40	0	1	4	**0**	5
2:50	4	0	6	**1**	11
3:00	1	4	3	**2**	10
3:10	5	1	**2**	0	8
3:20	1	1	**1**	0	3
3:30	1	0	2	**0**	3
3:40	0	0	1	**0**	1
3:50	1	3	9	**3**	16
4:00	3	5	5	**2**	11
4:10	0	0	0	**0**	0
4:20	0	0	2	**0**	2
4:30	0	0	**0**	0	0
Average	1	1	2	1	5
Total	25	19	47	18	10

Table 4.5. Percentages of CG lightning strikes that accumulate throughout the observing period of the four storms.

Storm	#1	#2	#3	#4
#STR	574	278	176	109
Back	84%	86%	86%	60%
Front	16%	14%	14%	40%
Left	56%	65%	43%	60%
Right	44%	35%	57%	40%
LB	49%	57%	37%	43%
RB	35%	29%	49%	17%
LF	7%	8%	6%	23%
RF	9%	6%	8%	17%

Table 4.6. Number of lightning strikes #STR within core quadrants and number of lightning strikes #STR within storm as a function of time, for storm 1. Averages and totals are also included.

Time	LFC	RFC	LBC	RBC	Storm
0:40	0	6	2	2	10
0:50	0	1	1	8	10
1:00	0	3	3	8	14
1:10	1	7	2	5	15
1:20	1	2	0	1	4
1:30	2	2	1	0	5
1:40	2	5	1	5	13
1:50	3	2	1	2	8
2:00	1	1	1	0	3
2:10	0	0	4	0	4
2:20	0	1	10	7	18
2:30	2	3	10	6	21
2:40	1	1	19	9	30
2:50	0	3	17	10	30
3:00	1	3	19	6	29
3:10	6	2	26	8	42
3:20	5	8	21	5	39
3:30	6	3	31	11	51
3:40	4	3	17	13	37
3:50	2	2	25	3	32
4:00	4	3	10	4	21
4:10	4	2	19	0	25
4:20	11	2	19	0	32
4:30	41	6	7	2	56
4:40	5	2	6	0	13
4:50	6	0	4	0	10
5:00	2	0	0	0	2
Average	4	3	10	4	21
Total	110	73	276	115	574

Table 4.7. Number of lightning strikes #STR within core quadrants and number of lightning strikes #STR within storm as a function of time, for storm 2. Averages and totals are also included.

Time	LFC	RFC	LBC	RBC	Storm
0:40	0	0	1	3	4
0:50	1	0	0	0	1
1:00	2	4	3	3	12
1:10	6	3	1	1	11
1:20	8	3	9	3	23
1:30	2	0	4	2	8
1:40	2	1	3	0	6
1:50	2	0	2	2	6
2:00	1	1	4	1	7
2:10	0	0	1	0	1
2:20	0	0	0	1	1
2:30	2	0	1	6	9
2:40	1	1	5	0	7
2:50	3	0	6	0	9
3:00	2	0	1	1	4
3:10	2	1	6	1	10
3:20	4	0	19	0	23
3:30	8	1	15	1	25
3:40	3	2	9	3	17
3:50	4	1	6	0	11
4:00	3	1	5	1	10
4:10	0	0	7	0	7
4:20	4	2	2	1	9
4:30	4	1	9	0	14
4:40	3	0	8	0	11
4:50	5	2	8	0	15
5:00	6	0	8	3	17
Average	3	1	6	1	11
Total	78	24	143	33	278

Table 4.8. Number of lightning strikes #STR within core quadrants and number of lightning strikes #STR within storm as a function of time, for storm 3. Averages and totals are also included.

Time	LFC	RFC	LBC	RBC	Storm
21:50	0	0	0	0	0
22:00	1	2	0	0	3
22:10	0	0	0	0	0
22:20	0	0	1	0	1
22:30	1	2	6	8	17
22:40	2	2	7	6	17
22:50	1	2	2	6	11
23:00	1	3	8	3	15
23:10	4	0	6	2	12
23:20	1	4	2	0	7
23:30	5	2	7	0	14
23:40	0	1	0	0	1
23:50	6	3	5	9	23
0:00	3	3	6	0	12
0:10	2	0	9	2	13
0:20	1	1	0	0	2
0:30	0	0	1	0	1
0:40	7	2	1	0	10
0:50	0	2	0	0	2
1:00	2	0	1	0	3
1:10	3	0	0	0	3
1:20	1	0	0	0	1
1:30	1	1	0	0	2
1:40	0	0	0	0	0
1:50	3	1	1	0	5
2:00	0	1	0	0	1
Average	2	1	2	1	7
Total	45	32	63	36	176

Table 4.9. Number of lightning strikes #STR within core quadrants and number of lightning strikes #STR within storm as a function of time, for storm 4. Averages and totals are also included.

Time	LFC	RFC	LBC	RBC	Storm
0:40	0	0	0	0	0
0:50	0	0	0	0	0
1:00	0	0	0	0	0
1:10	0	0	1	0	1
1:20	0	0	0	0	0
1:30	0	0	0	1	1
1:40	2	1	0	1	4
1:50	2	0	0	0	2
2:00	6	4	0	0	10
2:10	6	0	0	0	6
2:20	5	1	0	0	6
2:30	4	1	0	0	5
2:40	3	1	1	0	5
2:50	10	1	0	0	11
3:00	5	4	0	1	10
3:10	6	2	0	0	8
3:20	2	1	0	0	3
3:30	3	0	0	0	3
3:40	0	0	1	0	1
3:50	4	6	6	0	16
4:00	5	6	3	1	15
4:10	0	0	0	0	0
4:20	0	0	2	0	2
4:30	0	0	0	0	0
Average	3	1	6	0	11
Total	63	28	14	4	150

Table 4.10. Number of lightning strikes #STR within maximum rain rate intervals and number of lightning strikes #STR within storm as a function of time, for storm 1. Rain rate interval and storm areas (number of pixels) and lightning strike averages, totals, and weighted totals are also included.

Time	<0.25	0.25 to 2	2 to 4	4 to 8	8 to 16	16 to 32	32 to 64	>64	Storm
00:40	1	9	0	0	0	0	0	0	10
00:50	4	5	0	0	0	1	0	0	10
01:00	0	9	0	2	1	1	1	0	14
01:10	4	8	0	1	0	1	1	0	15
01:20	1	2	0	1	0	0	0	0	4
01:30	0	5	0	0	0	0	0	0	5
01:40	0	12	1	0	0	0	0	0	13
01:50	0	6	1	0	1	0	0	0	8
02:00	0	3	0	0	0	0	0	0	3
02:10	0	3	0	1	0	0	0	0	4
02:20	0	13	4	1	0	0	0	0	18
02:30	0	12	1	1	1	3	3	0	21
02:40	0	17	6	3	2	2	0	0	30
02:50	0	15	6	2	4	0	3	0	30
03:00	0	20	2	1	3	1	2	0	29
03:10	0	26	4	3	5	2	2	0	42
03:20	0	25	4	2	1	4	3	0	39
03:30	1	38	2	4	3	1	2	0	51
03:40	2	24	2	2	5	1	1	0	37
03:50	1	21	5	0	1	1	2	0	31
04:00	1	13	2	2	2	1	1	0	22
04:10	2	18	2	1	1	0	1	0	25
04:20	3	13	3	5	2	4	2	0	32
04:30	4	15	11	12	7	1	5	1	56
04:40	2	5	3	2	1	0	0	0	13
04:50	1	6	0	0	1	2	0	0	10
05:00	0	0	0	1	1	0	0	0	2
Average	1	13	2	2	2	1	1	0	21
Total	27	343	59	47	42	26	29	1	574
Area (# Pixels)	162	10888	1243	760	644	406	297	117	14517
Weighted Total	176	33	50	65	69	68	103	9	574

Table 4.11. Number of lightning strikes #STR within maximum rain rate intervals and number of lightning strikes #STR within storm as a function of time, for storm 2. Rain rate interval and storm areas (number of pixels) and lightning strike averages, totals, and weighted totals are also included.

Time	<0.25	0.25 to 2	2 to 4	4 to 8	8 to 16	16 to 32	32 to 64	>64	Storm
0:40	2	2	0	0	0	0	0	0	4
0:50	0	0	0	1	0	0	0	0	1
1:00	1	8	1	1	0	0	1	0	12
1:10	0	8	2	0	1	0	0	0	11
1:20	2	14	2	4	1	0	0	0	23
1:30	0	7	1	0	0	0	0	0	8
1:40	1	1	3	0	1	0	0	0	6
1:50	0	5	1	0	0	0	0	0	6
2:00	0	5	1	1	0	0	0	0	7
2:10	0	0	0	1	0	0	0	0	1
2:20	0	0	0	0	0	0	1	0	1
2:30	0	2	1	1	1	2	2	0	9
2:40	0	3	1	0	1	2	0	0	7
2:50	0	5	2	1	1	0	0	0	9
3:00	0	2	0	0	2	0	0	0	4
3:10	0	5	0	0	3	1	0	1	10
3:20	0	9	2	6	1	1	2	2	23
3:30	0	12	4	4	1	4	0	0	25
3:40	2	9	2	1	3	0	0	0	17
3:50	0	7	1	2	0	1	0	0	11
4:00	0	5	2	1	1	0	0	0	10
4:10	0	4	3	0	0	0	0	0	7
4:20	0	4	1	1	2	0	0	1	9
4:30	0	10	2	1	1	0	0	0	14
4:40	0	4	6	1	0	0	0	0	11
4:50	0	10	2	1	2	0	0	0	15
5:00	0	8	4	3	2	0	0	0	17
Average	0	6	2	1	1	0	0	0	10
Total	8	149	44	31	24	11	6	4	
Area (# Pixels)	398	16798	2286	1258	722	463	318	156	22399
Weighted Total	33	14	30	39	52	39	31	41	278

Table 4.12. Number of lightning strikes #STR within maximum rain rate intervals and number of lightning strikes #STR within storm as a function of time, for storm 3. Rain rate interval and storm areas (number of pixels) and lightning strike averages, totals, and weighted totals are also included.

Time	<0.25	0.25 to 2	2 to 4	4 to 8	8 to 16	16 to 32	32 to 64	>64	Storm
21:50	0	0	0	0	0	0	0	0	0
22:00	0	0	0	2	1	0	0	0	3
22:10	0	0	0	0	0	0	0	0	0
22:20	0	0	0	1	0	0	0	0	1
22:30	5	5	4	1	1	1	0	0	17
22:40	1	8	1	4	1	2	0	0	17
22:50	0	8	2	0	0	1	0	0	11
23:00	0	8	3	3	0	1	0	0	15
23:10	0	6	1	2	2	0	1	0	12
23:20	0	3	0	4	0	0	0	0	7
23:30	0	3	1	5	4	0	0	1	14
23:40	0	1	0	0	0	0	0	0	1
23:50	1	9	4	2	4	2	1	0	23
0:00	0	1	3	1	5	1	0	1	12
0:10	0	5	1	2	3	2	0	0	13
0:20	0	1	0	0	0	1	0	0	2
0:30	0	0	1	0	0	0	0	0	1
0:40	0	5	0	2	0	1	2	0	10
0:50	0	1	0	0	1	0	0	0	2
1:00	0	1	1	0	0	1	0	0	3
1:10	0	1	1	1	0	0	0	0	3
1:20	0	0	1	0	0	0	0	0	1
1:30	0	0	1	0	0	1	0	0	2
1:40	0	0	0	0	0	0	0	0	0
1:50	2	2	1	0	0	0	0	0	5
2:00	0	1	0	0	0	0	0	0	1
Average	0	3	1	1	1	1	0	0	7
Total	9	88	26	30	22	14	4	2	176
Area (# Pixels)	344	16085	2347	1684	1468	1056	910	852	24746
Weighted Total	49	8	21	33	28	25	8	4	176

Table 4.13. Number of lightning strikes #STR within maximum rain rate intervals and number of lightning strikes #STR within storm as a function of time, for storm 4. Rain rate interval and storm areas (number of pixels) and lightning strike averages, totals, and weighted totals are also included.

Time	<0.25	0.25 to 2	2 to 4	4 to 8	8 to 16	16 to 32	32 to 64	>64	Storm
0:40	0	0	0	0	0	0	0	0	0
0:50	0	0	0	0	0	0	0	0	0
1:00	0	0	0	0	0	0	0	0	0
1:10	0	1	0	0	0	0	0	0	1
1:20	0	0	0	0	0	0	0	0	0
1:30	0	1	0	0	0	0	0	0	1
1:40	0	1	1	2	0	0	0	0	4
1:50	0	2	0	0	0	0	0	0	2
2:00	0	1	4	2	2	1	0	0	10
2:10	0	2	2	0	1	1	0	0	6
2:20	0	3	1	1	1	0	0	0	6
2:30	0	2	0	0	0	3	0	0	5
2:40	0	3	0	1	1	0	0	0	5
2:50	4	6	0	1	0	0	0	0	11
3:00	2	6	0	1	0	1	0	0	10
3:10	0	2	2	1	3	0	0	0	8
3:20	0	2	0	0	0	1	0	0	3
3:30	0	1	1	0	0	0	1	0	3
3:40	0	1	0	0	0	0	0	0	1
3:50	2	5	3	2	2	1	1	0	16
4:00	3	7	0	2	3	0	0	0	15
4:10	0	0	0	0	0	0	0	0	0
4:20	1	0	0	0	0	0	0	1	2
4:30	0	0	0	0	0	0	0	0	0
Average	1	2	1	1	1	0	0	0	5
Total	12	46	14	13	13	8	2	1	109
Area (# Pixels)	398	16798	2286	1258	722	463	318	156	22399
Weighted Total	45	5	12	15	16	12	3	2	109

Table 4.14. Evolution of Storm 1. STSIZE is the storm size [km^2], H is the maximum 40 dBz height [km], R is the rainfall rate maximum above 2 km [mm h^{-1}], #STR is the number of strikes in the previous 10 minutes, and DR is the average distance of lightning strikes [km] from the center of the rainfall rate maximum.

TIME [UTC]	STSIZE [km^2]	H [km]	R [mm h^{-1}]	#STR	DR [km]
00:40	1700	7.3	40	10	21
00:50	1600	8.7	48	10	19
01:00	2000	8.3	64	14	15
01:10	1900	9.4	73	15	17
01:20	1800	8.5	50	4	19
01:30	1900	10.1	73	5	19
01:40	2300	10.1	75	13	17
01:50	2300	10.5	66	8	15
02:00	2200	9.2	89	3	16
02:10	2500	10.1	80	4	15
02:20	2700	9.2	78	18	14
02:30	2500	8.7	66	21	14
02:40	2400	9.2	69	30	15
02:50	2400	8.7	44	30	13
03:00	2900	9.4	42	29	15
03:10	2800	9.4	36	42	15
03:20	2600	8.9	66	39	14
03:30	2600	8.7	71	51	14
03:40	2800	8.5	71	37	13
03:50	2700	8	75	32	15
04:00	2700	6.6	69	29	15
04:10	2600	8.7	75	25	18
04:20	2400	8	80	32	14
04:30	2300	8.7	78	56	18
04:40	2000	10.3	89	13	13
04:50	1900	8.9	96	10	18
05:00	1800	9.8	91	2	14

Table 4.15. Evolution of Storm 2. STSIZE is the storm size [km^2], H is the maximum 40 dBz height [km], R is the rainfall rate maximum above 2 km [mm h^{-1}], #STR is the number of strikes in the previous 10 minutes, and DR is the average distance of lightning strikes [km] from the center of the rainfall rate maximum.

TIME [UTC]	STSIZE [km^2]	H [km]	R [mm h^{-1}]	#STR	DR [km]
00:40	1600	5.7	43	4	16
00:50	1700	6.3	66	1	10
01:00	1900	6.7	36	12	16
01:10	2500	9.4	66	11	25
01:20	3200	9.8	78	23	18
01:30	3300	9.6	66	8	15
01:40	3000	9.4	68	6	15
01:50	3100	8.7	84	6	17
02:00	3000	10.5	76	7	13
02:10	3300	9.6	84	1	12
02:20	3600	9.4	84	1	2
02:30	3800	6.5	68	9	10
02:40	3900	6.7	72	7	19
02:50	3400	5.9	66	9	15
03:00	3100	7.7	76	4	17
03:10	3200	8.7	88	10	12
03:20	2900	9.8	94	23	15
03:30	3200	9.2	96	25	16
03:40	3800	10.3	74	17	17
03:50	4000	9.8	84	11	18
04:00	3600	8.5	72	10	15
04:10	3400	8.7	68	7	18
04:20	3100	8.7	66	9	10
04:30	3300	8.7	66	14	16
04:40	3100	6.9	66	11	12
04:50	3500	6.9	64	15	17
05:00	3600	7.1	43	17	10

Table 4.16. Evolution of Storm 3. STSIZE is the storm size [km^2], H is the maximum 40 dBz height [km], R is the rainfall rate maximum above 2 km [mm h^{-1}], #STR is the number of strikes in the previous 10 minutes, and DR is the average distance of lightning strikes [km] from the center of the rainfall rate maximum.

TIME [UTC]	STSIZE [km^2]	H [km]	R [mm h^{-1}]	#STR	DR [km]
21:50	1200	10.5	64	0	0
22:00	1800	12.2	77	3	8
22:10	1700	12.9	77	0	0
22:20	2400	12.1	84	1	13
22:30	2700	12.4	87	17	19
22:40	2900	12.5	79	17	19
22:50	3700	12.1	81	11	21
23:00	3900	12.6	83	15	22
23:10	3600	12.0	85	12	22
23:20	3800	12.5	86	7	21
23:30	4100	12.6	96	14	16
23:40	5000	12.8	93	1	46
23:50	5200	12.7	91	23	17
00:00	5100	12.4	89	12	19
00:10	4300	12.9	91	13	19
00:20	4100	12.4	95	2	34
00:30	3800	12.2	91	1	10
00:40	3900	10.9	82	10	27
00:50	4000	10.6	81	2	15
01:00	3500	12.1	72	3	22
01:10	3800	10.4	76	3	29
01:20	3800	8.9	73	1	34
01:30	3900	8.5	71	2	23
01:40	4100	7.0	66	0	0
01:50	3600	6.1	44	5	25
02:00	3400	5.9	44	1	13

Table 4.17. Evolution of Storm 4. STSIZE is the storm size [km^2], H is the maximum 40 dBz height [km], R is the rainfall rate maximum above 2 km [mm h^{-1}], #STR is the number of strikes in the previous 10 minutes, and DR is the average distance of lightning strikes [km] from the center of the rainfall rate maximum.

TIME [UTC]	STSIZE [km^2]	H [km]	R [mm h^{-1}]	#STR	DR [km]
00:40	500	10.3	68	0	0
00:50	1300	8.5	67	0	0
01:00	1500	10.3	67	0	0
01:10	2000	9.6	68	1	13
01:20	2800	10.7	71	0	0
01:30	3100	12.1	80	1	23
01:40	3200	11.1	82	4	16
01:50	3300	10.8	79	2	57
02:00	3400	11	79	10	24
02:10	4000	10.9	80	6	28
02:20	3900	12.3	73	6	21
02:30	3400	12.1	75	5	27
02:40	3700	12.2	81	5	20
02:50	4000	12	87	11	42
03:00	4200	12.1	88	10	37
03:10	3000	12.3	88	8	26
03:20	2900	12.5	94	3	31
03:30	3300	12.9	96	3	26
03:40	3600	11.4	95	1	14
03:50	3300	11.1	76	16	21
04:00	2700	10.7	74	15	30
04:10	2000	10.5	78	0	0
04:20	1900	8.7	71	2	9
04:30	1300	6.2	67	0	0